HIGH FREQUENCY ACTIVITY PRECEDING EPILEPTIC SEIZURES

by

WEI-CHIH CHANG

A thesis submitted to
The University of Birmingham
For the degree of

DOCTOR OF PHILOSOPHY

School of Clinical and Experimental Medicine
The University of Birmingham
August 2010

Abstract

High frequency activity (>100 Hz, HFA) is suggested to be related to seizure genesis, but the mechanism of the HFA is not clear. In the present work HFAs and epileptic features including electrographic seizures (trains of hypersynchronous population spikes lasting ~46 sec) and interictal discharges (abrupt potential deflections, ~40 ms) were induced in rat hippocampal slices by increasing potassium concentration in artificial cerebrospinal fluid (8-10 mM, ACSF). We demonstrated that 1) the HFA was formed mainly by synchronous firing of pyramidal neurons while a subset of interneurons might contribute the HFA; 2) the frequencies of the HFAs were region-specific (186 Hz in CA1 and 240 Hz in CA3), and seizures were present only in CA1; 3) build-up of HFA preceding seizures was observed and it was disrupted by refractory periods triggered by interictal discharges, which were abrupt potential deflections present between seizures every 0.8 sec; 4) interictal discharges have both pro- and anti-effects on seizure genesis, and the dual consequences might be due to modifying HFA; 5) synaptic transmission through glutamatergic and γ-aminobutyric acid-ergic synapses were not essential in HFA formation but they were related to the modulations of HFA. Our findings suggested the crucial role of HFA in the seizure

genesis and the potential value in seizure prediction by monitoring the HFA.

To my parents, my wife and my family

謹獻予我的父母、妻子以及敬愛的家人們

Acknowledgements

I would like to thank Prof. John G.R. Jefferys and Dr Premysl Jiruska for their wise advice and patience. John showed me the prospects of the study and led me to think, to speak and to write properly like a scientist. Premysl taught me the skills and shared with me his knowledge. I thank the examiners, Prof. Attila Sik and Prof. Vincenzo Crunelli for their helping comments on my thesis. Dr Martin Vreugdenhil and Dr Andrew Powell helped me think about my work from different aspects. Barbara Harrison is always supportive to me and all the members of the laboratory. I also thank those people who worked with me previously in this group and the members just joined us for their substantial contributions to the thesis: Dr Jackie Deans, Dr Yuangen Li, Pierre-Philippe Saintot, Alexander Pietersen, Kalbinder Gill and Dr Atif Saghir. Without their assistance, this thesis can not be successful. The study was supported by Epilepsy Research UK.

I gratefully appreciate my wife, Ya-Tzu Chen, for her faithful support and encouragement; her happiness is the reason I work for. Especially I thank my mother, Ti Ho, and my father, Kuang-Chou Chang for their limitless support. Because of my parents, I can focus on my career without distraction.

Table of Contents

Results 63

List of Figures

In **Introduction** section

In **Materials and Methods** section

In **Results** section

In **Appendices** section

List of Tables

In **Results** section:

List of abbreviations (alphabetical)

ACSF	artificial cerebrospinal fluid
D-APV	D-(-)-2-Amino-5-phosphonopentanoic acid
Bic	(-)-Bicuculline methiodide
CSD	current source density
GABA	γ-aminobutyric acid
HFA	high frequency activity (>100 Hz)
high K^+ ACSF	artificial cerebrospinal fluid with high concentration of potassium (8-10 mM)
low Ca^{2+} ACSF	artificial cerebrospinal fluid with low concentration of calcium (0.5 mM)
MUA	multi-unit activity
NBQX	2,3-Dioxo-6-nitro-1,2,3,4-tetrahydrobenzo[f]quinoxaline -7-sulfonamide disodium salt
NMDA	N-methyl-D-aspartic acid

Introduction

Epilepsy

Approximately 1% of the populations in the developed countries suffer from epilepsy, making it is one of the most common neurological diseases (Engel and Pedley, 2008). Epilepsy and epileptic syndromes were classified into different categories according to International League Against Epilepsy (Berg et al., 2010), and this classification and the terminology for epilepsy are currently under review. Only patients with recurrent and unprovoked seizures are diagnosed with epilepsy (Hart and Sander, 2007). Epileptic seizures are paroxysmal and abnormal brain activities; and they can be categorised as 1) generalised epileptic seizures, which originate from both cerebral hemispheres, and 2) focal epileptic seizures, which start in the network limited in one hemisphere (Engel and Pedley, 2008). About 60-70% of focal epilepsies originate in the temporal lobes, as known as temporal lobe epilepsy (TLE). Most of TLE are from the two inner components of temporal lobe, hippocampal formation and amygdale, thus classified as mesial TLE (Hart and Sander, 2007). Hippocampal sclerosis is hard and shrunken hippocampus due to loss of neurons (atrophy) and proliferation of glial

cells, i.e. gliosis (Mathern et al., 2008). Hippocampal sclerosis was found in a majority of patients with mesial TLE, and for more than a hundred years ago it was suggested having pathological correlation to TLE. However hippocampal sclerosis is not a general hallmark for all patients with mesial TLE, neither the hippocampi with sclerosis are all epileptic. Whether hippocampal sclerosis causes seizure or it is a consequence of epilepsy is still uncertain (Mathern et al., 2008).

The unpredictable nature of the seizures is perhaps the most unpleasant aspect of epilepsy. Only two thirds of epileptic patients are steadily controlled by anticonvulsant drugs, and resective epilepsy surgery potentially benefits another 8-10% of patients who have intractable seizures. However, at least 25% of epileptic patients who mainly are classified as mesial TLE still suffer from the social and physical consequences of the sudden and unpredictable seizures (Litt and Lehnertz, 2002;Mormann et al., 2007). Thus for improving the quality of the patients' lives, seizure prediction has attracted growing interest in epileptology. If the seizure onset is predictable, several rapid anti-seizure treatments could be activated before the seizures, for instance brain stimulation or application of fast-acting substances. Even for those epileptic patients who had been controlled by medication, applications of drugs precisely before the seizures might reduce the doses or minimize the side effects.

An epileptic seizure is due to synchronous firing of neurons in the brain which causes a perceivable experience to the patients or observers (Hart and Sander, 2007). Electroencephalography (EEG) records electrical brain activity, and is a good approach to observe seizures (Figure I-01). Electrographic seizures can be further divided into “tonic” or “clonic” phases. These two phases initially described a category of epilepsy: when patients experience seizures, their skeletal muscles suddenly gain extreme tension and then the muscles start to contract and relax rapidly. In the EEG, tonic phase represents a series of population spikes and the clonic phase indicates the discrete but rhythmic clusters of population spikes (Figure I-01B).

“Ictus” in Latin is a stroke or a blow to indicate the seizure proper, thus the epochs between seizures are defined as interictal periods. Although seizures are the most remarkable features of epilepsy, they are not the only electrographic abnormality. Interictal discharges are transient and abrupt EEG deflections (de Curtis and Avanzini, 2001). They are observed during interictal periods in the EEG of epileptic patients (Figure I-01). The interictal discharges also reflect synchrony of hyperactive neurons, however the brain regions which can generate interictal discharges (i.e. irritative zones) are not identical with the seizure onset zones or epileptogenic zones (Rosenow and Luders, 2001). The relationship between interictal discharges and

seizures still remains unclear (Avoli et al., 2006;de Curtis and Avanzini, 2001).

For many years, prediction of seizure onsets by quantitative analyses of EEG focused on electrographic changes below 100 Hz during interictal periods or pre-ictal segments (Litt and Lehnertz, 2002;Mormann et al., 2007). However the mechanisms underlying the transition from normal (or pre-ictal) states to the epileptic seizures are still uncertain. Approximately 20 years ago the discovery of brain activity faster than 100 Hz started a new direction in epilepsy research (Allen et al., 1992;Fisher et al., 1992).

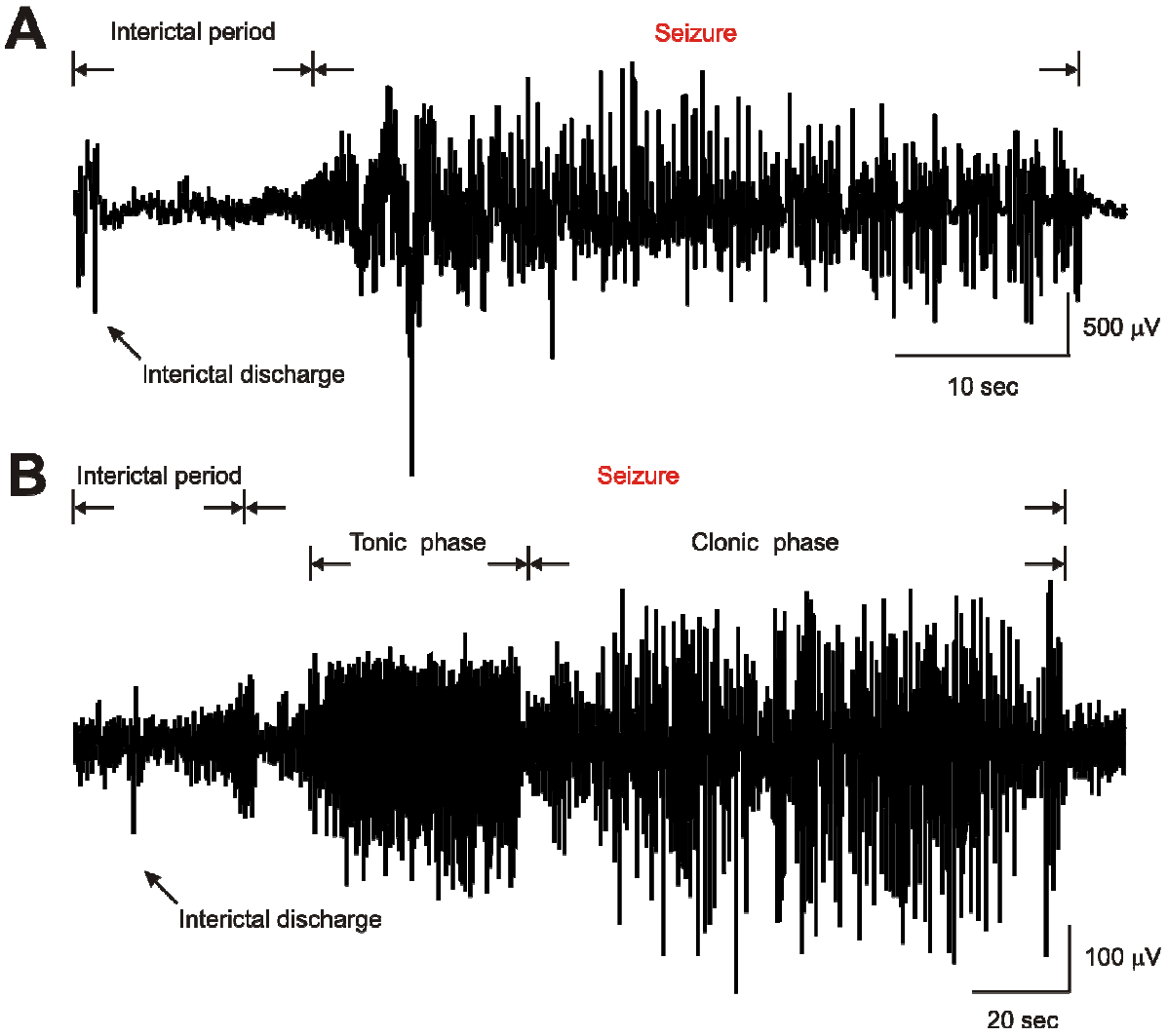

Figure I-01. EEG of epileptic seizures. Two patients were implanted with spencer (depth) electrodes. EEG was recorded from the electrode close to their amygdalo-hippocampal regions during seizures and few seconds before (courtesy of Dr P. Jiruska). **A**, EEG comprises an interictal period and a seizure. An interictal discharge is present in the interictal period. **B**, this seizure comprises tonic phase and clonic phase. An interictal discharge is also present in the interictal period.

High frequency activity (HFA)

Brain activity faster than 100 Hz, high frequency activity (HFA), is not unique to epileptic seizures, but is also found during normal physiological activity. Indeed the first descriptions of HFA were from physiological investigations.

Physiological HFA

When rodents are grooming, eating, drinking, immobile or even in slow wave sleep, “sharp waves” are present in hippocampal regions (Figure I-02), where a negative sharp wave was observed in stratum radiatum, which represented a summated depolarized field potential due to synchronous excitatory postsynaptic potentials (EPSPs), with an associated positive sharp wave in stratum pyramidale (Buzsaki, 1986). Years after the discovery of sharp waves, they were found to be associated with a fast network oscillation (~200 Hz, termed “ripple”) which was confined to the pyramidal layer of the CA1 region in rat hippocampus (Buzsaki et al., 1992). The ripples were also present in the CA3 pyramidal layer, though no spatial synchrony of these oscillations was found between the two regions, suggesting that this oscillation

was generated by local circuits. Although only ~10% pyramidal neurons and most of interneurons were involved in each cycle of the ripples, during the ripples the firing probabilities for both types of cell did increase several times; see Appendixes A.1 in detail (Csicsvari et al., 1999b;Ylinen et al., 1995). The membrane potential of the CA1 pyramidal neurons also presented oscillations, which could be phase-locked with the field ripples (Ylinen et al., 1995). The frequency of intracellular oscillations persisted either when the membrane potentials were depolarized or hyperpolarized, and only the correlated phases or the amplitudes were altered, suggesting that the oscillations were generated by networks of neurons. Thereafter they hypothesized that although CA3 did not directly contribute to the generation of the fast network oscillations, CA3 activated the inhibitory circuit in CA1 in the form of excitatory drive, and that the CA1 inhibitory circuit constructed suppressive windows so that the action potentials from CA1 pyramidal neurons could precisely aggregate between these windows to form the extracellular ripples (Buzsaki et al., 1992;Ylinen et al., 1995). The temporal correlations between the sharp wave ripples and the firing patterns of pyramidal neurons and interneurons have subsequently been observed in humans (Le Van et al., 2008).

Ripples which are superimposed on sharp waves can propagate from hippocampus

to the neocortex, thus this fast oscillation was proposed as a mechanism for long term synaptic modifications in their target regions (Chrobak and Buzsaki, 1996). These researchers concluded that when the behaviors of the experimental rats changed, some neurons switched their firing probabilities and/or changed the interactions to other neurons; thus the neurons construct a new rhythm or become able to respond to new rhythms (Csicsvari et al., 1999b). Later, two kinds of fast oscillations (both >100 Hz: a faster frequency-higher amplitude oscillation and a slower frequency-lower amplitude oscillation) were simultaneously observed in hippocampal CA1 regions. They could have different underlying mechanisms because the faster-frequency-higher amplitude oscillation is entirely due to CA1 local circuits but the slower frequency-lower amplitude oscillation is tightly correlated with the CA3 fast oscillation (Csicsvari et al., 1999a;Csicsvari et al., 2000). This finding raised the idea that oscillations even with similar frequencies might be due to different mechanisms.

Physiological HFAs were also observed in many cortical regions and correlated with physiological functions (Engel et al., 2009;Kandel and Buzsaki, 1997): for example, the oscillations in somatosensory cortex (>200 Hz) had been recorded in rodents and human, which might be related to the processing of sensory information from the thalamus to the normal nerocortex.

Pathological HFA

With developments in both digital equipment and invasive electrodes for clinical use, a neuronal activity between 80 and 120 Hz, which is faster than the traditional physiological oscillations, was found preceding slower electrographic epileptic features in patients (Allen et al., 1992;Fisher et al., 1992). This pathological HFA was present seconds before the seizure onset, and it was clearly recorded only on the seizure foci or the very neighboring regions close to the foci; this association led to the suggestion that HFA may play an important role in seizure genesis.

Years after the first discovery of the pathological HFA, Bragin and colleagues distinguished two different classes of HFAs from their clinical studies. The HFAs were found with two distinct frequency ranges in hippocampi of epileptic patients who were implanted with depth electrodes: one was from 80 to 160 Hz and the other was from 250 to 500 Hz (Bragin et al., 1999a). The slower HFA was observed bilaterally in both hemispheres during slow wave sleep or when the patients were in quiet state, thus it was suggested this form of HFA resembled to the sharp wave ripple found in rat hippocampus and entorhinal cortex. On the other hand, the faster HFA was present unilaterally and found only close to the seizure foci. Therefore they suggested that this

faster HFA might be epileptogenic and termed it as “fast ripple”. Later quantitative analyses also proved that the ratio between the occurrence of fast ripples and that of ripples was higher in hemisphere ipsilateral to the seizure onsets and that this higher ratio correlated with hippocampal atrophy (Staba et al., 2002).

Fast ripples were reproduced in a chronic epileptic animal model, in which kainic acid (KA) was injected into rats’ hippocampi unilaterally to develop neuronal loss resembling human hippocampal sclerosis and to induce spontaneous seizures several months later (Bragin et al., 1999b). In these epileptic rats the fast ripples were present in the KA-damaged regions, resembling the spatial correlation between HFA and seizure foci in patients. Bragin et al demonstrated the fast ripple may have different mechanisms from the sharp wave ripple: the pyramidal cells mainly contribute to the formation of the fast ripple. In contrast, interneurons played a central role in the formation of the sharp wave ripple. Furthermore, they also suggested that the fast ripple might reflect the underlying mechanisms responsible for epileptogenesis (Bragin et al., 1999b).

Two seizure onset patterns were found in KA injected epileptic rats: 1) low-voltage fast (rhythmic) onset, and 2) hypersynchronous onset, resembling the two distinct seizure onset patterns observed in epileptic patients (Bragin et al., 1999c). The fast

ripples were highly related to the hypersynchronous ictal onset thus the hypersynchronous ictal onset might share mechanisms with fast ripples (Bragin et al., 1999c). In studies using chronic epileptic animals models or brain tissues from patients with focal epilepsy, granule cells in the dentate gyrus were found to have aberrant axons, i.e. mossy fibre sprouting which conventionally is recognised as a hallmark of temporal lobe epilepsy and is implicated as an epileptogenic factor (Rakhade and Jensen, 2009). In the KA injection epileptic rat model fast ripples were found in a limited area (1 mm^3) in dentate gyrus, but the mossy fibre sprouting was found in a wider region. Besides, the fast ripples presented earlier in the development of the epileptic focus than the formation of axonal sprouting. Thus these authors concluded that the neuronal clusters responsible for fast ripples might be independent of the mossy fibre sprouting. On the other hand, the activity generated by these clusters might act as an endogenous stimulus that could recruit more neuronal connections into the pathological circuitry and thus cause its expansion (Bragin et al., 2000). A restricted region showing fast ripples in entorhinal cortex of epileptic patients was also reported, and these fast ripples proved to originate from strongly increased synchronous firing of neurons similar to that found in chronic rat epileptic model (Bragin et al., 2002b). The role of the fast ripple in epileptogenesis was thereby

suggested to be: first inhibition in the zone generating fast ripples becomes weaker, then as the fast ripples strengthen they invade other regions by overcoming their local inhibitory system, leading to the recruitment of more pathologically interconnected neuron clusters and subsequently to epileptic seizures (Bragin et al., 2000;Bragin et al., 2002a).

Moreover, the KA injected epileptic rats also revealed that the longer delays before the first appearance of pathological HFA were correlated to 1) the increased time to the first seizure occurrence, but 2) inversely correlated to the rates of seizures. This study indirectly reinforced the relationship between the HFA and the epileptogenesis and the seizure genesis (Bragin et al., 2004).

Mechanisms for the HFA

One of the possible mechanisms underlying the HFAs has been mentioned in the previous section. In normal (physiological) conditions the CA3 pyramidal burst firing cause EPSPs in stratum radiatum of CA1, which are in the form of sharp waves if observed extracellularly, and thus activate both CA1 principal neurons and interneurons. Enhanced synchronous interneuronal firing strongly constrains the firing

probabilities of the principal cells, so that pyramidal neurons can only fire between the inhibitory postsynaptic potentials (IPSPs) and form the a specific pattern, which is the ripples (Buzsaki, 1986;Buzsaki et al., 1992;Ylinen et al., 1995). The pathological HFA (fast ripples) found in epileptic patients or chronic animal models of epilepsy was proposed to have different mechanisms from physiological ripples; the fast ripples were mainly correlated with action potentials from pyramidal neurons, and rarely from interneurons, (Bragin et al., 1999b). However the mechanisms for pathological HFA have not yet been solidly proven.

The minimal latency between the presynaptic pyramidal discharges to the EPSP of neighboring interneuron was 2-3 ms (Gulyas et al., 1993). With this time-scale, local chemical synaptic transmission is too slow to fulfil the task of generating the very fast frequency of fast ripples (250-500 Hz), but non-synaptic modulations, like electrotonic coupling, ephaptic interactions or electrical field might succeed (Dudek et al., 1986;Jefferys, 1995). Electrotonic coupling refers to the current or cytoplasmic continuity through gap junctions between neurons. Ephaptic interaction exists between neurons in the absence of specialized contacts, in which inward membrane current of one neuron leads to an extracellular negativity and the net depolarisation of neighbouring neurons. The electrical field is due to large extracellular currents caused

by synchronous firing of neurons particularly in hippocampus or cortex (Jefferys, 1995).

Electographic seizures were present in hippocampal CA1 *in vitro* where synaptic transmission was blocked by low calcium concentration (<0.5 mM, low Ca^{2+}) in artificial cerebrospinal fluid (ACSF) (Jefferys and Haas, 1982). These electrographic seizures were found to be synchronous with ~50 ms delay between two recording sites separated by 1mm. The synchronisation was too quick and thus unlikely to be due to extracellular potassium diffusion alone. Electrical fields decay quickly in tens of microns (Holt and Koch, 1999). However there may be a chain reaction of electric field interaction exciting neighbouring cells, and that the small delays between successive delays leads to the 50 ms lag over 1mm. Alternatively gap junctions, or electrotonic coupling, might be also crucial. Another high-frequency oscillation was reported showing synchronisation in 120-μm range in hippocampal slices made from juvenile (postnatal day P18-26) rats, and the oscillation persisted after blocking glutamatergic and γ-aminobutyric acid (GABA) receptors together (Draguhn et al., 1998); however applying the gap junction blockers abolished the oscillations and cellular alkalinisation enhanced the oscillations. Cell damage might lead to increase of the number and/or strength of existing electrotonic junctions. Thus gap junctions seem promising to

synchronise neurons and form HFA.

Few years later, a study from our laboratory described a progressive development from a low amplitude-fast frequency oscillation to high amplitude-low frequency electrographic seizures in rat hippocampal slices perfused with low Ca^{2+} ACSF (Bikson et al., 2003); a hypothesis was suggested for the progression to seizure that neurons fire in aggregates, and the aggregates merge with each other and thus develop into seizures. In this report the transition was accelerated by introduction of low Ca^{2+} ACSF with lower osmolarity (80 mOsm/L lower), which supported the possible involvement of electrical field or ephaptic interactions in the seizure genesis. Our recent study, on the same low Ca^{2+} rat hippocampal slice model, showed that HFA mainly originated from the synchronous firing of pyramidal neurons in CA1 region. We demonstrated the gradual spatial expansions of the HFA and the increase of its synchrony preceding seizure onsets; this finding further supports the previous aggregate hypothesis (Jiruska et al., 2010a).

Hippocampus

The prevalence of mesial TLE made us focus on epileptogenesis and seizures in hippocampus. The trisynaptic pathway and the architecture of the neurons in the hippocampus were extensively studied since Ramon y Cajal's classic contributions using Golgi staining. The hippocampus comprises Cornu Ammonis (CA) and dentate gyrus (DG), and CA is sub-divided into CA1, CA2, CA3 and CA4 (Figure I-02). Clear strata are present in hippocampal CA formation (Figure I-02): 1) stratum oriens, basal dendrites of pyramidal neurons and some interneurons can be found in this layer; 2) stratum pyramidale, pyramidal neurons are the main excitatory cells in the hippocampus, and their bodies located in this layer; many interneurons are also present in this layer; 3) stratum radiatum, apical dendrites of pyramidal neurons extend into this layer, some interneurons are present (Johnston and Amaral, 2003). Further layers include: alveus, the most superficial layer containing axons of pyramidal neurons; stratum lucidum is between strata pyramidale and radiatum; stratum lacunosum-moleculare is the deepest layer close to the hippocampal fissure.

The trisynaptic pathway conducts the major excitatory signal flow along hippocampus, with glutamate as the neurotransmitter. First DG receives inputs from

the neighboring entorhinal cortex by the perforant pathway. Then, the granuale cells in DG signal through mossy fibres (bundles of axons of granule cells) to CA3 pyramidal neurons. Last, CA3 pyramidal neurons innervate CA1 pyramidal neurons by the Schaffer collateral pathway (Figure I-02). CA1 pyramidal neurons project through the subicular complex to the entorhinal cortex, which in turn is associated with many brain regions (Johnston and Amaral, 2003). The hippocampus also receives the cholinergic and GABAergic inputs from the septum, noradrenergic input from the locus coeruleus, serotonergic input from the raphe nucleus, dopaminergic input from the ventral tegmental area; and hippocampus is extensively innervated from the contralateral hippocampus (Johnston and Amaral, 2003).

Interneurons are more diverse than pyramidal neurons (Figure I-03). In the hippocampus all interneurons release GABA to induce inhibitory post-synaptic current. They can be classified into many subtypes by their firing patterns, molecular expressions and their terminations on different sub-cellular domains (Freund and Buzsaki, 1996;Klausberger and Somogyi, 2008). Three types of parvalbumin expressing interneurons are located in stratum pyramidale, and are distinguished by their innervation of different compartments of the pyramidal neurons: 1) axo-axonic (chandelier) cells, which exclusively innervate the initial segments of pyramidal cells;

2) basket cells, which innervate the cell bodies or the proximal dendrites of the pyramidal neurons; 3) bistratified cells, which innervate the basal dendrites or apical dendrites. These interneurons are innervated by pyramidal neurons locally, i.e. CA1 pyramidal neuron to CA1 interneuron, or distally, i.e. CA3 pyramidal neuron to CA1 interneuron (Ali et al., 1998;Buhl et al., 1996;Freund and Buzsaki, 1996;Klausberger and Somogyi, 2008). Oriens-lacunosum moleculare (O-LM) interneurons and back-projection cells have cell bodies located in stratum oriens, and also receive pyramidal inputs locally and distally by CA3 pyramidal neurons (Freund and Buzsaki, 1996;Klausberger and Somogyi, 2008).

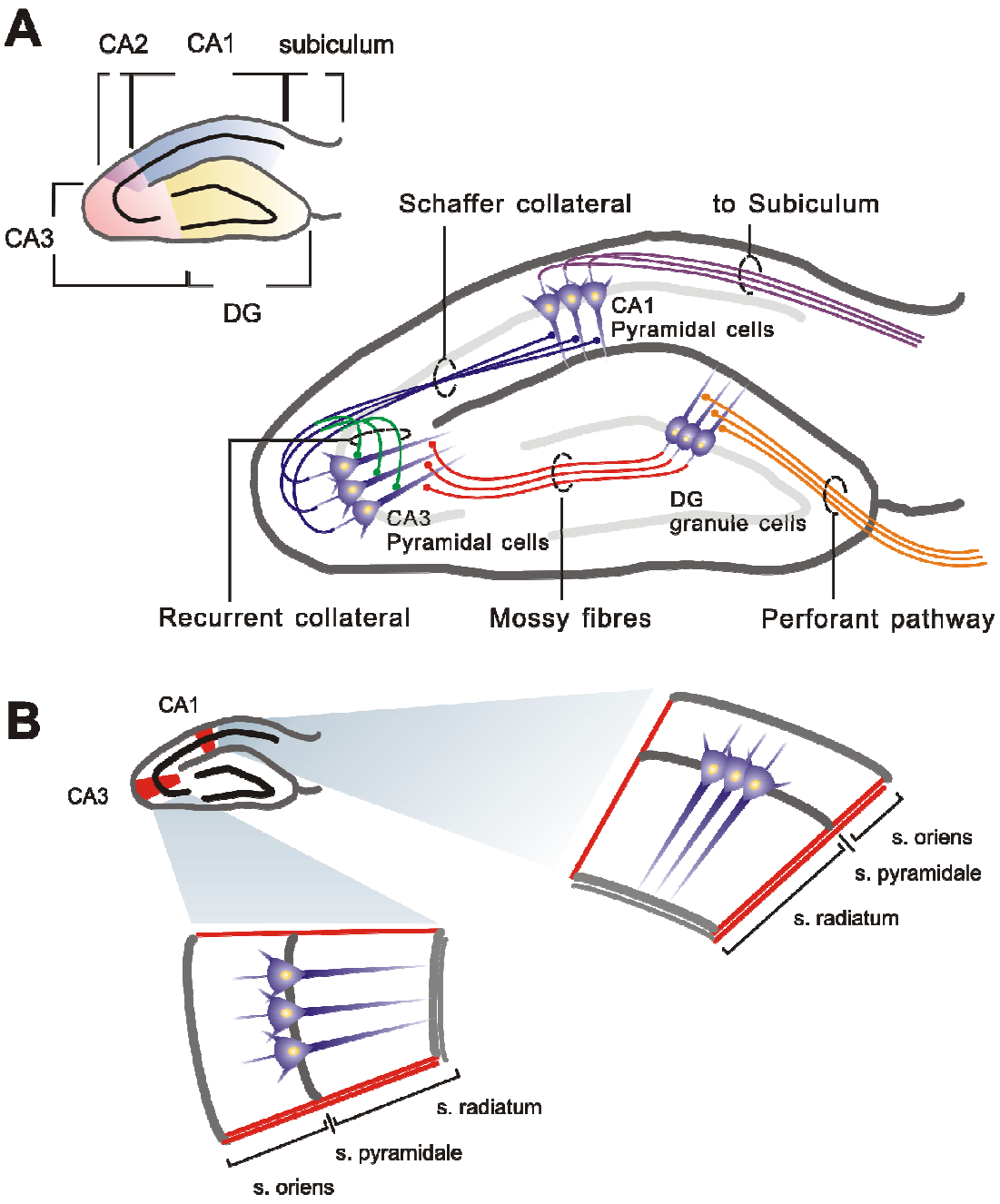
A
CA2
CA1
subiculum
CA3
DG
Schaffer collateral
to Subiculum
CA1
Pyramidal cells
CA3
Pyramidal cells
DG
granule cells
Recurrent collateral
Mossy fibres
Perforant pathway
B
CA1
CA3
s. oriens
s. pyramidale
s. radiatum
s. radiatum
s. pyramidale
s. oriens

Figure I-02. Hippocampal structure **A**, *inset*, a hippocampus is composed of Cornu Ammonis (CA) and dentate gyrus (DG, in yellow); and the CA is sub-divided as CA1 (in blue), CA2 (in purple) and CA3 (in red). CA1 is connected to entorhinal cortex through subiculum. Major circuit in hippocampus includes: DG granule cells receive entorhinal cortical inputs by perforant pathway; Mossy fibres are the axons of DG granule cells and project to CA3 pyramidal neurons; CA3 pyramidal neurons project through the Schaffer collateral pathway to CA1. These three pathways altogether are called the trisynaptic pathway. CA3 pyramidal neurons receive feedback innervation from themselves through recurrent collaterals. Recurrent collaterals are also present in CA1 pyramidal neurons but not as manifest as CA3 pyramidal neurons. CA1 pyramidal neurons output to subiculum and further to entorhinal cortex. **B**, hippocampal CA mainly comprises three layers: stratum oriens, stratum pyramidale and stratum radiatum. The laminations of CA1 and CA3 were enlarged in this schematic.

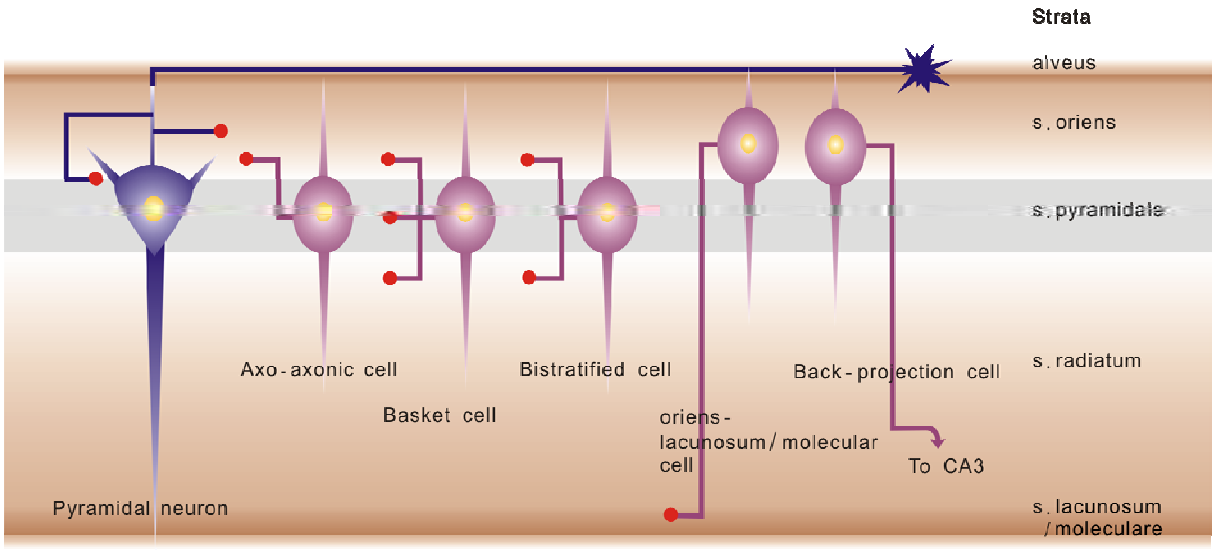

Figure I-03. Pyramidal neuron (blue) and interneurons (purple) in CA proper of the hippocampus. Recurrent collaterals of pyramidal neurons innervate other pyramidal neurons (or itself). Interneurons receive pyramidal inputs in s. oriens and/or s.radiatum (in CA3). Three types of interneurons locate in s. pyramidale. Axo-axonic cells innervate initial segments of pyramidal neurons. Basket cells innervate cell bodies or basal dendrites of pyramidal neurons. Bistratified cells innervate both basal dendrits and apical dendrites of pyramidal neurons. Two types of interneurons have cell bodies located in s. oriens. O-LM cells innervate pyramidal neurons in the LM layer. CA1 back-projection cells innervate CA3 pyramidal neurons.

High potassium rat hippocampal slice model

In this study, we used acute rat hippocampal slices (thus *in vitro*). The hippocampal slice preparation is a simplified preparation that removes long-range afferents mentioned above, and preserves the intrinsic trisynaptic pathway and the interactions between pyramidal neurons and local interneurons. The *in vitro* condition provides visualisation of the slice structure to help place electrodes, and makes pharmacological experiments much easier.

Changes in the concentrations of ions (Ca^{2+}, Mg^{2+} or K^{+}) in the perfusate, or additions of convulsant drugs, have been used to induce electrographic seizures either *in vivo* and *in vitro* (Jefferys, 2003). Low Ca^{2+} ACSF blocks synaptic transmission and reduces divalent cation screening of the cell membrane to depolarize neurons (Jefferys, 1995). In contrast, high potassium concentration in the ACSF (high K^{+}, 8-10 mM) reduces the transmembrane K^{+} gradient and incidently depresses IPSPs by reducing Cl^{-} gradient; thus eventually neurons are depolarized and potentially it enhances seizure genesis (Traynelis and Dingledine, 1988). Our preliminary tests showed that high K^{+} ACSF reliably induced a HFA and epileptic features comparable to those seen in low Mg^{2+} or the convulsant drug,

4-aminopyridine.

Aim of the study

The role of HFA in memory consolidation (i.e. sharp wave ripple) to deliver information from hippocampus to the neocortex had been extensively studied over the past decade (Chrobak and Buzsaki, 1996); on the other hand the importance of the pathological form of HFA is still uncertain, nor have the mechanisms for the pathological HFA been determined. Although the early studies described the HFA in epileptogenesis or during the preictal stages, the mechanisms of pathological HFA have not been thoroughly investigated (Allen et al., 1992;Bragin et al., 1999b;Bragin et al., 1999a;Fisher et al., 1992). Previous studies had proposed that the formation of HFA is due to non-synaptic mechanisms and demonstrated strong correlation between the HFA and seizure onset in a simplified *in vitro* model, where synaptic transmission in the hippocampal slices was abolished after introducing the low Ca^{2+} ACSF (Bikson et al., 2003;Jiruska et al., 2010a). However, although the non-synaptic mechanisms (electrotonic junctions, ephaptic interactions or electrical field) were implicated in the seizure genesis, the necessity of each mechanism in seizure genesis is still uncertain (Jiruska et al., 2010c).

Synchronous firing during HFA is likely to result in stronger synaptic drive to

postsynaptic targets, due to spatial summation and perhaps potentiation, which would be predicted to play a role in epileptogenesis and seizure onset. We will determine whether similar mechanisms for the HFA found in previous low Ca^{2+} studies will still predominate when synaptic transmission is intact; and thereby we could examine the questions whether the mechanisms of HFA in seizure genesis we suggested can be applied in animal models or even in patients. Also we question whether there is a solid distinction between physiological HFA and pathological HFA in terms of patterns of neuronal activities and mechanisms (Bragin et al., 2007;Klausberger and Somogyi, 2008).

To summarize, we performed our experiments using the high K^+ *in vitro* rat hippocampal slice model and addressed these issues: 1) to clarify the characteristics of the HFA; 2) to understand cellular mechanisms of the HFA; 3) to demonstrate spatio-temporal relationship between the HFA and electrographic seizures; 4) to discover any modification of the HFA. Eventually we hope to answer: what is the role of the HFA in seizure genesis?

Materials and Methods

Animals and slice preparation

Adult male Sprague-Dawley rats (aged 7-8 weeks; 140-200 g) were provided by Biomedical Service Unit of University of Birmingham. The animal procedures were approved by Home Office of the United Kingdom [Animal (Scientific Procedures) Act 1986], and all efforts were made to reduce numbers and the suffering of the animals. Animals were anesthetized deeply with intraperitoneal ketamine (60 mg / kg) plus medetomidine hydrochloride (0.25 mg / kg) and killed by cervical dislocation. The brains were quickly removed, and immersed in chilled and oxygenated (95 % O_2 and 5 % CO_2) sucrose artificial cerebrospinal fluid (ACSF) containing 189 mM sucrose, 2.5 mM KCl, 26 mM $NaHCO_3$, 1.2 mM $NaH_2PO_4 \cdot H_2O$, 10 mM glucose, 5 mM $MgCl_2$, and 0.1 mM $CaCl_2$. 400 μm sagittal hippocampal slices (0° along the midline) were made using an Integraslice 7550 PSDS (Campden Instruments Ltd.) where the cooling was maintained by Specimen Bath Cooler 7600 series (Campden Instruments Ltd.). Slices were incubated in a holding chamber containing oxygenated normal ACSF containing 125 mM NaCl, 3 mM KCl, 26 mM $NaHCO_3$, 1.25 mM $NaH_2PO_4 \cdot H_2O$, 10

mM glucose, 1 mM $MgCl_2$, and 2 mM $CaCl_2$ at room temperature for at least 1 hour. Osmolarity of both normal ACSF and sucrose ACSF was measured and required to be between 295 and 305 mmol/kg. Thereafter the slices were transferred to an interface recording chamber which was perfused with warm normal ACSF and maintained at 31-35℃. After recovery, the concentration of K^+ in the perfusing ACSF was raised to 8-10 mM (high K^+) for activating neurons and inducing epileptic events.

Extracellular electrophysiological recording

Spatiotemporal recording by platinum / iridium electrodes

For their fast response time, metal electrodes were used in our study. Homemade fine platinum (Pt) / iridium (Ir) wire (Pt 90 %/Ir 10 %, 0.025 mm in diameter, Teflon insulated; Advent Research Materials Ltd.) electrodes were located in pyramidal layer in hippocampal CA1 and CA3 to record the gross extracellular field potentials (Figure M-01A). The fabricating procedure is: Pt/Ir wires were inserted into borosilicate glass micropipettes which were pulled to form sharp tips, and then further protruded the broken pipette tips for hundreds microns; the recording sides of wires were neatly cut. Both ends of the micropipettes were sealed with super glue and silicon sealant, and the wires were connected to gold pins. The impedances of these Pt/Ir electrodes were 0.2-0.7 MΩ measured by an Audio Monitor and Impedance Tester (Neuralynx, Inc) at 1 kHz.

To record spatiotemporal profiles of electrographic epileptic events, nine Pt/Ir electrodes were placed in the stratum pyramidale along the hippocampus with equal inter-electrode distances (~550-600 μm, Figure M-01B). For current source density

analyses, field potentials were recorded from electrodes positioned in a line along the somatodendritic axes, with the electrodes equally spaced along a presumed somatodendritic axis in either hippocampal CA1 or CA3, with inter-electrode distances ~60 μm (Figure M-02). In both cases electrodes were positioned using micromanipulators under visual guidance by the stereomicroscopic graticule, Positions of the electrodes were recorded as photos by a digital eyepiece camera (World Precision Instruments, Inc.) and the inter-electrode distances were verified by both microscopic graticule and measurements by ImageJ programme.

The reference electrode was made from Ag-AgCl wire (99.99 % silver, 0.37 mm in diameter; Advent Research Materials Ltd.; the wire was immersed in bleach to oxidize the surface to AgCl) and was embedded in the recording chamber. Signals were amplified 500 times, low-pass filtered (<3 kHz) by a Lynx-8 Amplifier (Neuralynx, Inc) and digitized by a Power1401 signal acquisition system (Cambridge Electronic Design, Ltd.) with sampling frequency of 5 kHz and then stored and processed by a PC.

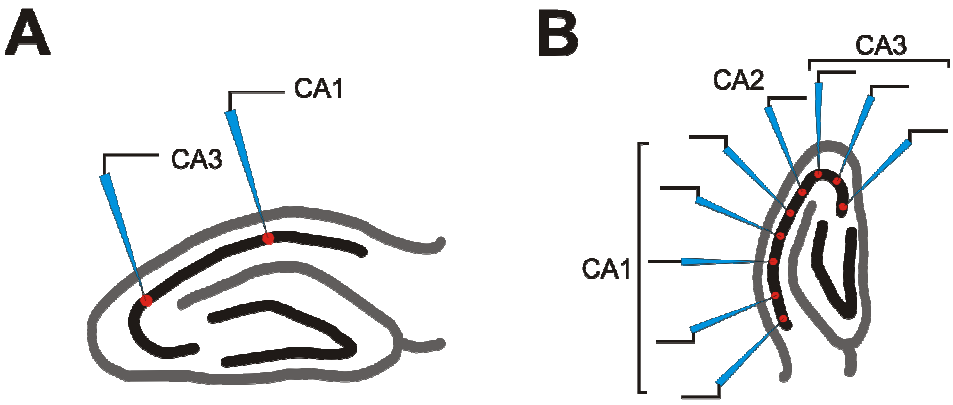

Figure M-01. Electrode arrangements for extracellular recordings. **A**, a schematic drawing shows a transverse hippocampal slice and two Pt/Ir electrodes which are located in the pyramidal layer in the CA1 and CA3 regions. **B**, for spatial recording of the HFA and the epileptic events, nine Pt/Ir electrodes were located along the pyramidal layer of the hippocampal slices with equal inter-electrode distances.

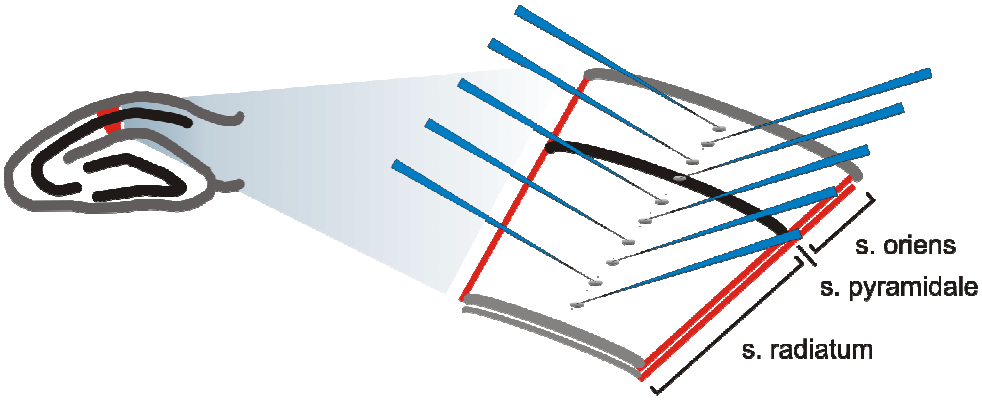

Figure M-02. Electrode arrangement used for current source density. A section of CA1 is enlarged to show the arrangement. Ten electrodes are positioned along the somatodendritic axis in CA1 with equal inter-electrode distances: three electrodes cover the s.oriens, one is in the s. pyramidle and six cover the s. radiatum (s. for stratum).

Tetrode recording

Tetrode is the abbreviation of tetra-electrodes, which means four electrodes were closely bound together. Tetrodes used in this study were homemade following a published protocol (Szymusiak and Nitz, 2010). In brief, ~60 cm tungsten fine wires (12.7 μm in diameter, with heavy formvar & butyral bond insulating coat; California Fine Wire Company) were bent to form a bundle of two wires ~30 cm long and mounted on an L-shape stand perpendicular to a magnetic stirrer plate, with the ends of the wires held with a crocodile clamp which was attached to a stirrer bar. The stirrer plate then was switched on and the bar spun slowly until 60-80 turns were made. A heat gun was used to melt the insulator for stabilising the twists. The wire bundle was gently cut out from the set-up, and crosstalk was tested to ensure that these four twisted wires were not connected electrically to each other. Then the wire bundle was strengthened and protected as for the Pt/Ir electrodes, in that the wire bundle was stuffed in a sharp micropipette and connected to gold pins, and then a tetrode was completed. The impedance of each channel of these tetrodes was 0.2-0.4 MΩ at 1 kHz.

Tetrodes were placed in stratum pyramidale. Signals were amplified 2000 times,

low-pass filtered (<6 kHz) by Lynx-8 Amplifier (Neuralynx, Inc) and digitized by a Power1401 signal acquisition system (Cambridge Electronic Design, Ltd.) with sampling frequency 20 kHz and then stored and processed by a PC.

Agents and chemicals

D-(-)-2-Amino-5-phosphonopentanoic acid (D-APV), 2,3-Dioxo-6-nitro-1,2,3,4-tetrahydrobenzo[f]quinoxaline-7-sulfonamide (NBQX) disodium salt and (-)-Bicuculline methiodide were purchased from Ascent Scientific (UK). Drugs were dissolved in water to stock solutions (1000x testing concentrations) and stored in -20℃ freezer. Drugs were defrosted and directly added to the perfusate during experiments.

Data analyses and statistics

Remove of mains noise and signal filtering

Signals were acquired by Spike2 programme (Cambridge Electronic Design, Ltd.), and were saved as Spike2 compatible files. The raw recordings had mains noise removed by an off-line procedure before all analyses. During the recordings a wire was left in the Faraday cage to capture phases of the mains noise synchronously with the electrophysiological recordings. The mains cycles (50 Hz in the United Kingdom) were acquired from this channel by a shared Spike2 script “Hum Remove” which was developed by us and CED. Artificial mains oscillations were then generated and calibrated to the averaged amplitudes and phase of the mains noise in every channel by the reference cycle. Then the artificial mains noise was subtracted from the original recordings to get clean physiological recordings (Jiruska et al., 2009).

A raw electrophysiological recording generally contains DC shifts and unwelcome artifacts. Even the activities of interest might interfere with each other. To improve detection of oscillations or events, off-line finite impulse response (FIR) filters or infinite impulse response (IIR) filters were applied in most cases; the epileptic features

and the activities within 100-250 Hz, 250-500 Hz and 500-1000 Hz, which represent the conventionally defined physiological ripples, fast ripples and multi-unit activities (MUA), were isolated. Although the IIR filter can be set for narrower notch filters of signals with steep band edges, this approach has major drawbacks in causing distortions of the waveforms and phase shifts; these waveform distortions and phase shifts might greatly mislead the correlations of interest, especially for the fast activities. Thus FIR filter was applied to ripples in 100-250 Hz, fast ripples in 250-500 Hz or MUA in 500-1000 Hz. Interictal discharges are combinations of HFA and slow (<100 Hz) deflections. However the FIR filter was not applicable in this lower frequency band thus IIR filter was used to reveal the patterns of interictal discharges between 10 to 100 Hz. Although we cannot avoid the phase shifts caused by IIR filter in the lower frequency band, we believed these shifts in slower time scales would not be as apparent as those caused in the faster time scales required by HFA.

Power spectra and spectrogram

Simple power spectra were acquired from the fast Fourier transform in Spike2, which show power of the signal in every ~5 Hz band in a given signal (1024 for FFT

size with data at 5 kHz sampling rate, or 4096 with data at 20 kHz sampling frequency). A Hanning window was used when we conducted power spectra. Due to different biological and recording conditions between slices and experiments, the power spectra were normalised to show the dominant frequencies. In these analyses, the peak power present between 100 to 500 Hz was used as a reference, and all wide-band power in the spectra were divided by this value; for those experiments concerning the temporal changes or different treatments of the HFA, the peak power between 100 to 500 Hz under control states was used to normalise spectra subsequently acquired from different experimental states.

The notion of the “first moment” was applied to the power spectra to describe distributions of the activities within a frequency band. In other words, the first moment is an arithmetic mean of the power spectrum derived from the powers across the range of frequencies. This analysis can supportively describe the changing frequency distribution of the activities between the power spectra, especially when the shift of the dominant frequencies was not significant. Because the power for high K^+ induced HFA was much smaller than that for the activities below 100 Hz, we made the first moment analyses on the 100-500 Hz in spectra only. The equation for first moment of spectra is:

$$F = \frac{\sum (P_Z \times F_Z)}{\sum P_Z}$$

F: the first moment frequency

P_Z: power of the Z^{th} bin on frequency domain

F_Z: the frequency of the Z^{th} bin

The fast Fourier transform depends on stationary signals and is less informative when dealing with the dynamic signals, particularly for the abrupt changes preceding the seizure onset. Thus for describing the temporal fluctuations on the HFA, Morlet wavelet transform analysis was conducted in this study by a homemade Matlab (The Mathworks) script. Wavelet analyses were calculated every 200 ms, overlapping 90 % with the previous window to smooth the signals, and the frequency domains indicated the power in every Hz. We also used wavelet transform by 50 ms windows without overlapping to show the spectrograms between several interictal discharges. Epileptic features brought extreme changes on the power of the signals – very large during the seizures and very low for the periods with HFA only – thus the power of the signals was logarithm transformed and further normalised in the following results if necessary.

Event detections and defining the characteristics of oscillations

Detections of every event including the HFA, interictal discharges or seizure onsets were crucial before further analyses. Different criteria and settings we used to detect events are described as the following.

Data were band pass filtered to present clear slow components of interictal discharges or the oscillations above 100 Hz as mentioned before. The timing of each interictal discharge was defined by large positive peaks in 10-100 Hz filtered signals with a minimal interval of 400 ms following the previous event (Figure M-03A). To detect other activities, standard deviation of a 200 ms background recording period was defined beforehand: in intact slices, the refractory period after interictal discharges is an idea background; in lesioned slices, background was assigned to a 200 ms HFA-free recording. Then thresholds were defined when they were greater than seven times the standard deviation of the background recording, and the time points of the activities were detected by their negative troughs crossing the threshold in individual filtered signals (100-250 Hz, 250-500 Hz and 500-1000 Hz). Minimal intervals were also applied corresponding to the fastest frequency boundaries, for instance 4 ms for the band between 100 to 250 Hz (Figure M-03B).

Timings of single-neuron activities were automatically generated after spike sorting procedures which are explained in the following section. Time points of seizure onset were manually set. With the timing information mentioned before, cross-correlation or auto-correlation analyses were performed by Spike2 or Matlab with customized scripts. By referencing to the detected events, averaged waveforms of the HFA were derived from wide-band traces and 100-250 Hz band pass filtered signals. The boundaries of the frequency bands required some flexibility as described in the following paragraph. Averaged waveforms of the interictal discharges were constructed from 10-100 Hz band-passed recordings, referencing to the detected peaks of the interictal discharges. Inter-pulse-interval histograms were also produced by these detected events.

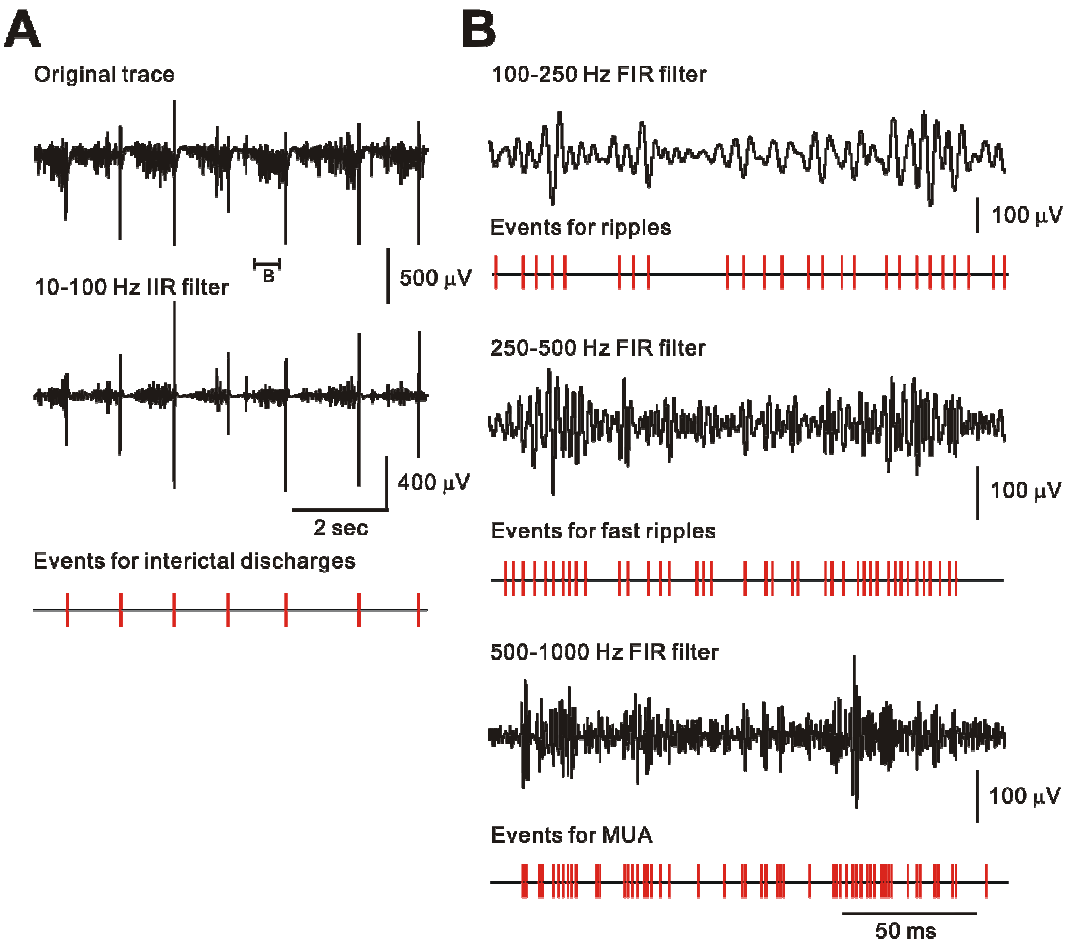

Figure M-03. Filtered recordings and detected events. **A**, the original trace and the 10-100 Hz filtered trace are shown; the events for interictal discharges are detected by peaks in 10-100 Hz band-passed signal shown as red ticks. **B**, a section of recording selected from A was band pass filtered by 100-250 Hz, 250-500 Hz and 500-1000 Hz respectively; and the events for ripples, fast ripple or MUA are marked on the troughs by thresholding 7 times of background recording in each trace.

Choice of frequency bands with more flexible ranges

Conventional frequency ranges for physiological ripples were not reliably applicable in our high K^+ HFA in hippocampal slices. We found that the high K^+ induced HFA had faster dominant frequencies in some cases; for instance, in CA3 the dominant frequency of the HFA was close to 250 Hz; thus use of a strict 100-250 Hz band pass filter on every experiment might lead to some information loss from the original HFA (Figure M-04B, *left panels*). Therefore we applied adaptive band pass filters from 100 Hz to 250 Hz, 300 Hz or even to 350 Hz to cover the majority of the activities depending on their power spectra in different regions of each slice. However we should be always aware that even from same recordings choices of band pass filters lead to distinct averaged waveforms or histograms of inter-pulse-interval of the HFA (Figure M-04).

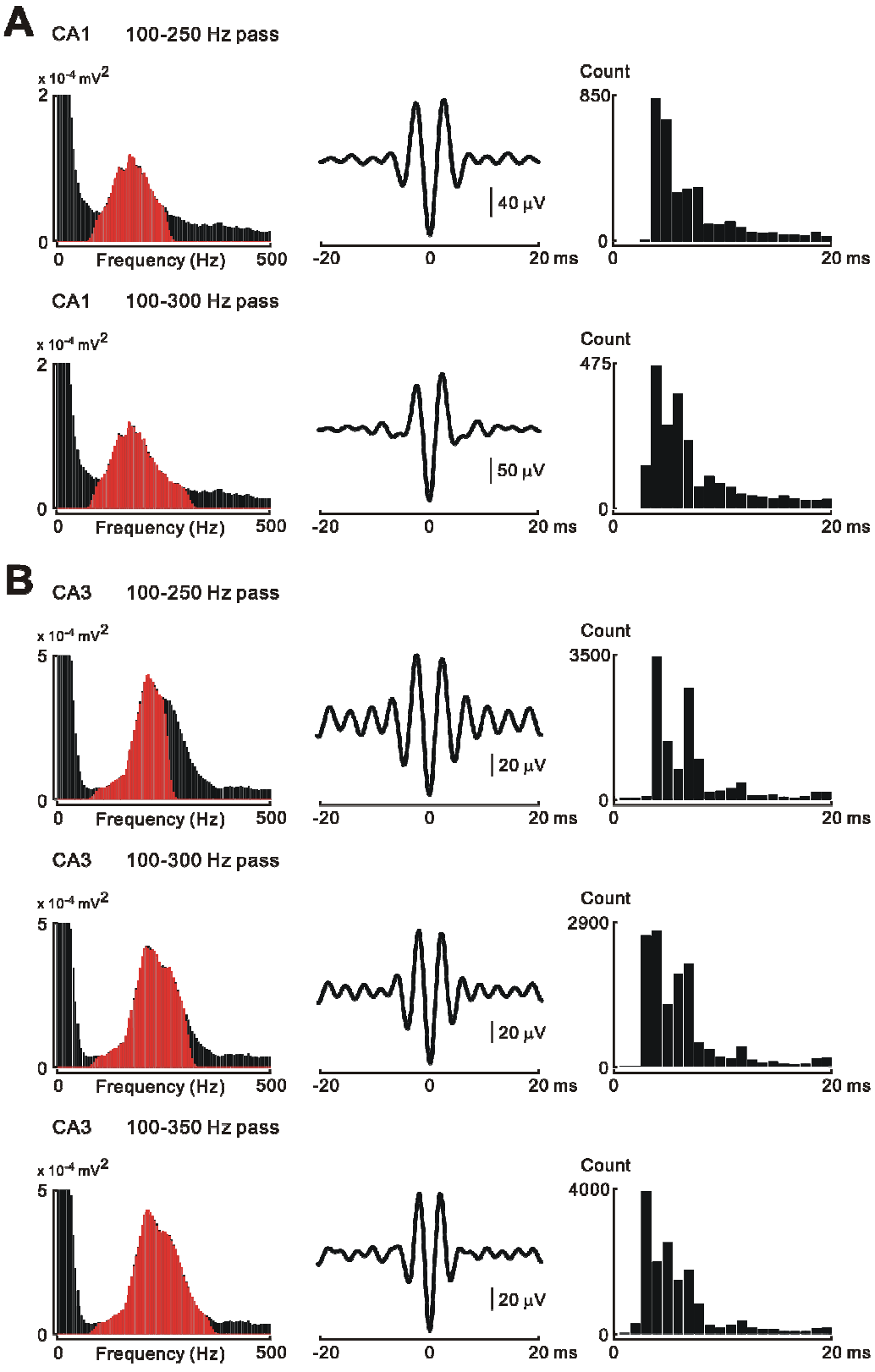
A
CA1 100-250 Hz pass
x 10-4 mV2
2
0
0 Frequency (Hz) 500
40 µV
-20 0 20 ms
Count
850
0
0 20 ms
CA1 100-300 Hz pass
x 10-4 mV2
2
0
0 Frequency (Hz) 500
50 µV
-20 0 20 ms
Count
475
0
0 20 ms
B
CA3 100-250 Hz pass
x 10-4 mV2
5
0
0 Frequency (Hz) 500
20 µV
-20 0 20 ms
Count
3500
0
0 20 ms
CA3 100-300 Hz pass
x 10-4 mV2
5
0
0 Frequency (Hz) 500
20 µV
-20 0 20 ms
Count
2900
0
0 20 ms
CA3 100-350 Hz pass
x 10-4 mV2
5
0
0 Frequency (Hz) 500
20 µV
-20 0 20 ms
Count
4000
0
0 20 ms

Figure M-04. Band pass filters on CA1 and CA3 activities. **A**, different widths of band pass filters affect the characteristics of the HFA identified from the same CA1 recording. *Left panels*, black power spectra were from the unfiltered recordings and the red spectra were acquired from band pass filtered data (100-250 Hz and 100-300 Hz); the amounts of signals included or excluded after filtering can be predicted by the overlaps on the spectra; *middle panels*, averaged waveforms of the HFA; *right panels*, inter-pulse-interval histograms of the HFA events. **B**, different widths of band pass filters affect the characteristics of the HFA identified from the same CA3 recording. The band pass filters were 100-250 Hz, 100-300 Hz and 100-350 Hz.

Current source density

Current source density (CSD) analysis was developed by Nicholson and Freeman in 1975, by which the subcellular events (i.e. membrane currents) can be predicted even from extracellular recordings (Nicholson and Freeman, 1975). CSD generates an estimation of the instantaneous current flows between recording sites: when a positive CSD was observed, the region close to the electrode was in the state of hyperpolarization and was defined as a current source; when the CSD showed as negative, the tissue near the electrode was depolarized and was defined as a current sink. We were interested in where are the origins of these epileptic features and the HFA, thus we recorded the field potentials along the somatodendritic axis in either CA1 or CA3.

The one-dimensional homogenous CSD equation is (Kloosterman et al., 2001):

$$CSD = \frac{\sigma\left[2\phi_{(Z)} - \phi_{(Z+1)} - \phi_{(Z-1)}\right]}{(\Delta Z)^2}$$

CSD: one-dimensional current source density

σ: the constant conductivity

$\phi_{(Z)}$: the potential recorded on the Z^{th} position of the electrode

ΔZ: the distance between the neighboring two electrodes

However the CSD equation should be modified when it encounters inhomogeneous tissue according to Lopez-Aguado *et al.* study (Lopez-Aguado et al., 2000;Lopez-Aguado et al., 2001):

$$CSD = \frac{\sigma_{(Z)}\left[\phi_{(Z)} - \phi_{(Z-1)}\right] - \sigma_{(Z+1)}\left[\phi_{(Z+1)} - \phi_{(Z)}\right]}{(\Delta Z)^2}$$

$\sigma_{(Z)}$: the conductivity at the Z^{th} position of the electrode

Single unit activity analyses

"Spikes" are the extracellular signs of action potentials. In this study the spikes were recorded by tetrodes and single neurons were distinguished by the following spike sorting procedures. A principle underlying tetrode recording and spike sorting is that the waveform and the amplitude of the spikes are influenced by several factors, notably the distances between the neuron and the recording electrode (Henze et al., 2000). Although only tens of micrometers separate the electrodes in one tetrode, these small differences are sufficient in the micro-environment to cause diverse transformations of the waveforms of the spikes and to produce significant decays of the waveforms between channels. In addition, the latency of the individual spikes together with their waveforms also depend on which compartments of the neuron are recorded (Henze et al., 2000). Thus a suite of four particular spikes represents the action potentials from a neuron, and other neurons will generate distinguishable sets of four waveforms (Figure M-05A). The spikes were confidently distinguished by the sorting procedures as the description below:

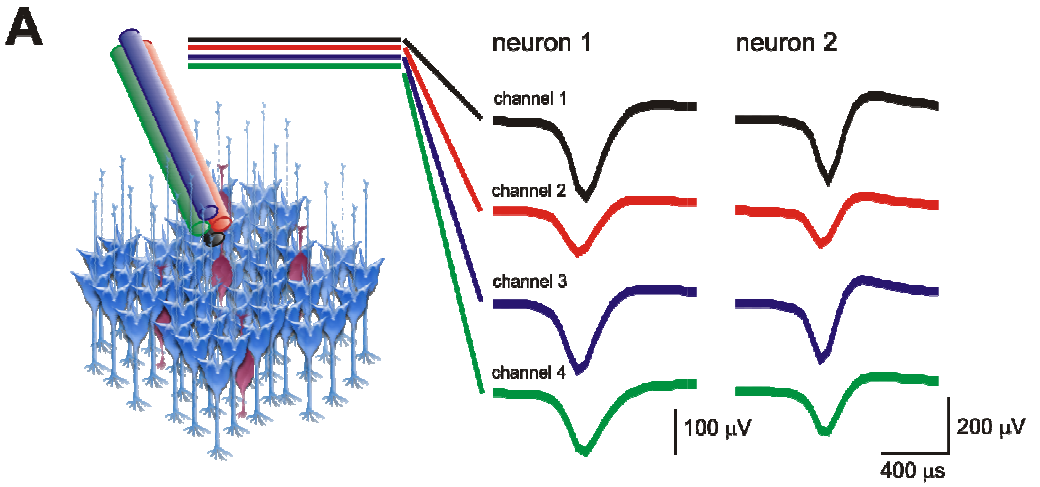
A
neuron 1
neuron 2
channel 1
channel 2
channel 3
channel 4
100 µV
200 µV
400 µs

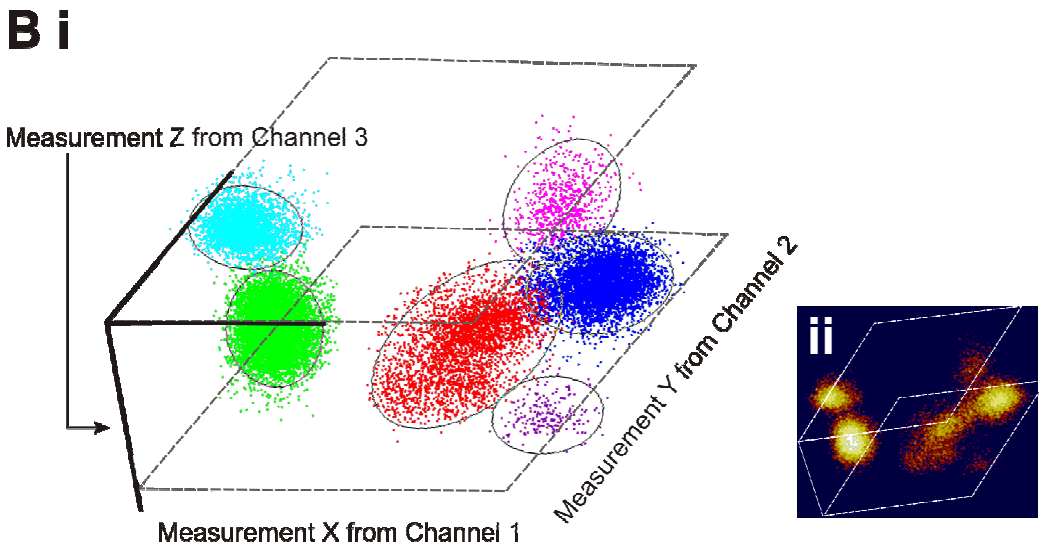
B i
Measurement Z from Channel 3
Measurement Y from Channel 2
Measurement X from Channel 1
ii

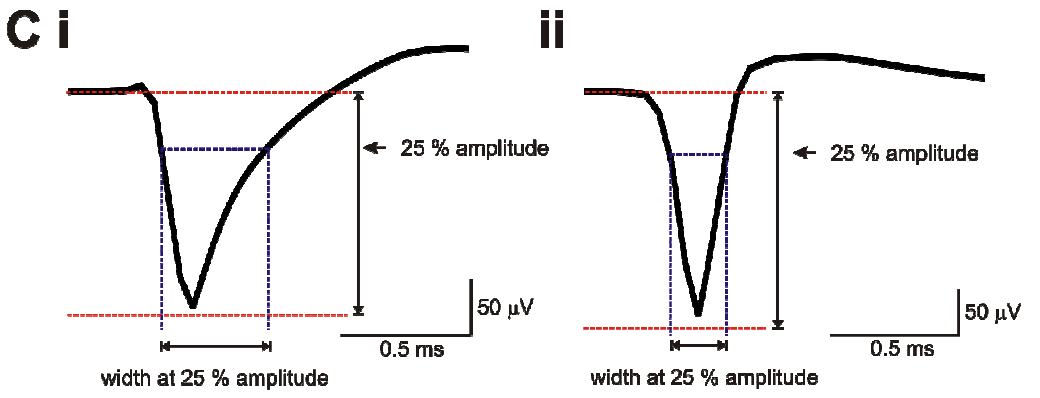
C i
25 % amplitude
50 µV
0.5 ms
width at 25 % amplitude
ii
25 % amplitude
50 µV
0.5 ms
width at 25 % amplitude

Figure M-05. Tetrode recording and spike sorting. **A**, tetrode recording; a schematic shows a tetrode approaching a group of neurons (blue, pyramidal neurons; purple, interneurons). Action potentials from neuron 1 present a suite of four waveforms recorded by the channels of the tetrodes, which are coded with four different colours; and neuron 2 has a distinct suite of four waveforms which is different to that from neuron 1. **B**, Spike clustering; *i*, a 3D raster plot can be produced by using three selected measurements of the spike waveforms and the spikes can be further categorised into different groups shown with colours. Ellipses for the Mahalanobis distances are surrounding each group (dash ellipses); *ii*, a clustering plot was transformed to the density plot to show the spreads of the events, and the overlaps are easily observed. **C**, measurements of the width at 25 % amplitude of the trough in a presumed pyramidal neuron (*i*) and an interneuron (*ii*).

Spike detection: Original traces were 700-5000 Hz band pass FIR filtered to present the unit spikes (i.e. action potentials). A positive and a negative threshold over seven times the standard deviation of background activity were set for spike detection. When the recording contained epileptic events like interictal discharges or seizures, two more boundaries were introduced to exclude those false spikes caused by filter artifacts due to these giant epileptic events. Once a peak or a trough from a spike crossed the trigger levels, a set of four “provisional spike templates (starting 0.5 ms before the peak or the trough, 1.5 ms wide)” were kept. Spike2 automatically compares and categorises the similar provisional templates into real templates, and discards infrequent templates. Generating templates was the very preliminary step to distinguish the spikes. To increase the spike “harvest” (in other words to reduce false negatives), we collected spikes with only 60 % accuracy of the templates (as the default setting in Spike2) and tolerated small variances. However these judgments incurred false positives and artifacts, thus we needed following steps to refine the categories.

Clustering: Clustering means to classify several objects into different groups by their intrinsic properties. A spike template comprises 32 data points to describe the

waveforms of the spikes in each channel. Every digit point can be used as an index for clustering, however discriminations between the spikes according to only the value of each points would be time consuming and less informative. Thus in this study we mainly used the measurements of the spike waveforms and principal component analysis to cluster spikes by Spike2 built-in functions. 1) Clustering by measurements of the spikes, such as their peak (or trough) amplitudes, timings of the events, areas or slopes of the spikes…etc.; any three measurements of the spikes from the four channels of the tetrodes can be selected to construct a three dimensional scatter plot (Figure M-05B*i*). Each dot in the plot is a spike, which also represents an action potential, and is known as an event. Changing the combination of measurements led to a new spatial distribution of these spikes in the plot, and new clusters might be found with different combinations of measurements. 2) Clustering by principal components: principal component analysis simplified all the variances of the spikes to several “principal components” in order, which represent the major features of the spike waveforms. The clustering then was plotted based on the first three principal components.

In both approaches, the spikes were automatically categorised into n groups and coded with different colours in Spike2, where n was equal to the number of the real

templates. In general a neuron produces action potentials with same amplitudes and similar time constants (waveform); only when the pyramidal neurons fire in a bursting pattern the amplitudes and waveforms of the action potentials change within the burst. Thus the spikes from the same neurons, which reflect the action potentials, will be similar even though the extracellular environment was dynamic. With these intrinsic similarities, these spikes were closely located in the 3D clustering (scatter) plots. However the false negative or false positive categorisations needed to be re-classified, and these steps were done manually (Harris et al., 2000). Several functions offered by the Spike2 programme were used to improve our judgments. 1) The boundaries used to keep or to discard events in clustering were always ambiguous and subjective. Mahalanobis distance is a statistic measurement similar to standard deviation but it can be applied in multiple dimensions (see Main Manual for Spike2 for Windows, version 6, 16-19, 2006). Thus built-in Mahalanobis distances of the clusters were applied to exclude events with greater variances. Mahalanobis ellipses were set on 2.5 times the standard deviations of the groups to reject spikes (Figure M-05B*i*). 2) Colour-coded clustering plot can be switched to monochromatic density plot. Sub-groups might be automatically merged or fused into greater ones by the programme if they appeared

to represent the same neuron. With the density contract different neurons could easily be re-grouped and separated (Figure M-05B*ii*). 3) Inter-spike intervals were always monitored (Csicsvari et al., 1999b). A neuron rarely produces two action potentials in 1 ms because of the refractory periods caused by sodium channel inactivation. Thus any 2 spikes with an interval shorter than 1 ms in a sorted group implied that at least one of these events were from other neurons. In this study, spikes with inter-spike intervals below 2 ms were discarded. In practice this stricter rule can eliminate the contaminating spikes from different sources (Harris et al., 2000).

Classification of the units: The sources of the sorted spikes were further defined as from pyramidal neurons or from interneurons by three criteria: 1) the averaged spike width at 25% maximal amplitude of the trough. Spikes in wide-band data were averaged and the duration at 25% maximal amplitude of the trough was measured by customised Matlab scripts semi-automatically (Figure M-05C*i* and C*ii*). According to Csicsvari *et al*. spikes with width at 25% amplitude greater than 0.33 ms are likely from a pyramidal neuron, but the spikes with width at 25% amplitude less than 0.22 ms are more likely from an interneuron (Csicsvari et al., 1998;Csicsvari et al.,

1999b). 2) The auto-correlations of these spikes. Pyramidal neurons in hippocampus are prone to fire in a bursting pattern, thus the auto-correlation of a pyramidal neuron generally shows two robust peaks near time 0; and a very fast exponential decay reflects their lower firing rate. In auto-correlations from several pyramidal neurons, we found more pairs of peaks with fixed intervals were observed. Interneurons fire in faster rates but less with burst firing, thus the auto-correlation from an interneuron is flatter than that from pyramidal neurons. 3) The firing rates of the neurons. Pyramidal neurons fire at a low frequency which was demonstrated below 1.5 Hz, but the interneurons fire at high frequencies which were much higher than 1.5 Hz *in vivo* (Csicsvari et al., 1998;Csicsvari et al., 1999b). However this is an *in vitro* study, and furthermore the neuronal activities were enhanced by increased extracellular potassium, so that even the pyramidal neurons fire more frequently than those under physiological conditions (*in vivo*), thus the firing rate was taken as supplementary information to the other criteria. These three criteria were used together to increase our confidence.

Time points of the single unit activities, here the starting points of each set of saved spikes, were automatically given by Spike2 programme. These time points were 0.5

ms preceding the real troughs (or peaks) of the spikes. This discrepancy was corrected before we conducted the cross-correlations between the HFA and the spikes.

Difficulties in spike sorting

Wire electrodes can record signals as far as 140 μm, but in practice only spikes from few neurons within 50 μm of the electrodes are captured with distinguishable spike amplitudes (Buzsaki, 2004;Henze et al., 2000). As shown in Figure M-06A, spikes protrude from the HFA (arrows). Most spikes quickly decayed with increasing distance from the neurons to the electrodes, and they join to the "background" (Buzsaki, 2004). Our study suggested the HFA is the summation of the spikes from many pyramidal neurons and interneurons, thus the spikes may be involved in the HFA with different latencies (Figure M-06B), and the latencies between HFAs and spikes naturally produced the smooth phase correlations. However in experiments where HFA was not well-developed but some spikes were apparent, false HFA was generated when we applied filters; and in these cases the latencies between the spikes and the event of the false detected HFA were always fixed (Figure M-06C).

Even we had excluded a great many of the sorted spikes in our analyses on the criteria outlined above, we still struggled to remove the fixed artifact present in the phase histogram, which is present as a robust bar at ~1/4 π protruded from a smooth distribution (Figure R-16A*iii*, comparing to Figure R-06A*iii* or R-06B*iii*, *top*)

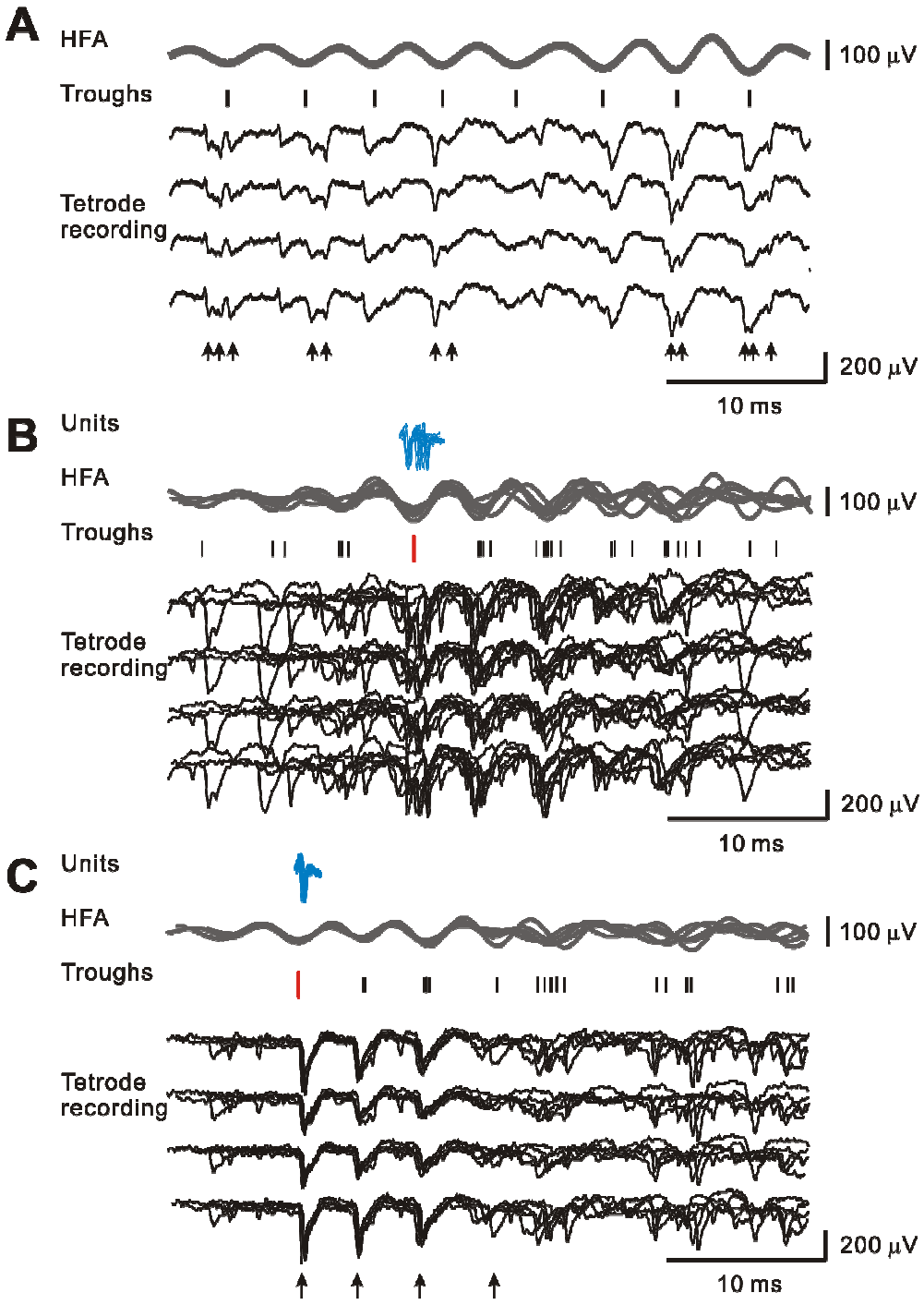
A
HFA
100 μV
Troughs
Tetrode recording
200 μV
10 ms
B
Units
HFA
100 μV
Troughs
Tetrode recording
200 μV
10 ms
C
Units
HFA
100 μV
Troughs
Tetrode recording
200 μV
10 ms

Figure M-06. False detections of the HFA due to filter artifacts from unit spikes. **A**, the HFA comprises spikes. A period of tetrode recordings and the 100-250 Hz filtered HFA from these recordings. The troughs of the HFA are marked as ticks. Several spikes are present in individual cycles of the HFA (arrows). **B**, unit spikes and the HFA. Seven periods of tetrode recordings were overlapped aligning with the troughs of the HFA (red tick). Discrepancies of the tetrode recordings and the "jittering distribution" of the spike timing around the HFA (blue spike traces) are clear. **C**, unit spikes and the falsely detected HFA. Five periods of tetrode recordings were overlapped aligning with the trough of the HFA (red tick). The aligned spike as recorded in each of the 4 channels shows a complete lack of jitter against the trough of the HFA. It is followed by three (or four) repeated spikes with reducing amplitudes and increasing inter-spike intervals characteristics of pyramidal burst firing (Henze et al., 2000). Besides, these repeated spikes from these periods are fixed on the same latency after the trough of the HFA (blue spike traces).

Statistics

Data were presented as the means ± standard errors. All statistics tests were conducted by SPSS 15.0 (SPSS Inc.). The differences between groups were examined by Student's t test or one-way ANOVA. Significance was verified by 95 % confident level, and confidence over 99 % was also marked.

Cross-correlation between the individual unit spikes and the HFA were tested by Kolmogorov-Smirnov test against uniform distribution. Spikes without difference from uniform distribution were excluded for further analyses. Z value is derived from the test, which is a scale showing the difference between the experimental cross-correlation to the theoretical uniform distribution.

Analyses of regressions in linear, quadratic and exponential trends were applied on the study of the temporal build-up of the HFA. K-means clusters or two steps clusters were applied to classify observations.

Experimental processes in schematics

To clarify the different experimental designs, the experimental processes in this study are presented in schematics.

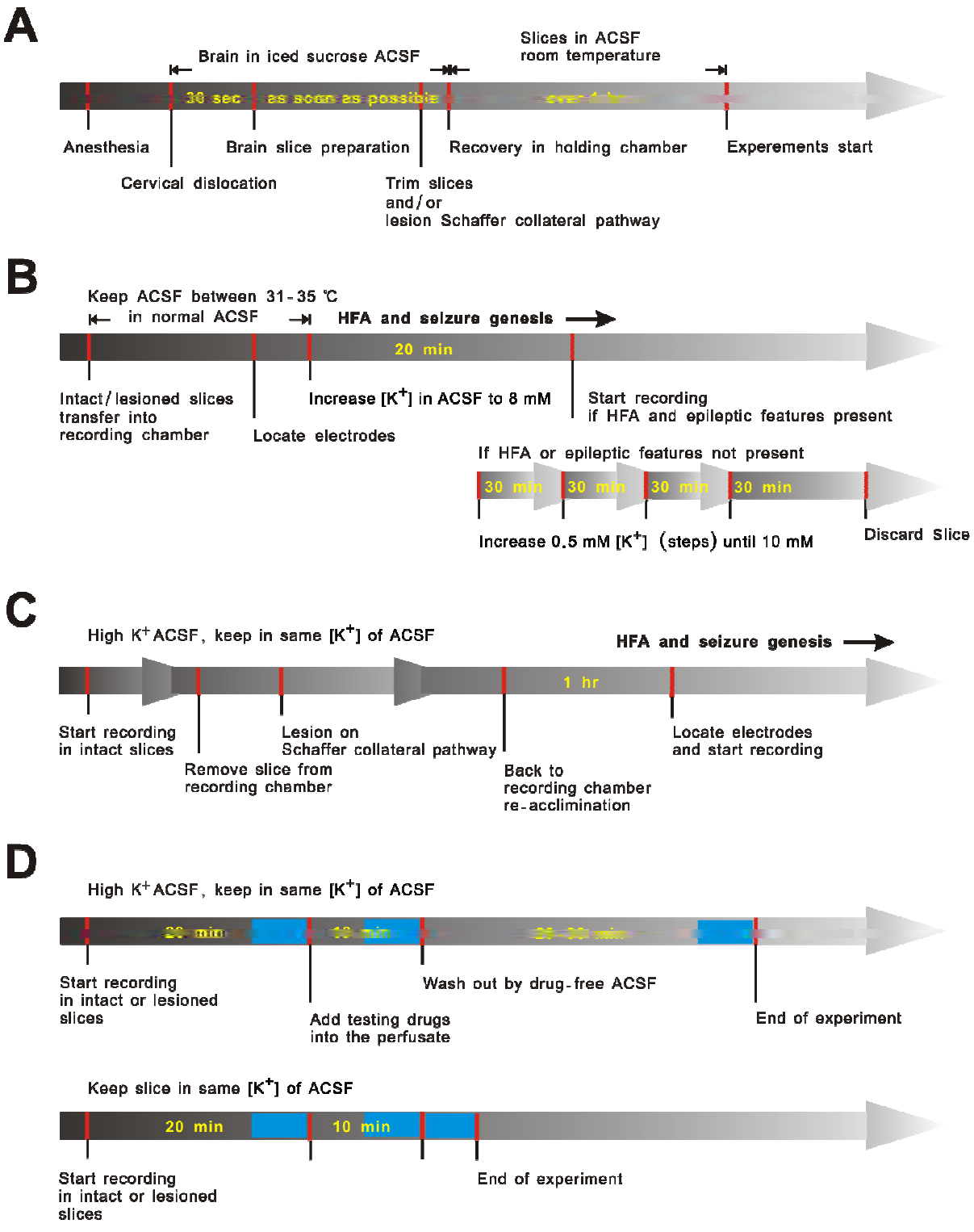
A
Brain in iced sucrose ACSF
Slices in ACSF
room temperature
30 sec
as soon as possible
Anesthesia
Brain slice preparation
Recovery in holding chamber
Experements start
Cervical dislocation
Trim slices
and/or
lesion Schaffer collateral pathway
B
Keep ACSF between 31-35 ℃
in normal ACSF
HFA and seizure genesis
20 min
Intact/lesioned slices
transfer into
recording chamber
Increase [K+] in ACSF to 8 mM
Start recording
if HFA and epileptic features present
Locate electrodes
If HFA or epileptic features not present
30 min
30 min
30 min
30 min
Increase 0.5 mM [K+] (steps) until 10 mM
Discard Slice
C
High K+ACSF, keep in same [K+] of ACSF
HFA and seizure genesis
1 hr
Start recording
in intact slices
Lesion on
Schaffer collateral pathway
Locate electrodes
and start recording
Remove slice from
recording chamber
Back to
recording chamber
re-acclimination
D
High K+ACSF, keep in same [K+] of ACSF
Start recording
in intact or lesioned
slices
Wash out by drug-free ACSF
Add testing drugs
into the perfusate
End of experiment
Keep slice in same [K+] of ACSF
20 min
10 min
Start recording
in intact or lesioned
slices
End of experiment

Figure M-07. Experimental processes in schematics. **A**, processes for slice preparation. **B**, processes to induce HFA and epileptic features; the second route was chosen when HFA or epileptic features were not present. [K^+] was increased every 30 min if HFA or epileptic features did not present. Slices were discarded when no HFA or epileptic features were present and [K^+] at 10 mM. **C**, these processes were only applied in comparisons of seizure genesis before and after lesion on the Schaffer collateral pathway (see Figure R-12). **D**, first route was applied to test antagonists of receptors; the second route was applied to test whether background HFA was enhanced with time (see Figure R-20**D** and **E**). Blue squares show in which data was analyzed and comparisons were made.

Results

Electrographic epileptic features in high K^+ hippocampal slice model

Hippocampal slices were allowed to recover in an incubating chamber supported by normal ACSF for at least an hour before use, and then the slices were transferred to the interface recording chamber where perfusate was flowing (now normal ACSF). Two Pt/Ir electrodes were placed in the stratum pyramidale of hippocampal CA1b and CA3b individually (Figure R-01A, *left panel*). The concentration of potassium in ACSF was then increased from 3 mM to 8-10 mM (high K^+ ACSF) to enhance neuronal activities. In general, the possibility of neurons firing in groups grew with increasing extracellular potassium concentration, and much higher potassium concentration accelerated the aggregates developed. However we normally kept the $[K^+]$ below 10 mM because spreading depression was easily induced when $[K^+]$ exceeded 10 mM in our preliminary experiments. Emergence of several electrographic epileptic features including seizures and seizure-free segments which are known as interictal periods required 8 mM potassium and over 20 minutes to “develop” (Figure R-01A, *right panel* and B). If no epileptic feature was found, the potassium concentration was increased

by 0.5 mM every 30 min and ceiling at 10 mM; empirically 9 mM [K^+] brought us stable recordings as shown in this thesis.

During the interictal periods, singular “deflections” were observed at ~1 Hz both in CA1 and CA3 regions and they were synchronised between these two regions; their correlation will be detailed in the following section; these singular deflections were called interictal discharges (Figure R-01C*i*). In this high K^+ model seizures were present only in the CA1 (Figure R-01B, C*ii* and C*iii*), and most of the seizures started from the CA1b region (38 of 84 seizures in total, i.e. 45%, 8 of 15 slices, Table R-01). The proportions of onsets in adjacent subregions within individual slices are shown as an interpolation between those sites to indicate the centre of the distribution of onsets for seizures and interictal discharges (Figure R-02; the proportion regarding interictal discharges will be detailed in the following part).

Seizures can be further defined as a tonic phase and a subsequent clonic phase. Intense population spikes were present during the tonic phase of seizures (Figure R-01C*ii*). The big, discrete but rhythmic spikes with afterdischarges during the clonic phase resembled CA3 interictal discharges, and they also synchronised to CA3 interictal discharges (Figure R-01C*iii*).

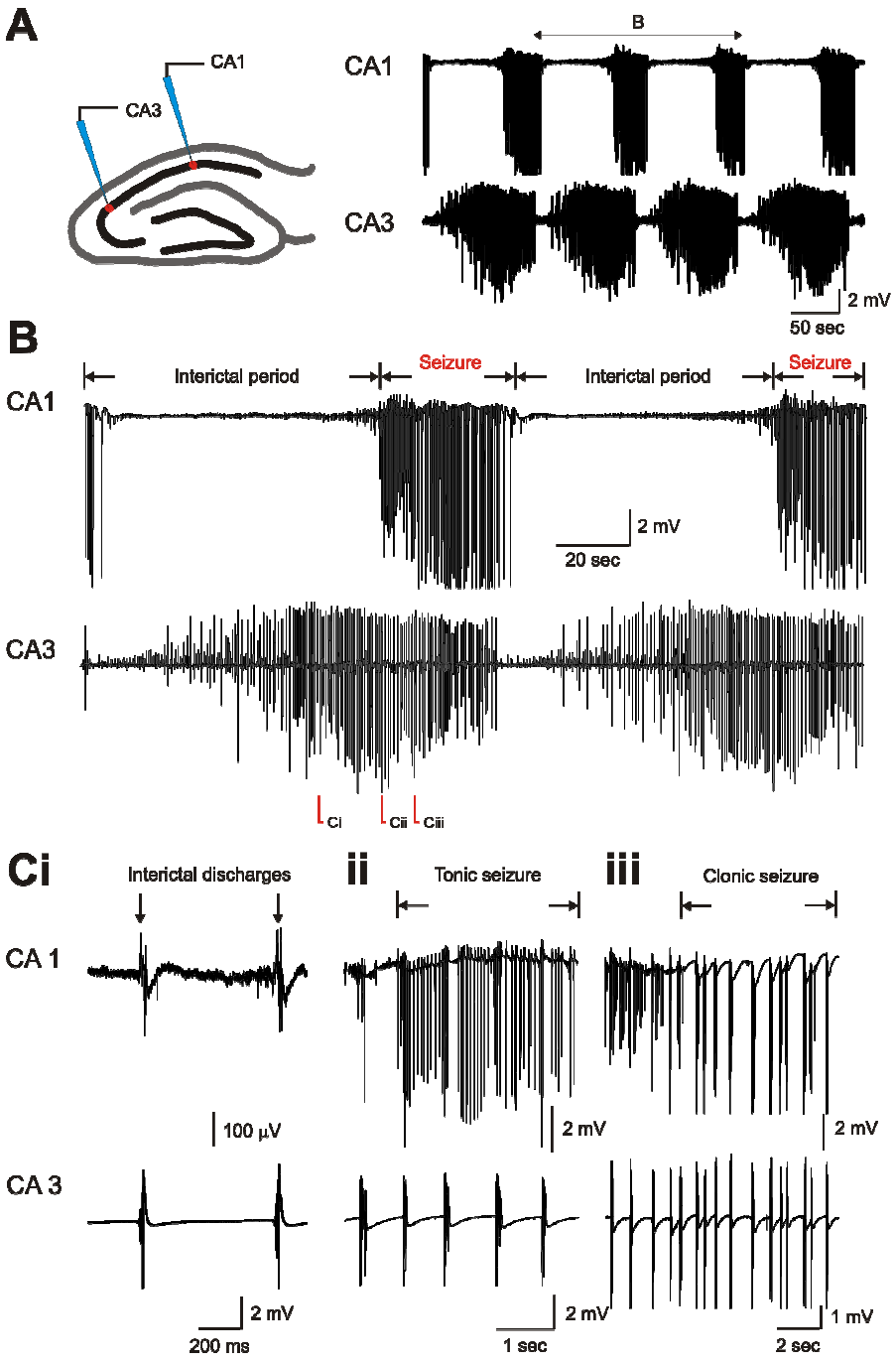
A
CA1
CA3
B
CA1
CA3
2 mV
50 sec
B
Interictal period
Seizure
Interictal period
Seizure
CA1
2 mV
20 sec
CA3
Ci
Cii
Ciii
Ci
Interictal discharges
ii
Tonic seizure
iii
Clonic seizure
CA 1
100 µV
2 mV
2 mV
CA 3
2 mV
200 ms
2 mV
1 sec
1 mV
2 sec

Figure R-01. High K^+ induced electrographic epileptic features in hippocampal slices. **A**, *left panel*, a schematic indicates two Pt/Ir electrodes are located in stratum pyramidale in both hippocampal CA1 and CA3 regions; *right panel*, original wide-band electrophysiological recordings from CA1 and CA3 respectively. **B**, two segments of recordings for CA1 and CA3 are expanded from A. CA1 recording comprises seizures (ictal periods) and the seizure-free periods (interictal periods); and CA3 recording presents brief discharges with variable amplitudes, but no seizure pattern is present. **C**, epileptic features were expanded (as indicated in B); *i*, two interictal discharges are shown in both CA1 and CA3 regions; *ii*, a tonic seizure is present in CA1,and CA3 shows interictal discharges; *iii*, a clonic seizure follows the tonic seizure in CA1 and CA3 presents interictal discharges only.

	Interictal discharges					Seizures				
Region	CA3a	CA3b	CA3c	CA4	Total	CA1a	CA1b	CA1c	CA2	Total
Slices No.										
01		4	36		40	2				2
02			80		80	4				4
03		63	17		80	4				4
04	16	64			80	1	3			4
05	12	87	1		100		3	2		5
06		65	115		180		7	2		9
07		32	26	2	60		3			3
08		67	13		80		3	1		4
09	53	43	3	1	100	4		1		5
10	26	106	8		140		7			7
11	3	37			40		2			2
12		175	5		180			9		9
13		63	136		199		10	1		11
14	1	39	120	33	193	9				9
15		43	77		120	6				6
Total	111	888	637	36	1672	30	38	16		84
%	**7**	**53**	**38**	**2**		**36**	**45**	**19**		

Table R-01. Summary of where the interictal discharges and seizures initiated in hippocampal slices exposed to high K^+. More than half of the interictal discharges started from CA3b (888 of 1672 interictal discharges, 53%) and the majority of the seizures rose from CA1b (38 of 84 seizures, 45%).

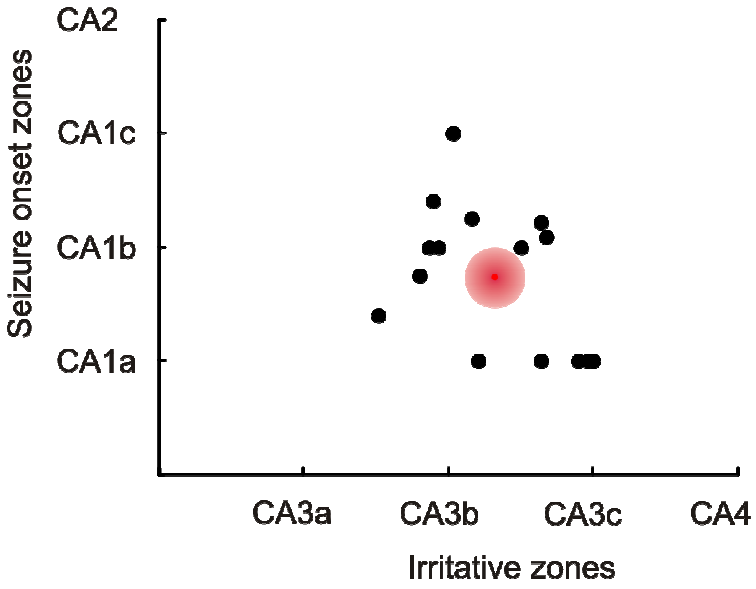

Figure R-02. Correlation between the irritative zones and the seizure onset zones in the high K^+ epileptic *in vitro* model. This figure was derived from the Table R-01. The locations where interictal discharges or seizures initiated were quantitated. Irritative zone is the place interictal discharges initiated the most; and seizure onset zone is the place seizure initiated the most. Thus each black dot comprises the arithmetic irritative zone and seizure onset zone for each of experiments (15 slices). No linear regression was found in these observations. Red circle indicates the average of these experiments (as the centre of the cluster) and imply the irritative zone and seizure onset zone in this mode.

HFA induced in high K^+ hippocampal slice model

A key question was whether HFA similar to that seen in the low Ca^{2+} model is also present in this high K^+ hippocampal slice model. During the interictal periods, a very fast activity was easily observed from the raw recording, either superimposed on interictal discharges or existing alone (Figure R-03A, black traces). After applying a digital 100-250 Hz band pass filter to the original recordings, which is the frequency band for the physiological sharp wave ripples, the fast activity found in the high K^+ model was still robust (Figure R-03A, red traces). Thereafter the fast activity found in this model was also termed a HFA as that found in the low Ca^{2+} model.

The HFA was present in both CA1 and CA3, however we found the peak frequencies of these HFAs, shown by the averages of normalised power spectra, differed between regions in the same slices, with means of 186 Hz in CA1 and 240 Hz in CA3 (21 slices for CA1 HFA average and 20 slices for CA3 HFA average, Figure R-03B*i* and C*i*). It is not possible to determine a standard error for these mean frequencies because they are the means of averaged spectra, and not an average of some measure of the centre of the peak in each of the individual spectra. However, by taking the dominant frequencies from 4 interictal periods for each of 13 slices, it is

possible to determine the mean and standard error for a measure of the peak of each of the spectra: the averaged dominant frequencies of the HFA in CA1 was 186.7±6.9 Hz, and that in CA3 was significant faster with 221.9±5.5 Hz in the same slices (p<0.01).

To extract the HFAs from original recordings, the flexible band pass filters for CA1 and CA3 were different. In general, 100-250 Hz band pass filter was applied in CA1 and 100-300 Hz was applied in CA3, but they were adjusted according to individual experiments, as we mentioned in Materials and Methods. The HFA was detected as events by thresholding at seven times the standard deviation of the voltage recorded during 200 ms epochs of the background activity. In the same slices, the inter-event-interval histograms show the mode at 4 ms for CA1 HFA (19 slices, Figure R-03B*ii*) and at 3 ms for CA3 HFA (18 slices, Figure R-03C*ii*). The general waveforms of the HFAs were acquired by averaging from wide-band raw recordings or from high frequency band pass filter data (100-250 Hz for CA1, 100-300 Hz for CA3), using the troughs of the detected HFA events as the reference points. In CA1, the averaged waveform of the filtered HFA gave durations of the first trough-to-trough cycle and the peak-to-peak cycle in 5.0 ms and 4.8 ms (19 slices, Figure R-03B*iii*, *top*); and those durations were 4.8 ms and 5.0 ms in the wide-band HFA (17 slices, Figure R-03B*iii*,

bottom). In CA3 of same slices, the band-passed HFA had the durations of 3.8 ms and 4.0 ms in the first trough-to-trough cycle and the peak-to-peak cycle (18 slices, Figure R-03C*iii*, *top*); the raw HFA had 4.6 ms and 4.4 ms in those two durations (16 slices, Figure R-03C*iii*, *bottom*). The durations of the HFA cycles and the inter-event-intervals of the detected HFA events closely corresponded to the peaks of power spectra found in CA1 and CA3. Thus these analyses indicated that two distinct HFA cycles were present in hippocampal CA1 and CA3 respectively.

The HFAs in both CA1 and CA3 superimposed on a positive slow component which can be observed in the wide-band averaged HFA (Figure R-03B*ii* and C*ii*, *insets*; B*iii* and C*iii*, *bottoms*). We suggested that the positive slow component might be due to hyperpolarisation contributed by the local interneurons, or a passive component generated when the basal dendrites were activated.

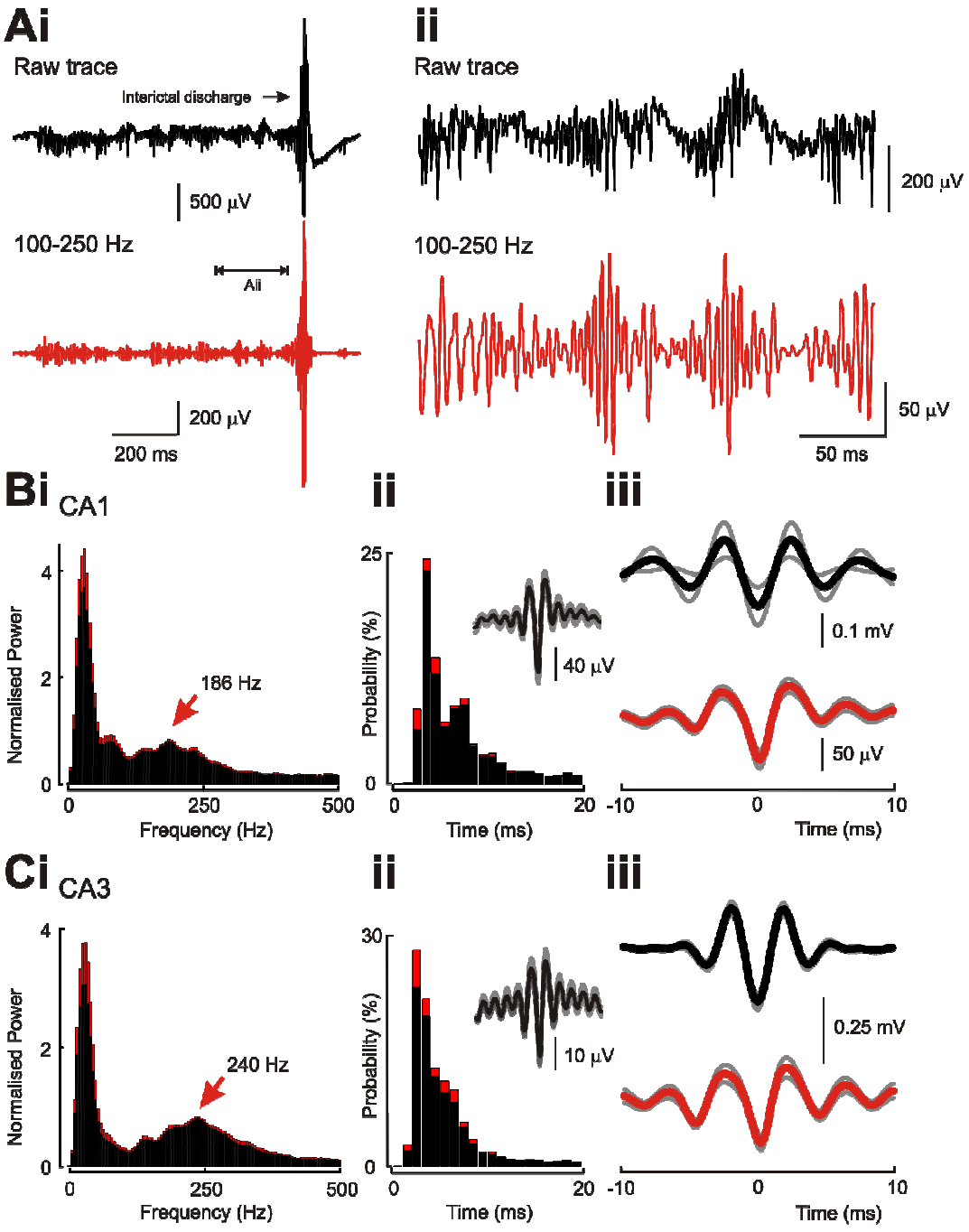
Ai
Raw trace
Interictal discharge
500 μV
100-250 Hz
Aii
200 μV
200 ms
ii
Raw trace
200 μV
100-250 Hz
50 μV
50 ms
Bi CA1
Normalised Power
186 Hz
Frequency (Hz)
ii
Probability (%)
40 μV
Time (ms)
iii
0.1 mV
50 μV
Time (ms)
Ci CA3
Normalised Power
240 Hz
Frequency (Hz)
ii
Probability (%)
10 μV
Time (ms)
iii
0.25 mV
Time (ms)

Figure R-03. HFAs in the high K^+ epileptic model. **A***i*, a selected interictal period including an interictal discharge is presented as unfiltered recording (black trace) and 100-250 Hz band pass filtered signals (red trace); the oscillation present in the filtered trace is HFA; *ii*, a section in *i* is further enlarged to see the details. **B**, properties of HFA in hippocampal CA1; *i*, a normalised power spectrum indicates the strongest HFA at 186 Hz (over 3 interictal periods in each of 21 slices; standard errors are presented in red); *ii*, inter-pulse-interval histogram of HFA between 100-250 Hz shows a peak value at 4 ms (slices=19 and all HFA included, standard errors are presented in red); *ii*, *inset*, an averaged 40 ms long recording from CA1 showing the HFA in full frequency band (slices=17); *iii*, *top*, an averaged HFA waveform filtered between 100-250 Hz shows that the trough to trough latency of the first cycle is 5.0 ms and the peak-to-peak duration is 4.8 ms (slices=19 and all HFA included; standard errors are presented as gray traces); *iii*, *bottom*, an averaged HFA waveform from wide frequency range with 4.8 ms trough to trough latency of the first cycle and 5.0 ms for the peak-to-peak cycle (slices=17, all HFA included; standard errors in gray). **C**, properties of HFA in same hippocampal CA3; *i*, a normalised power spectrum indicates the strongest HFA at 240 Hz (over 3 interictal periods in each of 20 slices; standard errors are presented in red); *ii*, inter-pulse-interval histogram of HFA between 100-300 Hz shows a peak value at 3

ms (slices=18 and all HFA included, standard errors are presented in red); *ii*, *inset*, an averaged 40 ms long recording from CA1 showing the HFA in full frequency band (slices=16); *iii*, *top*, an averaged HFA waveform filtered between 100-300 Hz shows that the trough to trough latency of the first cycle is 3.8 ms and the peak-to-peak duration is 4.0 ms (slices=18 and all HFA included; standard errors are presented as gray traces); *iii*, *bottom*, an averaged HFA waveform from wide frequency range with 4.6 ms trough to trough latency of the first cycle and 4.4 ms for the peak-to-peak cycle (slices=16, all HFA included; standard errors in gray).

Origin of the HFA - study of CSD

The key question of this section is whether the mechanisms of the HFA in the high K^+ model are due to the distal synaptic modulations from CA3 like the physiological sharp wave ripples (Buzsaki et al., 1992;Ylinen et al., 1995), or whether the HFA is caused by pyramidal neurons spontaneous firing in groups in a local area as the suggestions for the HFA in the KA-induced chronic epileptic animal model and clinical epileptic studies (Bragin et al., 1999b). To study the mechanisms of the HFA, first we used CSD analyses. The principle behind CSD is using a series of discrete extracellular field potentials to estimate the instantaneous, spatially continuous current changes across the cell membrane: when CSD is negative, it represents a current sink where the current flows into the neurons, thus the cell membrane depolarised; on the other hand, when CSD is positive, it represents a current source that current comes out from the cells, thus the cell membrane might be hyperpolarised. In theory a passive current sink or source can be incurred by the balancing membrane current respectively due to neighboring active sources or sinks due to membrane hyperpolarisations or depolarisations. To acquire the CSD ten Pt/Ir wire electrodes were placed along the somatodendritic axes in either hippocampal CA1 and CA3 with

equal spacing (~60 μm); where three electrodes were located in the stratum oriens, one electrode was placed in the stratum pyramidale and another six electrodes were in the stratum radiatum. The extracellular field potentials were recorded. Our preliminary observations indicated that, except during the interictal discharges no potential deflection in slow rhythm was found in dendritic layers accompanied with the HFA. Thus for CSD of the HFA only, field potentials from these ten electrodes were 100-250 Hz band pass filtered and the troughs on the stratum pyramidale recording were detected by thresholding at 7 times the standard deviation of the background recording. Filtered signals were then averaged according to these detected troughs in each experiment, and then CSD was calculated from the averaged field potentials in CA1 and CA3 respectively. Further, CSDs were averaged across different slices (9 slices for averaged CA1 HFA CSD; 7 slices for averaged CA3 HFA CSD). Averaged CSDs are presented in Figure R-04A*ii* and B*ii*.

CSDs were translated into pseudocolour maps, where cold colours represent current sinks and hot colours represent current sources (Figure R-04A*iii* and 4B*iii*). In both CA1 and CA3 the HFA was led by a sink in the stratum pyramidale, and the corresponding sources were observed in the stratum oriens and radiatum; phase reversals occurred at 120 μm or 60 μm from pyramidal layer in stratum radiatum or

stratum oriens respectively. The sink then propagated to the stratum radiatum and the stratum oriens. Thereafter a strong source quickly followed the sink in the stratum pyramidale. Since no dendritic inputs were observed during the HFA, the CSD indicated that in both CA1 and CA3 the HFA might start from a spontaneous depolarisation in the stratum pyramidale and the depolarisation later back-propagates into the layers containing the apical dendrites and basal dendrites, and this depolarisation was quickly followed by a current source of somata of these neurons. The CSD pattern along the somatodendritic axis led us to suggest that spontaneous, synchronous action potentials from pyramidal neurons make the major contribution to the HFA. However, it remains unclear whether the interneurons also participated in the generation of the HFA. Also, the mechanisms which led to the source that quickly following the pyramidal layer sink were still unclear; more evidence was needed to tell whether this current source represented hyperpolarisations of somata or it was a passive source corresponding to strong dendritic depolarisations. Furthermore, the similar CSD patterns found in CA1 and CA3 failed to explain the distinct slower and faster rhythms of HFAs respecitively found in these two regions.

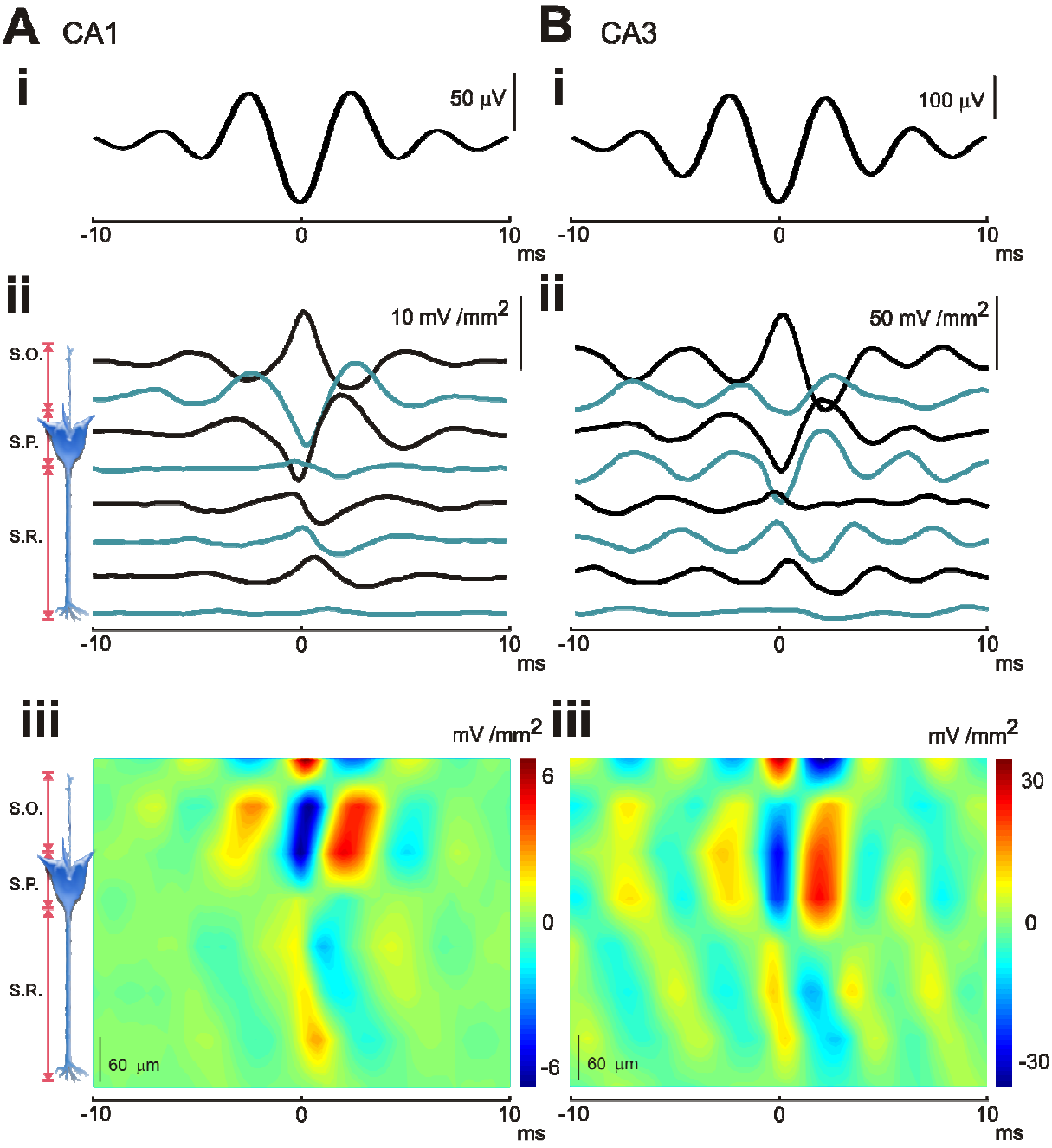
A CA1
B CA3
i
50 μV
100 μV
-10
0
10
ms
ii
10 mV /mm2
50 mV /mm2
S.O.
S.P.
S.R.
iii
mV /mm2
6
0
-6
30
-30
60 μm

Figure R-04. CSD of HFA in hippocampal CA1 and CA3. **A***i*, an averaged CA1 HFA waveform (100-250 Hz, 17 slices); *ii*, an averaged CSD of HFA was derived from ten Pt/Ir electrode recordings along the somatodendritic axis in CA1, and averaged by the timing of the most negative amplitude in stratum pyramidale (9 slices and all HFA included); the schematic of pyramidal neuron indicates the recording positions; adjacent traces are shown with two different colours for clarity; *iii*, the averaged CSD of CA1 HFA was interpreted into a colour map, in which cold colours represent negative CSD, or current sink, and hot colour, positive CSD, or current source. **B***i*, an averaged CA3 HFA waveform (100-300 Hz, 16 slices); *ii*, an averaged CSD of HFA were also derived from ten Pt/Ir electrode recordings along the somatodendritic axis in CA3, and averaged by the timing of the most negative amplitude in stratum pyramidale (6 slices and all HFA included); *iii*, the averaged CSD of CA1 HFA was interpreted into a colour map.

Neuronal activity and the HFA - studied by tetrodes

To further explore the cellular mechanisms of the HFA, neuronal activities were studied by tetrode recording and spike sorting. In these experiments, tetrodes were placed in hippocampal CA1 and field potentials were recorded. In 11 hippocampal slices, 76 pyramidal neurons and 36 interneurons were identified by spike sorting. Pyramidal neurons were identified by a wider waveform than that for interneurons (duration >0.33 ms at 25% amplitude, Figure R-05A*i*), and auto-correlations for pyramidal neurons show two peaks around ±4 ms (the peak at time 0 in all auto-correlation histograms in this study was removed) and very fast exponential decay (Figure R-05A*ii*). These peaks imply the burst firing patterns of hippocampal pyramidal neurons (Fox and Ranck, Jr., 1981;Ranck, Jr., 1973). Interneurons were characterised by their narrower spike waveform than in pyramidal neurons (duration <0.22 ms at 25% amplitude, Figure R-05B*i*), and their auto-correlations showed slower exponential decay (Figure R-05B*ii*) due to their fast firing rate and shorter refractory periods (Bean, 2007).

The study of the temporal relationship between the HFA and the neuronal activities in CA1 comprised steps of statistic judgments. First we needed to see whether

individual neuronal activity was correlated with the HFA. Kolmogorov-Smirnov tests on the latencies between the unit spikes for individual cells and the troughs of HFA were conducted to see whether the uniform distributions were not present. In other words, if the latencies from a neuron presented a uniform distribution, the neuronal activity was not correlated wih the HFA. In our experiments only one pyramidal neuron and one interneuron showed uniform distributions in their latencies between the HFA and unit spikes. Most pyramidal neurons and some interneurons showed systematic firing patterns during the HFA as the bands seen in the stacking scatter plots for all pyramidal neurons and interneurons (Figure R-05A*iv* and B*iv*). Z values were generated during the Kolmogorov-Smirnov tests, and these values showed the discrepancy between the observed distributions and the null hypothesis of uniform distributions. In other word, the Z value demonstrates the strength of the correlations.

Thereafter we constructed phase cross-correlations between the HFA and the unit spikes from individual cells, where the troughs of the HFA were denoted as 0 and the adjacent peaks of the HFA were denoted as ±π (±2.4 ms, Figure R-06). The phase histograms were then divided by the total number of the HFA in different recordings to give the firing probability of the neurons. Next we would like to know whether these neurons form a single group. Modes in individual phase histograms were

Kolmogorov-Smirnov tested against normal distribution. For the pyramidal neurons, the distribution of the modes was significantly different from a normal distribution and presented great numbers of cells on the trough of the HFA; thus we decided to keep the major cluster and discard several neurons (Figure R-06A*ii*). Four pyramidal neurons, including the one not modulated by the HFA, were excluded because of their larger deviations to the major cluster, which this discrimination was based on k-means cluster analysis (blue box in Figure R-06A). We found that the majority of the pyramidal neurons increased their firing probability by ~5 times at the trough of the HFA (72 cells, Figure R-06A*iii*). For the interneurons, their mode distribution was also significantly different to a normal distribution, and they were classified into two clusters also by k-means clusters (blue and red boxes, Figure R-06B*ii*). Group 1 interneurons increased their firing probability by ~5 times at the trough of the HFA (27 cells because one interneuron with insignificant modulation was excluded, Figure R-06B*iii*, *top*). Interestingly the firing probability of Group 2 interneurons increased on the rising (decaying side of the trough) phase of the HFA, and thus we suggested that this group of interneurons might be involved in the HFA modulation (8 cells, Figure R-06B*iii*, *bottom*).

According to the tetrode recording and the CSD analyses, we concluded that the HFA was mainly formed by action potentials from pyramidal neurons but some of the interneurons also took a part in the structure of the HFA. A subset of interneurons fired against the phase of the HFA in the experiments, thus we suggested these interneurons might be activated by the HFA-generating pyramidal neurons and they could feedback to modify the HFA pattern. This circuit might be one of the potential mechanisms to induce hyperpolarisation, as shown as the current source in pyramidal layer just followed the depolarization (current sink). However more detailed information, like intracellular recordings for individual cells, is required to verify the mechanisms.

The phase histograms shown in this section also brought us a notion about how often a neuron participated in the HFA. In general each pyramidal neuron and interneuron participated in the whole entirety of HFA with a very low frequency: for almost all the pyramidal neurons, the summation of the averaged probabilities was ~2.6 % during a cycle of the HFA; and the summated probabilities from interneurons were ~5.3 % and ~2.3 % respectively for the group 1 and 2. Higher firing probability of interneurons might suggest that 1) interneurons were more susceptible in the high K environment, and 2) the interneurons in CA1 can be more active in this model.

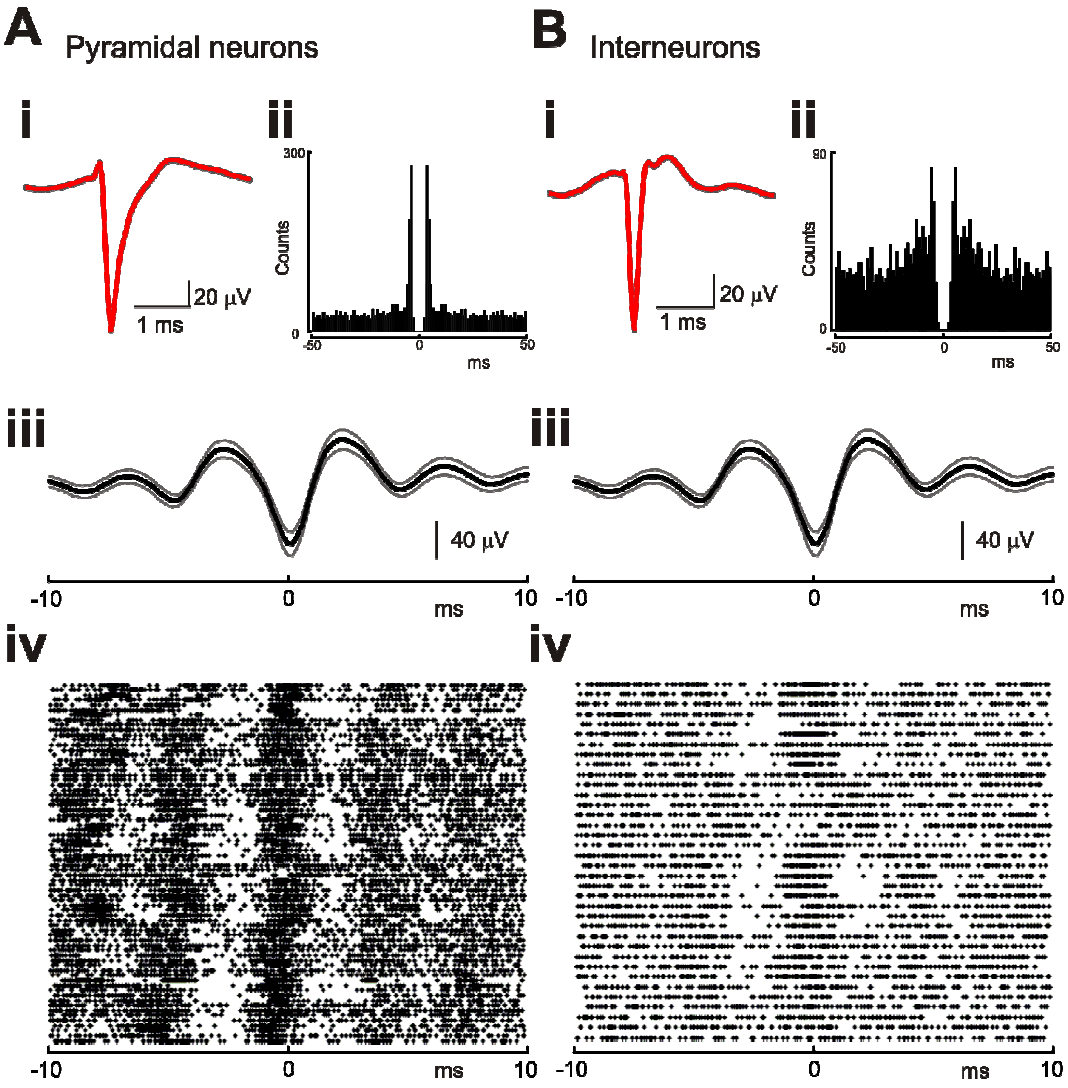
A
Pyramidal neurons
B
Interneurons
i
ii
iii
iv
20 μV
1 ms
Counts
300
0
-50
0
50
ms
40 μV
-10
0
10
ms

Figure R-05. Neuronal activities corresponded to the HFA in CA1. **A***i*, an averaged unit spike from a CA1 pyramidal neuron (wide-band), which shows a wider duration than interneurons; *ii*, an auto-correlation histogram indicates that this pyramidal neuron fired in bursts thus two robust peaks are present ~4 ms apart from zero; *iii*, an averaged wide-band waveform of the CA1 HFA where gray traces indicates the standard errors of the average; *iv*, a scatter plot demonstrates the activities from 76 pyramidal neurons temporally corresponded to the HFA, where every dot is an event around the HFA and each row represents events from one neuron. **B***i*, an averaged selected unit spike from a CA1 interneuron (wide-band), which shows a narrower duration than pyramidal neurons; *ii*, an auto-correlation histogram shows a more even pattern than that for pyramidal neurons; *iii*, an averaged wide-band waveform of the CA1 HFA (gray traces are for stand errors); *iv*, a scatter plot demonstrates the activities from 36 interneurons temporally corresponded to the HFA.

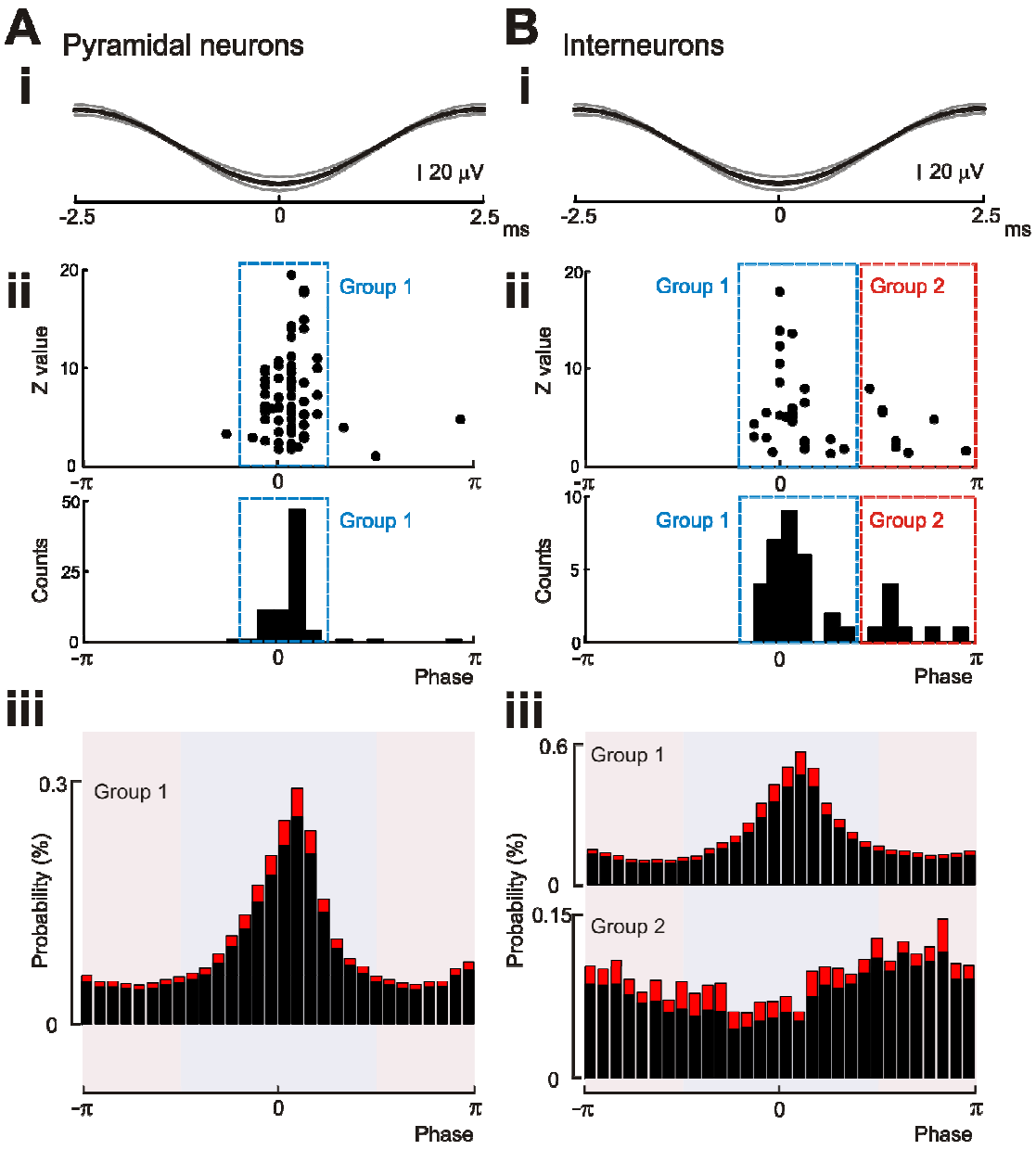
A
Pyramidal neurons
i
I 20 μV
-2.5
0
2.5
ms
ii
Z value
20
10
0
Group 1
-π
0
π
Counts
50
25
0
Group 1
Phase
iii
Probability (%)
0.3
0
Group 1
B
Interneurons
i
I 20 μV
-2.5
0
2.5
ms
ii
Z value
20
10
0
Group 1
Group 2
Counts
10
5
0
Phase
iii
Probability (%)
0.6
0
Group 1
0.15
Group 2
Phase

Figure R-06. Temporal correlations between neuronal activities and the HFA in CA1. **A***i*, an averaged 100-250 Hz band-passed HFA waveform which shows one cycle only (gray traces present the standard errors); *ii*, *top panel*, a scatter plot comprises the mode of the phase cross-correlation between unit activity and the HFA (x-axis) and the Z value derived from uniform test (y-axis); every dot represents a neuron (n=76); *ii*, *bottom panel*, cumulative numbers of neurons in every mode of phases; the blue dashed boxes indicate the group into which the pyramidal neurons were statistically classified (n=72); *iii*, averaged phase cross-correlation histogram shows this group of pyramidal neurons (n=72) increased their firing during the trough of HFA (shading with light blue). **B***i*, a cycle of averaged 100-250 Hz band-passed HFA waveform; *ii*, *top panel*, a scatter plot comprises the mode of the phase cross-correlation and the Z value; 36 interneurons are included; *ii*, *bottom panel*, cumulative numbers of neurons in every mode of phases; the dashed boxes indicate the two groups into which the interneurons were statistically classified (28 cells in group 1 and 8 cells in group 2); *iii*, *top panel*, averaged phase cross-correlation histogram shows that group 1 of interneurons (n=27) increased their firing during the trough of HFA (shading with light blue) as did most of the pyramidal neurons; *iii*, *bottom panel*, another phase cross-correlation histogram shows that group 2 interneurons (n=8) were prone to fire

during the rising phase of the HFA.

Spatial and temporal profiles of HFA

HFA was implicated exclusively in seizure foci in both clinical observations and chronic animal models (Bragin et al., 2007;Bragin et al., 1999b). Moreover, detections of HFA only seconds preceding the seizure onsets were described by early studies (Allen et al., 1992;Fisher et al., 1992). These reports suggested the HFA is spatiotemporally related to the seizure genesis. Thus it is also important to know the spatial and temporal profile of the high K^+ induced HFA in hippocampal slices. Nine Pt/Ir electrodes were placed along the hippocampus in the stratum pyramidale and field potentials were acquired (Figure R-07A). The loci of the electrodes from subiculum to hilus in order were: CA1a-1, CA1a-2, CA1b, CA1c-1, CA1c-2, CA2, CA3a, CA3b, and CA3c. Power spectra were analysed from every electrode and normalised by the dominant frequencies within 100-300 Hz for both CA1 and CA3, which is the frequency band for the HFA; data included five discrete interictal periods from each of 10 slices. According to the spatial power spectra, the dominant frequencies of HFA were uniform in CA3 regions but a more complex in hippocampal CA1. However a difference in their dominant frequencies between these two regions can be clearly observed in the spectra (Figure R-07B). The dominant frequency

seems to switch abruptly between CA1 and CA3. The spatial differences of the dominant frequencies between 100 to 500 Hz were tested by ANOVA (Figure R-07C). Dominant frequencies in CA1b, CA1c-1 and CA1c-2 are significantly slower than those from every sub-region in CA3 (5 interictal periods in each of 10 slices, $p<0.01$). The spatial differences were also tested in terms of their spreads in frequency. First moment analyses were conducted in every locus of recordings by multiplying the frequencies to their normalised powers as a function of location (ANOVA, Figure R-07D). In this test, CA1c-1 showed a significantly slower frequency distribution than those in CA1a-1 ($p<0.01$), CA1a-2 ($p<0.05$), CA2 ($p<0.01$) and CA3c respectively (5 interictal periods in each of 10 slices, $p<0.05$).

Fifty-six discrete interictal periods from 14 slices were used for studying the temporal profile of the activities (Figure R-08A). The signals were Morlet wavelet transformed to time and frequency domains using 0.2 sec calculating windows. A suppression of activity was present after the end of the previous seizure, which was easily observed in the original traces or the spectrograms. After tens of seconds the activity recovered, and increased further in intensity before the next seizure (Figure R-08B). The enhancement in the band for the HFA was clearly apparent, and the build-up of the HFA was consistent in these slices. Due to the different durations of the

interictal periods, every interictal period was first divided into 9 equal segments. The powers within HFA band (100-500 Hz), slow component band (10-100 Hz) and multi-unit activity band (MUA, 500-1000 Hz) were summated and averaged every 0.75 second. The power of the HFA was very low after the end of last seizure, and it was greatly enhanced preceding the next seizures, to about 6 times the minimal intensities (Figure R-08C*i*). The build-up of the HFA can be fitted with a quadratic or an exponential regression (with R square = 0.95 and 0.94 respectively), but less well fitted with a linear regression (R square = 0.76). The gradual progression of the slow components and the MUA were also observed. The growing slow components can be fitted with linear, quadratic and exponential with 0.68, 0.91 and 0.92 in their R squares; for the MUA the confidences for fitting with linear, quadratic and exponential regressions are 0.98, 0.99 and 0.99 (Table R-02).

Although MUA indicated the increase in global neuronal firing preceding the seizure onsets, the activity of individual neuron was not distinguished. Therefore once again tetrode recording was introduced to bring us the neuronal behaviors from a reasonable number of hippocampal cells preceding the seizure onset in the high K^+ slice model. We studied the firing patterns of individual neurons during the normalized interictal periods (neurons=23, Figure R-09A). Interictal periods were equally divided

into ten segments. Firing probability was calculated from that, spikes of individual neurons in each segment were normalized by total events of the neurons in the whole interictal periods. Activities from both pyramidal neurons and interneurons were suppressed after the previous seizures correspondent to the blank apparent in the spectrogram. Then the interictal periods were equally divided into 10 segments; and for individual neurons the spikes numbers in each segment were nomalised by the total number of firing from the same cells during the interictal periods. Thus we acquired the temporal changes of the firing probability during the interictal periods (Figure R-09B). Two trends of the firing probabilities for pyramidal neurons were observed: 1) the maximal firing probability was present in the last five segments, and the averaged trend can be well fitted with a quadratic regression (R square=0.93, $p<0.01$) but not a linear one (R square=0.27, $p>0.05$, n=9, Figure R-09B, *top*); 2) the maximal firing probability was present in the first five segments, and the averaged decreasing trend can be poorly fitted with an exponential regression and a linear regression (R squares=0.75 and 0.55, $p<0.05$, n=4, Figure R-09B, *middle*). Most of the interneurons (9 from 10 cells) increased their firing probability during the interictal periods, which can be fitted with a logarithmic regression (R square=0.94, $p<0.01$, Figure R-09B, *bottom*).

In these single neuron development profiles, we found that only the interneuron profiles corresponded to the build-up of MUA; however the interneurons are unlikely the key for either the HFA or even seizures. We had two suggestions for the pyramidal cell profiles in our observation: 1) unit spikes from pyramidal neurons were merged into the population spikes (or the HFA), thus less pyramidal spikes could be detected approaching the seizure onsets; 2) increased firing probability of pyramidal neurons is not responsible for the seizure onsets, but more silent pyramidal neurons might be recruited preceding seizures (Jiruska et al., 2010a); 3) some pyramidal activities were not distinguished from recording which might be due to the drawbacks of spike sorting.

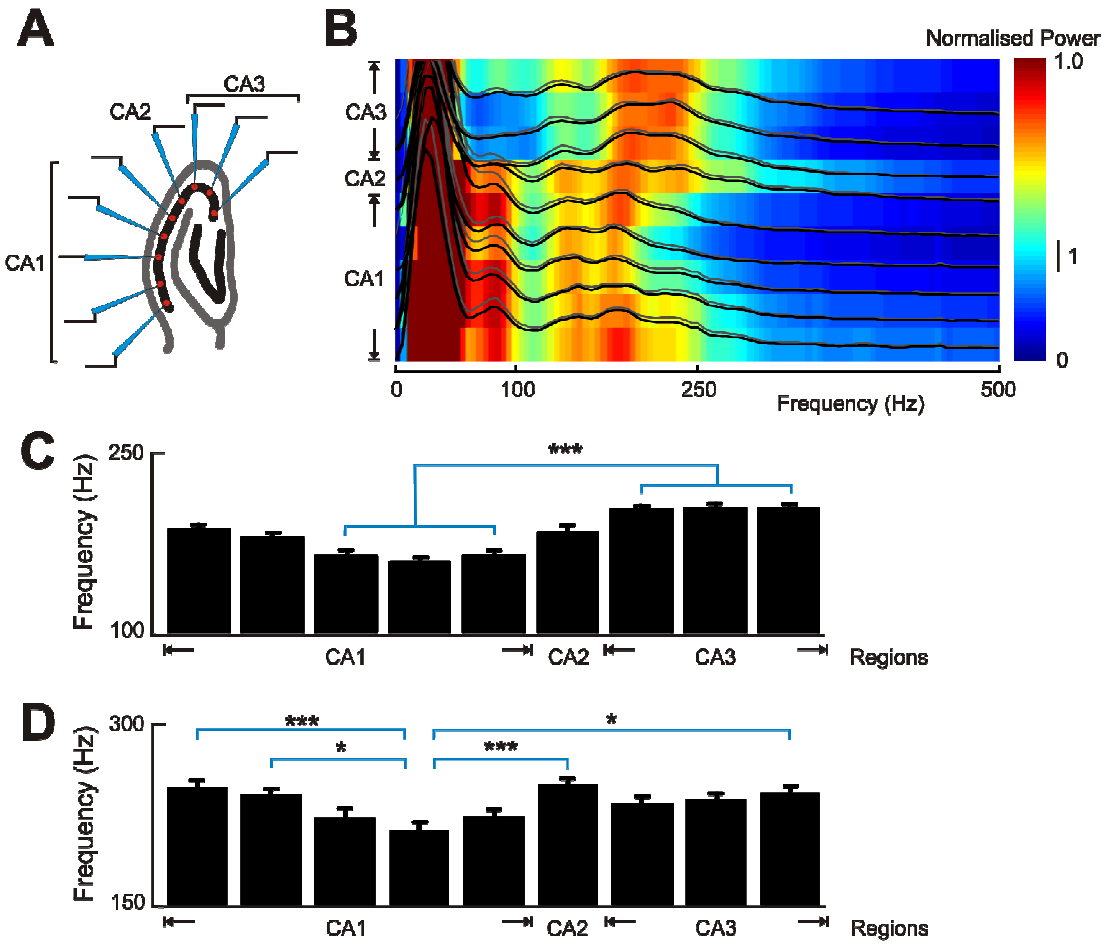
A
CA3
CA2
CA1
B
Normalised Power
1.0
1
0
CA3
CA2
CA1
0
100
250
500
Frequency (Hz)
C
250
100
Frequency (Hz)
***
CA1
CA2
CA3
Regions
D
300
150
Frequency (Hz)
***
*
*
***
CA1
CA2
CA3
Regions

Figure R-07. Spatial differences of HFA. **A**, a schematic shows electrode arrangement on a hippocampal slice; they are marked as CA1a-1, CA1a-2, CA1b, CA1c-1, CA1c-2, CA2, CA3a, CA3b and CA3c from subiculum to CA4. **B**, power spectra from each recording position were normalised and averaged across ten slices (5 discrete interictal periods in each slice); the power spectra were stacked together according to the hippocampal orientation (shown as thick lines and the thinner lines are for their standard errors), and they were coded in colour to present the strengths; an obvious frequency difference between CA1 and CA3 within HFA band can be observed. **C**, average dominant frequencies between 100 to 500 Hz showing the spatial differences crossing the hippocampal slices. The dominant frequencies for the HFA from CA1b, CA1c-1 and CA1c-2 are significantly lower than that from all CA3 regions (ANOVA, $p<0.01$) **D**, first moment analyses on the spatial difference of HFA as a function of location; in these analyses powers for frequencies under 100 Hz were excluded and only 100-500 Hz were included; a significant differences were found between CA1a-1, CA1a-2, CA2, and CA3c to CA1c-1 (*, $p<0.05$; ***, $p<0.01$).

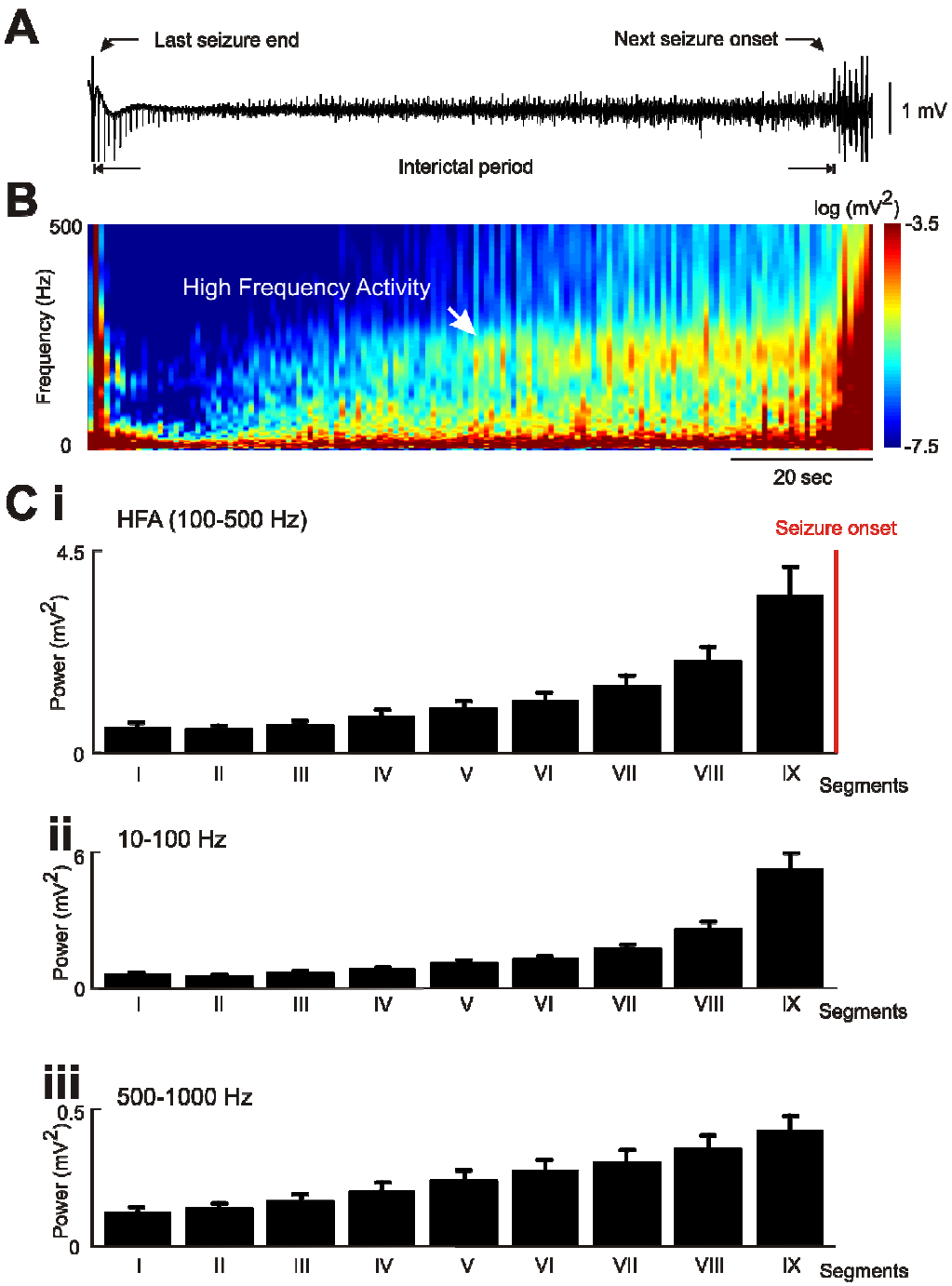
A
Last seizure end
Next seizure onset
1 mV
Interictal period
B
log (mV2)
500
-3.5
Frequency (Hz)
High Frequency Activity
0
-7.5
20 sec
C i
HFA (100-500 Hz)
Seizure onset
4.5
Power (mV2)
0
I II III IV V VI VII VIII IX
Segments
ii
10-100 Hz
6
Power (mV2)
0
I II III IV V VI VII VIII IX
Segments
iii
500-1000 Hz
0.5
Power (mV2)
0
I II III IV V VI VII VIII IX
Segments

Figure R-08. Temporal build-up of HFA in CA1. **A**, a selected wide-band recording of interictal period from CA1 which starts from the last seizure and ends at the next seizure onset. **B**, a spectrogram with time and frequency domains was translated from the recording in A; powers were logarithm transformed to enhance the colour contrast, in which hot colours represent the stronger power and cold colours are for the weaker power; a gap is clear after the last seizure and the HFA band around 200 Hz (white arrow) develops clearly before the next seizure onset. **C**, interictal periods were divided into 9 segments with equal lengths (14 slices, 56 interictal periods in total), in which the powers between 100-500 Hz, 10-100 Hz or 500-1000 Hz were summated together and averaged within each segment; the trends of build-up of HFA (100-500 Hz), slow component (10-100 Hz) and multi-unit activity (500-1000 Hz) are shown in *i*, *ii*, *iii* respectively.

	Regressions in intact slices		
	Linear	Quadratic	Exponential
Activity			
HFA	0.76	0.95	0.94
Slow component	0.68	0.91	0.92
MUA	0.98	0.99	0.99

Table R-02. Summary for the trends of the activities preceding seizures. The fitness to the regressions was showed by R squares for every activities (p<0.01).

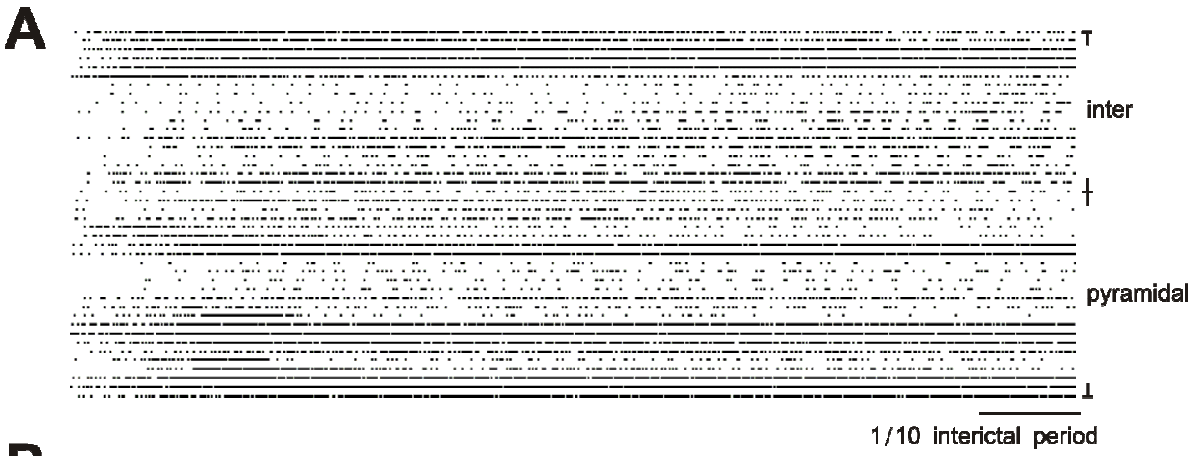
A
inter
pyramidal
1/10 interictal period

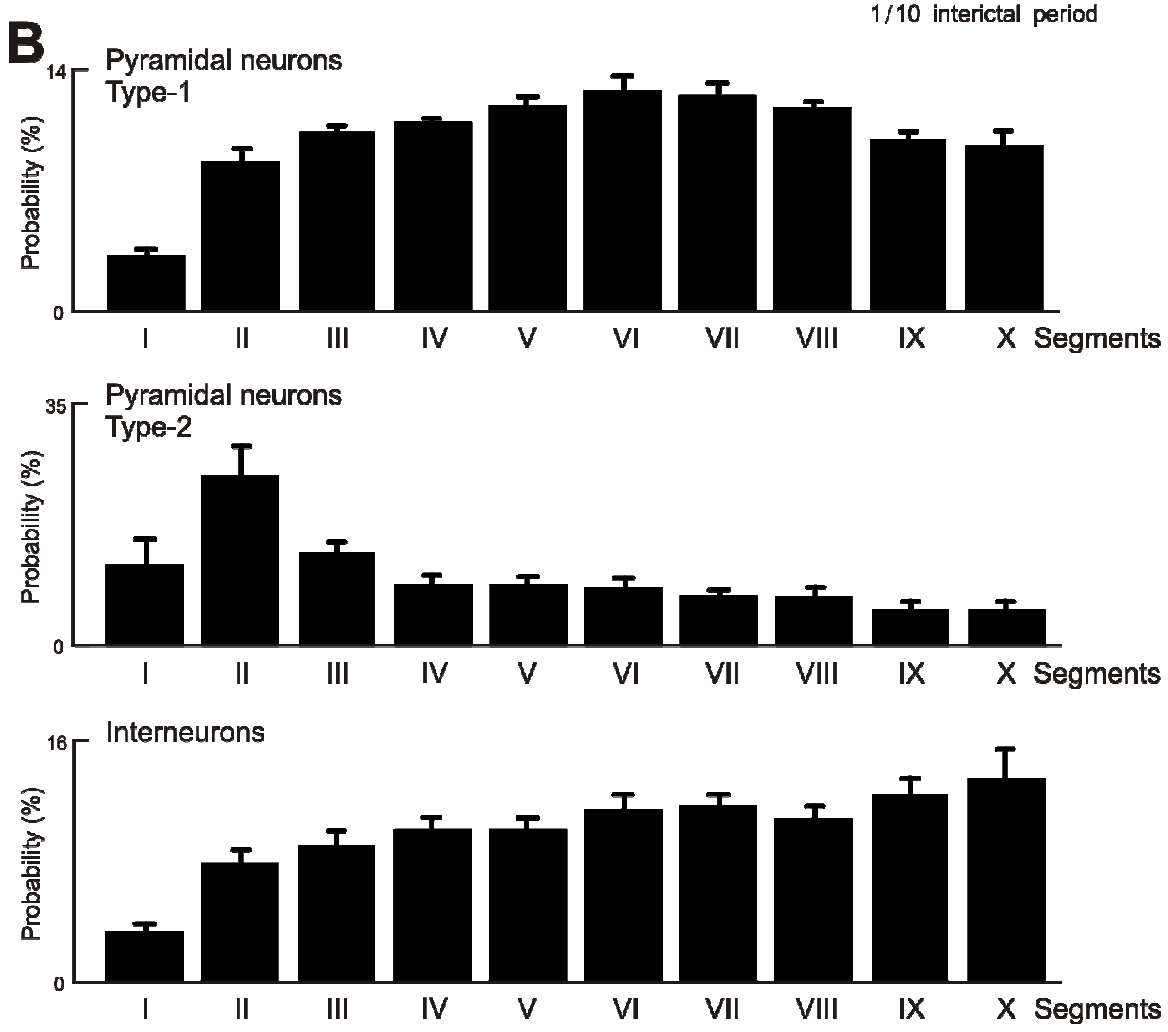
B
Pyramidal neurons
Type-1
Probability (%)
14
0
I II III IV V VI VII VIII IX X Segments
Pyramidal neurons
Type-2
Probability (%)
35
0
I II III IV V VI VII VIII IX X Segments
Interneurons
Probability (%)
16
0
I II III IV V VI VII VIII IX X Segments

Figure R-09. Unit activities during the interictal periods in CA1. **A**, a scatter plot presents unit spikes during the interictal periods (neurons=23). Interictal periods were normalised into same length and the dots represent unit spikes during the interictal periods; each row comprises spikes from one neuron during an interictal period, where their cellular types are labeled at the right end. **B**, firing probabilities of the pyramidal neurons and interneurons during the interictal periods. Interictal periods were equally divided into ten segments, and the firing probabilities for each neuron in every segment were analyzed. Pyramidal neurons present two firing trends (neurons=9 or 4 for each type) during interictal periods and the firing trend for interneuron is more consistent (neurons=9).

Interictal discharges

Interictal discharges were present synchronously in CA1 and CA3 of the high K^+ hippocampal slices between seizures (Figure R-10A, arrows), and these discharges persisted robustly in CA3 when seizures appeared in CA1 (Figure R-01C*ii* and C*iii*). Interictal discharges were present at a mean of every 0.8 sec (alternatively 1.25 Hz, 5512 interictal discharges,16 slices, Figure R-10B). We analysed the temporal relationships between interictal discharges (10-100 Hz filtered) in hippocampal CA1 and CA3 and their sub-regions, and found that interictal discharges started mainly from either CA3b (888 of 1672 interictal discharges, i.e. 53%, 8 of 15 slices) or CA3c (637 of 1672 interictal discharges, i.e. 38%, 6 of 15 slices; Table R-01 and Figure R-02); thus the CA3b was predominantly the “irritative zone, where the interictal discharges initiate” in this high K^+ hippocampal model and the interictal discharges in CA1 followed those in CA3 (Figure R-10C). The propagation of the interictal discharges took 6 ms to travel from CA3b to CA1b (in total 1690 sec of discrete interictal periods, from 12 slices, Figure R-10C, *bottom*), where most seizures started (8 of 15 slices, Table R-01).

The subcellular events during the interictal discharges in CA1 and CA3 were

analysed by CSD. Somatodendritic recordings from CA1 and CA3 were 10-100 Hz filtered and averaged by the positive peaks on stratum pyramidale as the reference. In CA1, the interictal discharges were led by a sink in the stratum radiatum with a corresponding source located in the stratum pyramidale, later a current sink was present in the stratum pyramidale (Figure R-10D, *left panels*). In CA3, the interictal discharges started with current sinks mainly on stratum oriens and also on stratum radiatum, with a corresponding current source in stratum pyramidale. Then a current sink followed after the source in pyramidal layer (Figure R-10D, *right panels*). Therefore the interictal discharges in the high K^+ model required synaptic inputs since each interictal discharge started with sinks on their dendritic layers, however the mechanisms of interictal discharges in their initiation zone in CA3 and their projection zone in CA1 might be slightly different due to the distinct leading parts (stratum radiatum in CA1 and stratum oriens in CA3).

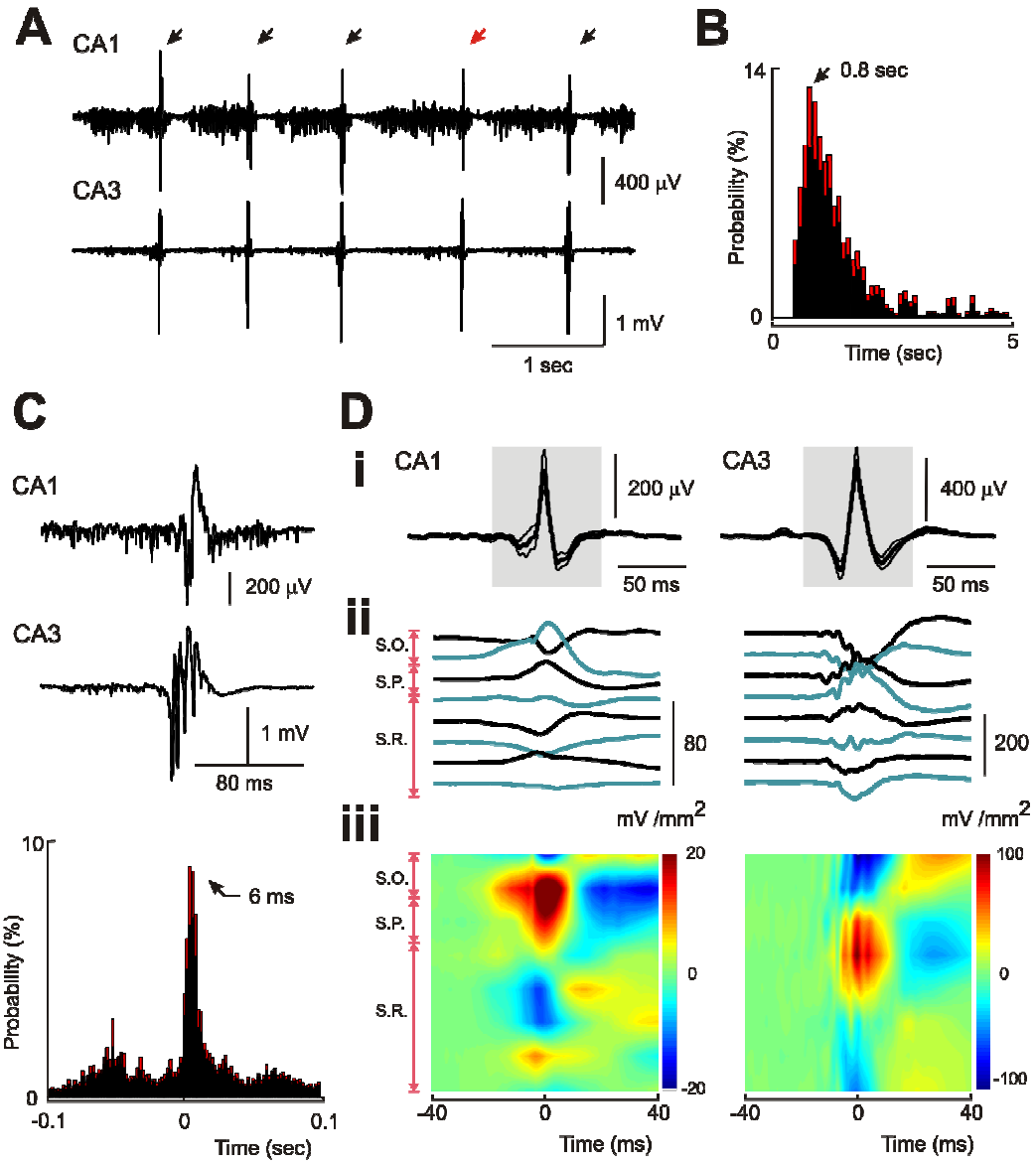
A
CA1
CA3
400 μV
1 mV
1 sec
B
14
0.8 sec
Probability (%)
0
0
5
Time (sec)
C
CA1
200 μV
CA3
1 mV
80 ms
10
6 ms
Probability (%)
0
-0.1
0
0.1
Time (sec)
D
i
CA1
200 μV
50 ms
CA3
400 μV
50 ms
ii
S.O.
S.P.
S.R.
80
200
iii
mV /mm2
mV /mm2
S.O.
S.P.
S.R.
20
0
-20
100
0
-100
-40
0
40
Time (ms)
-40
0
40
Time (ms)

Figure R-10. Interictal discharges induced by high K^+ ACSF in hippocampal slices. **A**, synchronous recordings (>10 Hz) of CA1 and CA3 show aligned interictal discharges (arrows). **B**, inter-interictal discharges-interval histogram indicates the mode of the interval of the interictal discharges is 0.8 sec (5512 interictal discharges, 16 slices); red columns are standard errors. **C**, *top two panels*, selected interictal discharges from CA1 and CA3 were expanded from A (red arrow); *bottom panel*, a CA3-CA1 interictal discharges cross-correlation histogram indicates that interictal discharges started from CA3 and interictal discharges in CA1 happened 6 ms after (in total 1690 sec of discrete interictal periods, from 12 slices). **D**, CSD presents the slow component of interictal discharges from CA1 (left panels) and CA3 (right panels), which derived from 10-100 Hz band pass filtered original recordings; *i*, averaged 10-100 Hz waveforms of CA1 and CA3 interictal discharges where thick traces show the means and thin traces show the standard errors (13 slices); the shaded areas were for CSD analyses; *ii*, 10-100 Hz band-passed CSD of CA1 and CA3 interictal discharges were averaged by the timing of highest peaks in stratum pyramidale, and hippocampal layers are indicated to the left; *iii*, interictal discharges CSD were coded by colours indicating the polarities of the CSD, where positive, warm colour represents current source; and negative, cold colour represents current sink.

Interference of the HFA by interictal discharges

The build-up of the HFA was described in the previous paragraph; however this development does not progress continuously. The fluctuation of the HFA can be observed even in the raw traces. The activities were strongly suppressed after each of the interictal discharges in both CA1 and CA3 (Figure R-11A and B, arrows on traces); this refractory period was more obvious from the spectrogram which showed no activity (segments with clear cold colour) was recorded within the 200 ms period after an interictal discharge in CA1 (Figure R-11A); longer refractory periods were observed in CA3 (Figure R-11B).

An alternative approach to detect the refractory period used cross-correlations between the interictal discharges and the events of HFA or MUA. The original recordings were filtered and presented as slow components (10-100 Hz), ripples (100-250 Hz, slower HFA), fast ripples (250-500 Hz, faster HFA) or MUAs (500-1000 Hz) individually. The interictal discharges were marked on their peaks. By thresholding at 7x the standard deviation of background recording, the troughs of ripple, fast ripples and MUA were detected; and the cross-correlations were generated between them. The occurrences of the HFAs and MUA were enhanced ~100 ms before each interictal

discharge in CA1 and the probability of HFA was strongly suppressed after the interictal discharge for 200 ms or more (6 slices, Figure R-11C); similar cross-correlations were present in the activities in CA3, but 300 ms or more refractory periods were found in CA3 (13 slices, Figure R-11D).

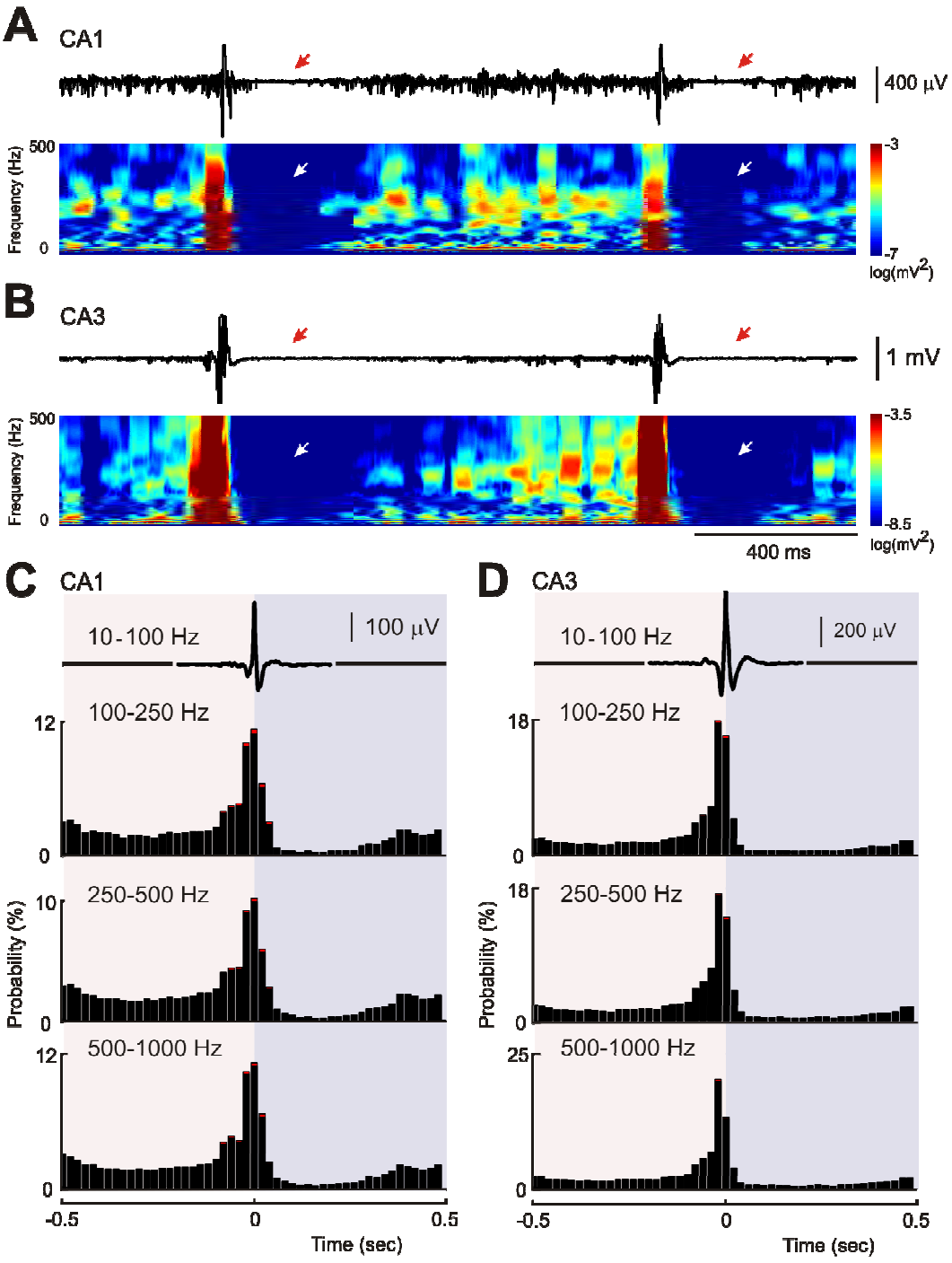
A
CA1
400 μV
Frequency (Hz)
500
0
-3
-7
log(mV2)
B
CA3
1 mV
Frequency (Hz)
500
0
-3.5
-8.5
log(mV2)
400 ms
C
CA1
10-100 Hz
100 μV
100-250 Hz
250-500 Hz
500-1000 Hz
Probability (%)
12
0
10
0
12
0
-0.5
0
0.5
Time (sec)
D
CA3
10-100 Hz
200 μV
100-250 Hz
250-500 Hz
500-1000 Hz
Probability (%)
18
0
18
0
25
0
-0.5
0
0.5
Time (sec)

Figure R-11. HFA is disrupted by interictal discharges. **A**, selected CA1 recording (>10 Hz) including two interictal discharges with the spectrogram of this recording. Arrows indicate refractory periods after each interictal discharge, where no activity observed within this period. **B**, selected synchronous CA3 recording (>10 Hz) and its spectrogram as those from CA1 in A. Refractory periods are also indicated by arrows. **C**, CA1 event cross-correlation histograms between interictal discharges and activities in different frequency bands (6 slices). *Top panel*, averaged CA1 interictal discharge (10-100 Hz); *lower panels*, cross-correlations between interictal discharges and the ripple band (100-250 Hz), fast ripple band (250-500 Hz) and multi-unit activity (500-1000 Hz) respectively. Activities were enhanced hundred ms before the interictal discharges, but suppressed after the interictal discharges for 200 ms or more, that is the refractory period. **D**, CA3 event cross-correlation histograms between interictal discharges and activities in different frequency bands (13 slices). *Top panel*, averaged CA3 interictal discharges (10-100 Hz); *lower panels*, cross-correlations between interictal discharges and the ripple band, fast ripple band and multi-unit activity respectively. Activities were also enhanced hundred ms before the interictal discharges, but suppressed after the interictal discharges 300 ms, which is much longer than that from CA1. In panel C and D, pink shading represents the period

before interictal discharges and blue shading represents the period after interictal discharges.

Seizure genesis is modified by interictal discharges

The HFA is strongly related to seizure onsets and the HFA is modified by the interictal discharges as shown in previous sections. We hypothesized that the seizure onset might be influenced if we removed the source of interictal discharges in CA3. The Schaffer collateral pathway is the only axonal projection from CA3 pyramidal cells to CA1 in our hippocampal slice preparation. Thus physical lesion on the Schaffer collateral pathway will remove the CA3 synaptic inputs onto CA1 neurons (Figure R-12A). In this section, comparisons were made before and after lesioning in the same slices. After the Schaffer collateral pathway was lesioned, no interictal discharge was observed in CA1, though CA3 interictal discharges persisted as before; the durations of interictal periods and seizures were also changed (Figure R-12B). The interictal periods were significantly shorter, from 60.4±4.4 sec in intact slices (28 discrete interictal periods) to 40.3±2.0 sec in CA1 of the same slices after lesions (30 discrete interictal periods), i.e. a 30.9±5.9 % reduction (Figure R-12C*i*, 6 slices, $p<0.01$). The seizure durations also decreased after slice lesioning. The original seizures comprised tonic phases and clonic phases, and the total seizure duration was 46.5±4.7 sec (29 seizures, Figure R-12C*ii* and D*i*, 6 slices). After the lesions, the

clonic phases were lost and the seizure duration in CA1 become 12.4±0.7 sec, that is a 68.0±4.6 % reduction in seizure duration (31 seizures, Figure R-12C*ii*, 6 slices, $p<0.05$). Instead of the clonic phases of seizures, some pre-bursts or after-bursts were present preceding or following seizures in the lesioned slices (Figure R-12D*ii*). The pre-bursts are small population spikes with weaker strength, and resemble, but never develop into, the ordinary tonic seizures. Although the after-bursts had excessive strength as clonic seizure, the after-bursts presented an arrhythmic pattern with couples of bursts only. Those two events were never found in intact hippocampal slices in high K, thus we conclude they implied a modified mechanism for the seizure genesis from that present in intact slices.

The seizure onset patterns also changed after lesioning slices. In the intact slices, most seizure onsets “aligned” with the interictal discharges, and the seizure onset zones changed little during each experiment (Figure R-12E*i*). After lesioning, the hypersynchronised pattern of the seizure onset was lost (Figure R-12E*ii*) and the seizure onset zone became more changeable. In summary, we believed the interictal discharges have dual effects on the seizure genesis. First, the shorter interictal periods after lesioning the Schaffer collaterals suggest interictal discharges delay seizure onset. Second, and in contrast, the briefer seizure duration after lesioning

suggests the CA3 input may exacerbate the seizures. These experiments indicated that the clonic phase of the CA1 seizures driven by CA3 interictal discharges, and disconnecting CA3 from CA1 might protect the tissue from long lasting seizures. Moreover, whether the transformations of the seizure onset patterns imply a pro- or anti- seizure role of interictal discharges is still uncertain.

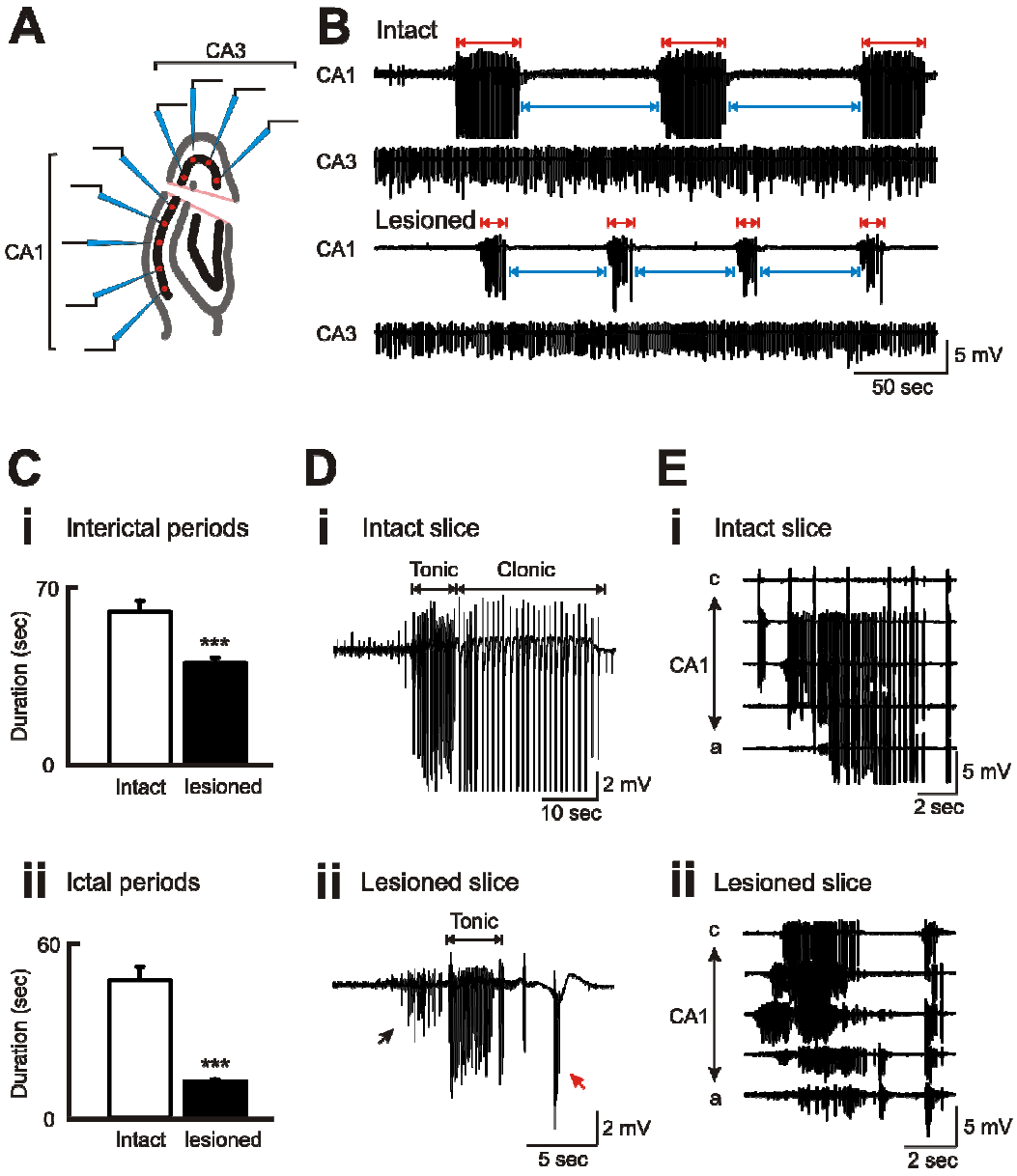
A
CA3
CA1
B
Intact
CA1
CA3
Lesioned
CA1
CA3
5 mV
50 sec
C
i Interictal periods
70
0
Duration (sec)
***
Intact lesioned
ii Ictal periods
60
0
Duration (sec)
***
Intact lesioned
D
i Intact slice
Tonic Clonic
2 mV
10 sec
ii Lesioned slice
Tonic
2 mV
5 sec
E
i Intact slice
c
CA1
a
5 mV
2 sec
ii Lesioned slice
c
CA1
a
5 mV
2 sec

Figure R-12. Epileptic features modified after lesioning slices between CA1 and CA3. **A**, a schematic shows a lesioned slice and the Pt/Ir electrode arrangement. **B**, electrographic wide-band recordings from CA1 and CA3 from intact slice and lesioned slice. The lengths of interictal periods and seizures in CA1 changed from the intact slice to the lesioned slice, but there was no significant difference of CA3 patterns between these two conditions. **C***i*, the difference of the lengths of interictal periods from intact to lesioned slices; the interictal periods decreased significantly from 60.4± 4.4 sec to 40.3±2.0 sec (30.9±5.9 reduction, 28 and 30 interictal periods respectively, in 6 slices, ***, $p<0.01$); *ii*, the difference of the seizure lengths from intact to lesioned slices; the seizure lengths decreased significantly from 46.5±4.7 sec to 12.4±0.7 sec (29 and 31 seizures respectively, in 6 slices, 68.0±4.6 % reduction, ***, $p<0.01$). **D**, different seizure patterns in intact and lesioned slices (wide-band); seizures comprised of tonic and clonic parts when they presented in intact slices (shown as D*i*); a seizure lost the clonic part when the slice was lesioned (shown as D*ii*), and they sometimes preceded by pre-bursts (black arrow) or after-bursts (red arrow). **E**, different seizure onset pattern in intact and lesioned slices (signals >10 Hz); *i*, hyper-synchronised seizure onset pattern can be observed in intact slices; *ii*, when the slice lesioned, seizures lost the hyper-synchronised onset patterns and the seizures

can be led by any region in CA1.

The HFA without the interference of the interictal discharges

Our next study was addressed whether the effect of interictal discharges on seizure genesis is mediated by modifications on the HFA. After lesioning the Schaffer collateral pathway, the HFA was still present in CA1 (Figure R-13A). This observation re-emphasized that the origins of the HFA are not CA3 dependent, which resembles the situation for the physiological sharp wave ripples. The peak frequency of the HFA in CA1 switched from 186 Hz in intact slices to 234 Hz in lesioned slices according to their averaged power spectra (Figure R-13B*i*, 19 slices), and the peak frequency of the HFA in CA3 was at 240 Hz in intact slices and at 249 Hz in lesioned slices (Figure R-13C*i*, 16 slices). Alternatively comparing the averages of the dominant frequency in CA1, the mean was 186.7±6.9 Hz (13 slices, four interictal periods in each slice) in intact slices and increased to 216.5±7.2 in lesioned slices (4 interictal periods in each of 6 slices, $p<0.05$); but no significant shift was found in CA3. First moment analyses on the distributions of the spectra (100-500 Hz) were conducted in both CA1 and CA3 from intact or lesioned slices. In CA1, the first moment of the frequency spectra had significantly shifted from 235±6 Hz in intact slices to 265±2 Hz (Figure R-13B*ii*, $p<0.01$); in CA3, the first moment of the frequency spreads had significantly

increased from 252±5 Hz to 281±4 Hz (Figure R-13C*ii*, $p<0.01$). As we found in the intact slices, in lesioned slices the first moment of frequency in CA1 is lower than that in CA3 ($p<0.01$). Thus the HFAs in these two regions had been relocated to faster frequencies when the Shaffer collateral pathway was lesioned.

The properties of the HFA in lesioned slices were studied by their inter-pulse-interval and the averaged waveforms to support the phenomena that the changed spectra reflected the altered waveforms and rhythms of the HFAs in lesioned slices. HFA in CA1 of lesioned slices gave a mode of the inter-pulse-interval histogram at 4 ms, and the first cycle of the trough-to-trough duration was 4.0 ms in both wide band averaged HFA or band-pass (100-300 Hz) averaged HFA (Figure R-13B*iii*, 18 slices). HFA in CA3 of lesioned slices presented a mode in the histogram at 3 ms, and the first cycle of the trough-to-trough duration was 3.6 ms in both wide band averaged HFA or band-pass (100-300 Hz) averaged HFA (Figure R-13B*iii*, 18 slices). The HFA situated on the positive slow component was also clear in both CA1 and CA3 of lesioned slices. Thus the hypothesis that the hyperpolarisation was due to local inhibitory circuits was still supported.

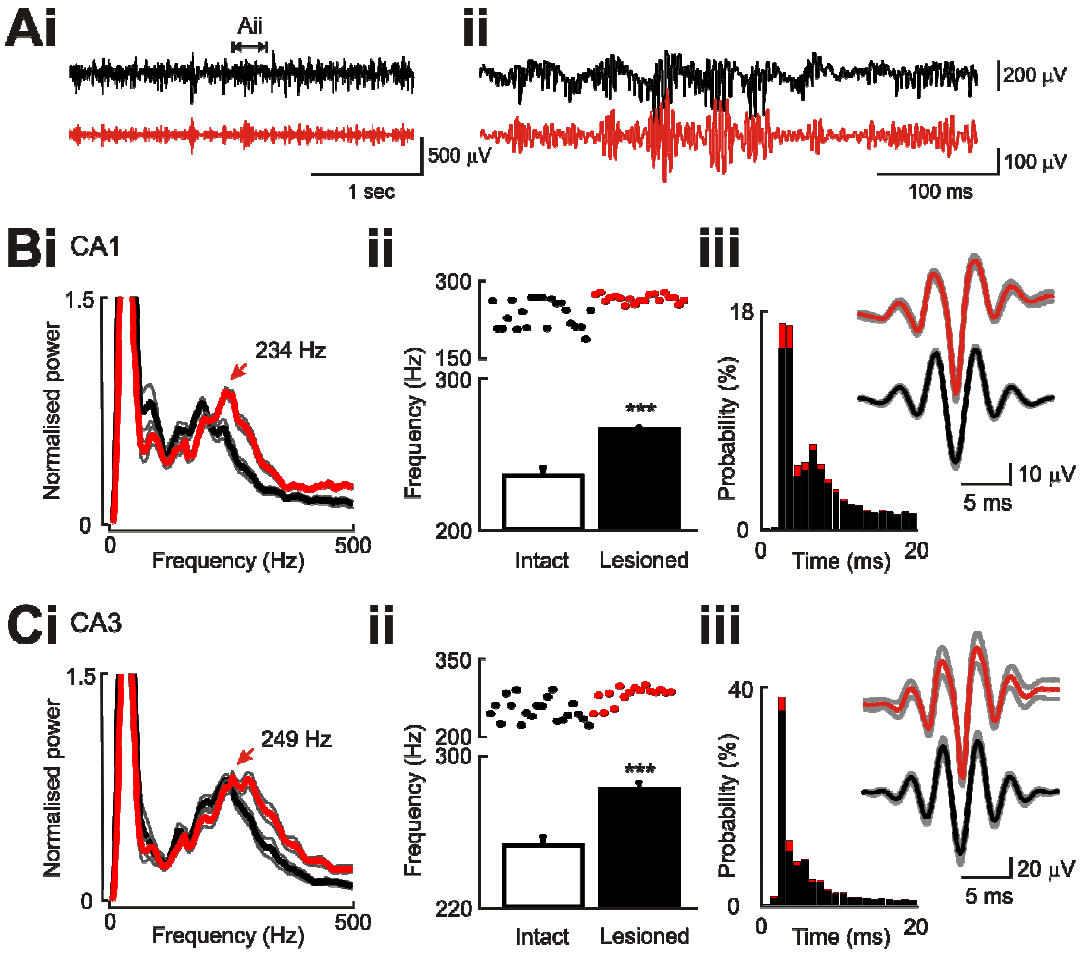
Ai
Aii
500 µV
1 sec
ii
200 µV
100 µV
100 ms
Bi CA1
Normalised power
1.5
0
234 Hz
0
500
Frequency (Hz)
ii
300
150
300
200
Frequency (Hz)
***
Intact
Lesioned
iii
18
0
Probability (%)
0
Time (ms)
20
10 µV
5 ms
Ci CA3
Normalised power
1.5
0
249 Hz
0
500
Frequency (Hz)
ii
350
200
300
220
Frequency (Hz)
***
Intact
Lesioned
iii
40
0
Probability (%)
0
Time (ms)
20
20 µV
5 ms

Figure R-13. Modifications on HFA in lesioned slices. **A***i*, a wide-band recording from CA1 in a lesioned slice (black) and its 100-250 Hz filtered trace (red); interictal discharges were abolished after CA3 was removed; *ii*, expansions from A*i*; the HFA can be observed in the filtered trace. **B**, features of CA1 HFA in lesioned slices; *i*, the power spectra indicate the dominant frequency of HFA was shifted from 186 Hz to 234 Hz when slices lesioned (19 slices, all interictal periods were included, red spectrum is for lesioned slices and black spectrum is for intact slices); *ii*, the shifting of frequencies of HFA were analysed by first moment; *top panel* shows individual first moments from intact slices (21 slices, black dots) and lesioned slices (19 slices, red dots); *lower panel* shows that HFA has significantly higher frequency distribution in lesioned slices (***, $p<0.01$); *iii*, inter-pulse-interval histogram shows a peak at 4 ms (18 slices); *iii*, *inset*, the averaged HFA waveforms from wide-band recording (red trace, S.E. in gray) or within 100-300 Hz (black trace, S.E. in gray) both show the first cycles at 4.0 ms (18 slices). **C**, features of CA3 HFA in lesioned slices; *i*, the power spectra indicate the dominant frequency of HFA was shifted from 240 Hz to 249 Hz when slices lesioned (16 slices, interictal periods were included; black spectrum is for intact slices and red spectrum for lesioned slices); *ii*, first moment analyses; *top panel* shows individual first moments from intact slices (20 slices, black dots) and lesioned slices (16 slices, red

dots); *lower panel* shows that HFA has significantly higher frequency distribution in lesioned slices (***, $p<0.01$); *iii*, inter-pulse-interval histogram shows a peak at 3 ms (16 slices); *iii*, *inset*, the averaged HFA waveforms from wide-band recording (red trace, S.E. in gray) or within 100-300 Hz (black trace, S.E. in gray) show the first cycles both at 3.6 ms (18 slices).

Different build-up of the HFA when the CA3 inputs were removed

Next we studied the dynamics of the HFA, the slow component and the MUA during the interictal periods to see whether they were affected after withdrawing the interictal discharges. The temporal build-up of these activities was analyzed in the lesioned slices. According to the raw traces and the spectrograms, the development of the HFA was also present in the lesioned slices (Figure R-14A and B); however the trends present in lesioned slices differed from those observed in intact slices. The HFA in the intact slices was strongly suppressed after the previous seizures but in the lesioned slices the HFA still survived after the previous seizure though it was partially depressed, which is clearly demonstrated by the original trace or the spectrogram (Figure R-14A and B).

In addition to the differences in the starting strengths of the HFA, the development of the HFA, the slow component and the MUA during interictal periods in the lesioned slices were also investigated. As in the intact slices, interictal periods in 16 lesioned slices (73 discrete interictal periods) were equally divided into nine segments, and the power of activities between 100-500 Hz, 10-100 Hz and 500-1000 Hz were summated and averaged for each 0.75 seconds. In these lesioned slices, the build-up of the HFA

was better fitted with linear regression than that in intact slices (R square=0.99). The power of the HFA in the lesioned slices was significantly stronger than that in the intact slices except for the last segment preceding the seizures (p<0.01, Figure R-14C*i*). The quadratic increases of the slow component in intact slices were not present in lesioned slices, the increase of slow component in the lesioned slices was linear instead (R square=0.98, Figure R-14C*ii*). Both in the intact or the lesioned slices, development of the MUA was steadily fitted a linear regression, though the power of the MUA in lesioned slices was even stronger (p<0.01, Figure R-14C*iii*; Table R-03).

In these comparisons of the activities between intact slices and lesioned slices, we found that the interictal discharges not only caused ~200 ms refractory periods, but also suppressed the global HFA in the early and middle segments during the interictal periods. Thus we suggested that interictal discharges prolong the seizure genesis because they inhibit the formation of the HFA. Less power and slower build-up of MUA during the interictal periods in intact slices is further evidence to support an inhibitory condition induced by the distal synaptic inputs from CA3. Interestingly, even the HFA was suppressed by the interictal discharges, the level of the HFA just preceding the seizure onsets is not different to the level of the HFA in lesioned slices before seizures. Whether this maximal power implies a threshold of HFA for initiating a seizure is still

uncertain.

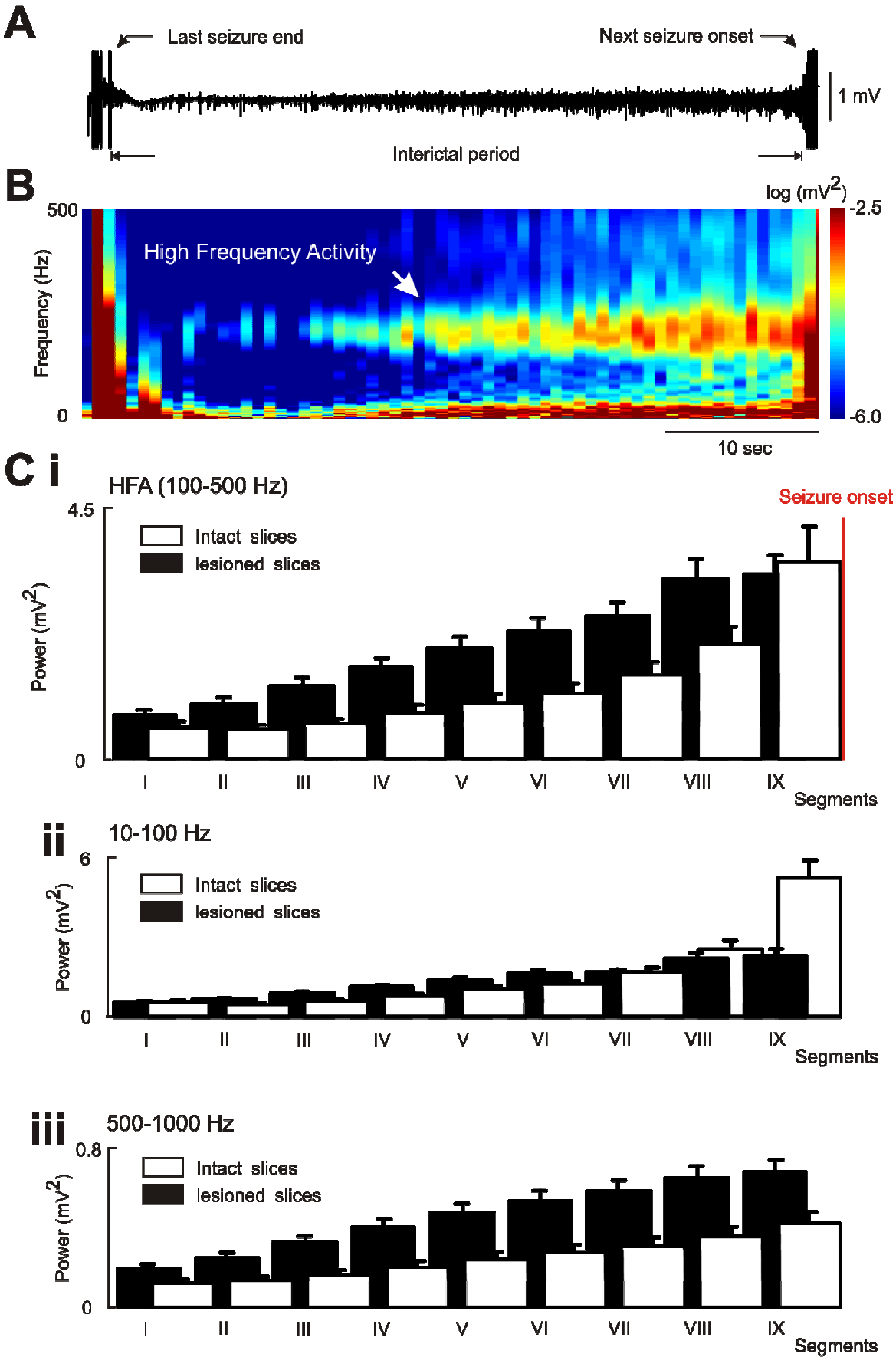
A
Last seizure end
Next seizure onset
1 mV
Interictal period
B
log (mV2)
500
High Frequency Activity
Frequency (Hz)
0
-2.5
-6.0
10 sec
C i
HFA (100-500 Hz)
Seizure onset
4.5
Intact slices
lesioned slices
Power (mV2)
0
I
II
III
IV
V
VI
VII
VIII
IX
Segments
ii
10-100 Hz
6
Intact slices
lesioned slices
Power (mV2)
0
I
II
III
IV
V
VI
VII
VIII
IX
Segments
iii
500-1000 Hz
0.8
Intact slices
lesioned slices
Power (mV2)
0
I
II
III
IV
V
VI
VII
VIII
IX
Segments

Figure R-14. Temporal build-up of the HFA in CA1 of the lesioned slices and the comparisons between those in intact slices and lesioned slices. **A**, a selected wide-band recording of interictal period in CA1 from a lesioned slice. **B**, a spectrogram with time and frequency domains was translated from the recording in A; powers were logarithm transformed; in lesioned slices, activities were continuous after the last seizure and the HFA band which is above 200 Hz (white arrow) also develops clearly before the next seizure onset. **C**, interictal periods were divided into 9 segments with equal lengths (16 slices, 73 interictal periods in total); the trends of build-up of HFA (100-500 Hz), slow component (10-100 Hz) and multi-unit activity (500-1000 Hz) from lesioned slices are shown in *i*, *ii*, *iii* respectively with black bars; the summated powers of the activities for each frequency band from intact slices are presented with white bars for comparisons.

	Regressions in lesioned slices		
	Linear	Quadratic	Exponential
Activity			
HFA	0.99	0.99	0.97
Slow component	0.98	0.99	0.97
MUA	0.99	0.99	0.94

Table R-03. Summary for the trends of the activities proceding seizures in lesioned slices. The fitness to the regressions was showed by R squares for every activities (p<0.01).

Neuronal activity and the HFA when distal inputs were removed

MUA cannot represent the individual neuronal activities during the progress of interictal periods as the distinct neuronal firing patterns we demonstrated for the intact slices; besides different rhythms of the HFA were observed between the intact and the lesioned slices, which suggests distinct cellular mechanisms might be involved in this divergence. Thus we conducted tetrode recording in the lesioned slices as well to find the differences. In 11 lesioned slices (one to three tetrodes were used for simultaneously recording), 186 pyramidal and 9 interneurons neurons were isolated by spike sorting. As we observed in the intact slices, the pyramidal neurons were identified by their wider waveforms and auto-correlations containing bursting patterns and fast exponential decay; we even saw an additional pair of peaks (±11 ms) in the auto-correlations for pyramidal neurons which represents more consistent bursts (Figure R-15A*i* and A*ii*). In contrast, the interneurons were identified by the narrower waveforms and the flatter auto-correlations (Figure R-15B*i* and B*ii*). In many lesioned slices, the HFA did not develop well. In particular we found that the digital filtering of pyramidal spikes might cause false detections of HFA in these slices as explained in the Materials and Methods. Therefore we had to exclude many neurons for following

analyses of temporal correlations between the HFA and neuronal activities.

Forty-seven pyramidal neurons and nine interneurons (simultaneous recording from one to three tetrodes in CA1 region of 6 lesioned slices) were first Kolmogorov-Smirnov tested for their correlations with the HFA. Only one pyramidal neuron showed uniform distribution, and the other pyramidal neurons presented modulated cross-correlations to the HFA (Figure R-15A*iii* and *iv*). Although the activities of the 9 interneurons were modulated by the HFA, the pattern was not consistent (Figure R-15B*iii* and *iv*).

Cross-correlations between neurons and HFA were re-constructed in the phase domain, where the troughs of the HFA were denoted as 0 and the peaks were ±π (±2.0 ms, Figure R-16). Modes of individual phase histograms from the pyramidal neurons presented a normal distribution, thus these pyramidal neurons increased their firing probability in the same phase to the HFA and that was also on the trough of the HFA (pyramidal neurons=46, Figure R-16A*ii* and *iii*). An abrupt peak at around 0.5 ms (1/4π) might be due to the filter artifact as explained in Materials and Methods (Figure R-16A*iii*). Modes of the phase histograms from the interneurons were less consistent and did not differ from either a normal distribution or a uniform distribution. Thus they were pooled together (interneurons=9, Figure R-16B*ii*). For these

interneurons, they increased their firing probability after the troughs of the HFA (Figure R-16B*iii*).

CSD also tested the causes of HFA in CA1 of a lesioned slice. The HFA was led by a current sink in pyramidal layer and then it propagated to both dendritic layers; the sink was followed by a source in the pyramidal layer (Figure R-17). Thus the current flows and the underlying mechanisms of HFA were similar to those found in intact slices. In summary, the HFA in lesioned slices was still mainly due to the pyramidal neurons, and the interneurons may also play the modifying role. Interestingly, a relatively greater proportion detected neurons were pyramidal cells in the lesioned slices than in the intact. Although the detection of specific neurons has a large element of chance, and depends upon the locations of the tetrodes, this large difference might imply a possibility that fewer interneurons were active when the CA3 inputs were removed.

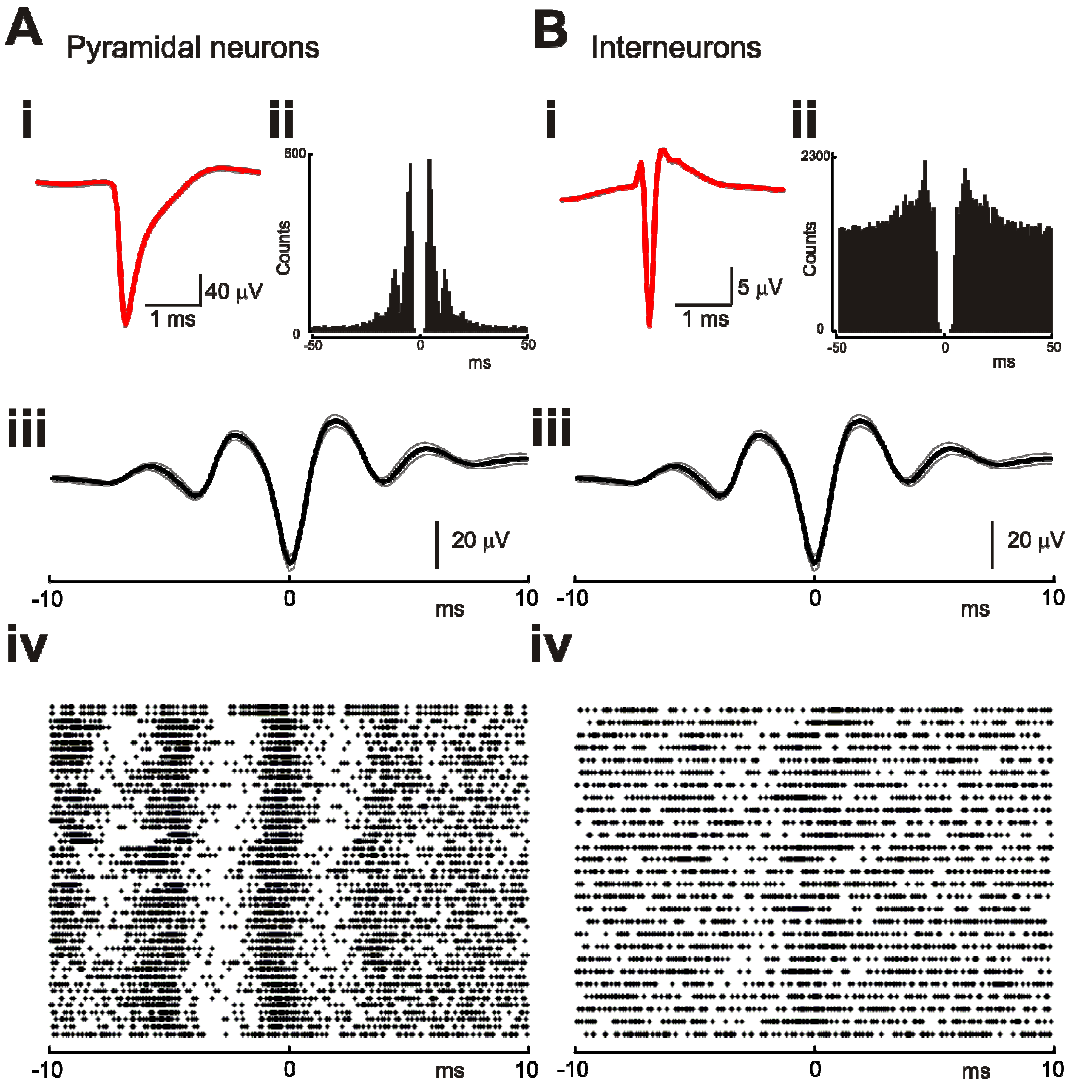
A
Pyramidal neurons
B
Interneurons
i
ii
iii
iv
40 µV
1 ms
5 µV
1 ms
Counts
800
2300
0
-50
0
50
ms
20 µV
-10
0
10
ms

Figure R-15. Neuronal activity corresponded to the HFA in CA1 of the lesioned slices. **A***i*, an averaged unit spike from a CA1 pyramidal neuron in a lesioned slice (wide-band), which shows a wider duration than interneurons; *ii*, the auto-correlation histogram indicates that this pyramidal neuron fired in bursts, thus two pairs of peaks are present ~4 ms and ~11 ms; *iii*, an averaged wide-band waveform of the CA1 HFA in lesioned slices where gray traces indicate the standard errors of the average; *iv*, a scatter plot demonstrates the activities from 47 pyramidal neurons temporally related to the HFA, where every dot is an event around the HFA and each row represents events from one neuron. **B***i*, an averaged unit spike from a CA1 interneuron in a lesioned slice (wide-band), which shows a narrower spike width than that from pyramidal neurons; *ii*, an auto-correlation histogram shows a very even pattern with ± 4~5 ms refractory period; *iii*, an averaged wide-band waveform of the CA1 HFA (gray traces are for standard errors); *iv*, a scatter plot demonstrates the activities from 9 interneurons temporally related to the HFA. For viewing convenience, the correlation for every neuron is present three times (thus 27 rows for 9 neurons).

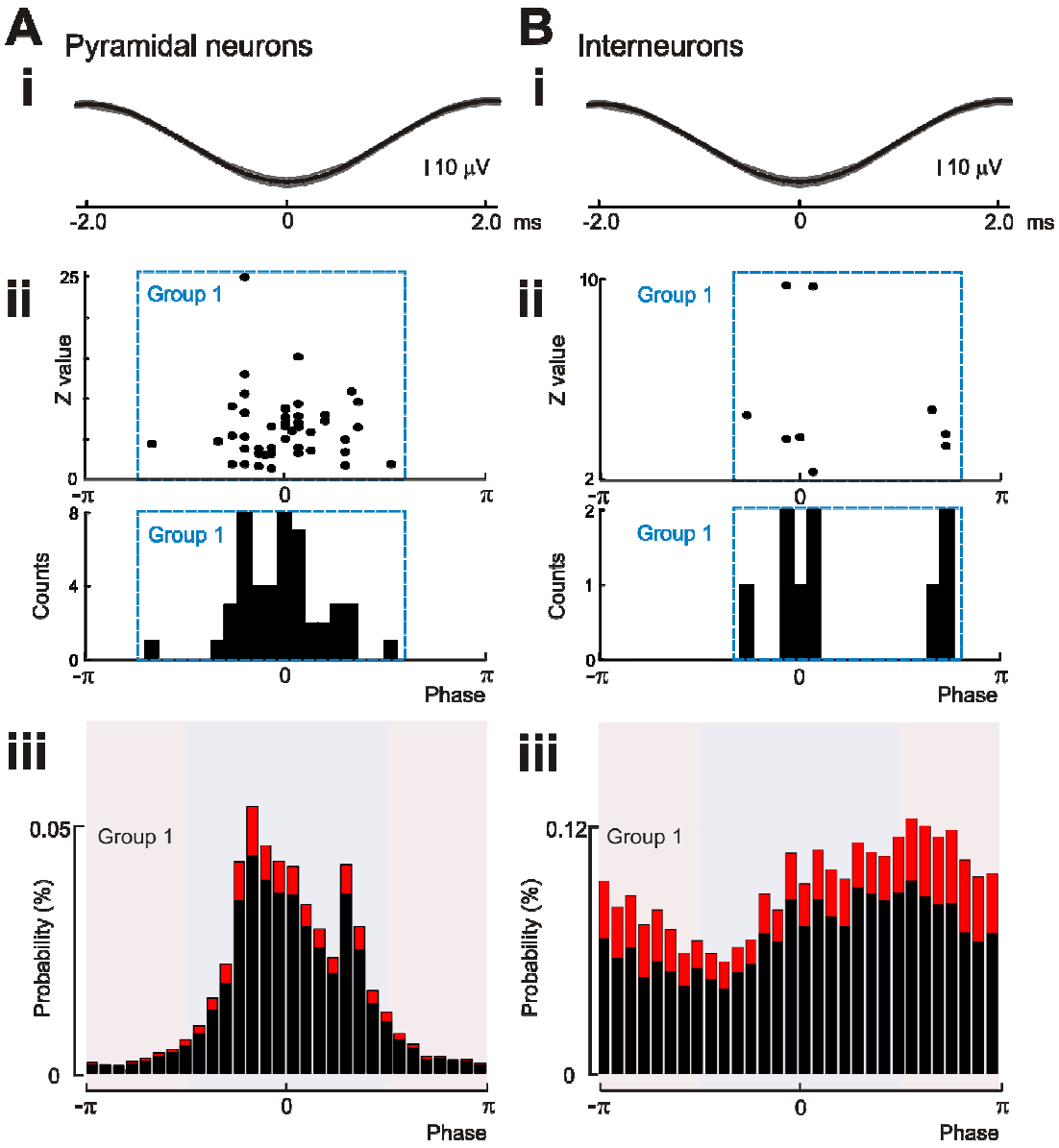
A
Pyramidal neurons
i
10 μV
-2.0
0
2.0 ms
ii
Group 1
Z value
25
0
-π
0
π
Group 1
Counts
8
4
0
-π
0
π
Phase
iii
Group 1
0.05
Probability (%)
0
-π
0
π
Phase
B
Interneurons
i
10 μV
-2.0
0
2.0 ms
ii
Group 1
Z value
10
2
-π
0
π
Group 1
Counts
2
1
0
-π
0
π
Phase
iii
Group 1
0.12
Probability (%)
0
-π
0
π
Phase

Figure R-16. Temporal correlations between neuronal activities and the HFA in lesioned CA1. **A***i*, an averaged 100-300 Hz band-passed HFA waveform which shows one cycle only (gray traces present the standard errors); *ii*, *top panel*, a scatter plot comprises the mode of the phase cross-correlation between unit activity and the HFA (x-axis) and the Z value derived from uniform test (y-axis); every dot represents a neuron (n=47); *ii*, *bottom panel*, cumulative numbers of neurons in every mode of phases; the blue dashed boxes indicate the group into which the pyramidal neurons were statistically classified; *iii*, averaged phase cross-correlation histogram shows the group of pyramidal neurons increased their firing rates during the trough of HFA (n=46; one neuron was discarded because it showed uniform cross-correlation to the HFA; the trough is shaded with light blue). **B***i*, a cycle of averaged 100-300 Hz band-passed HFA waveform; *ii*, *top panel*, a scatter plot comprises the mode of the phase cross-correlation and the Z value; nine interneurons are included; *ii*, *bottom panel*, cumulative numbers of neurons in every mode of phases; the dashed boxes indicate the one group into which interneurons were statistically pooled; *iii*, averaged phase cross-correlation histogram shows that interneurons (n=9) increased their firing rates

on the rising phase of the HFA.

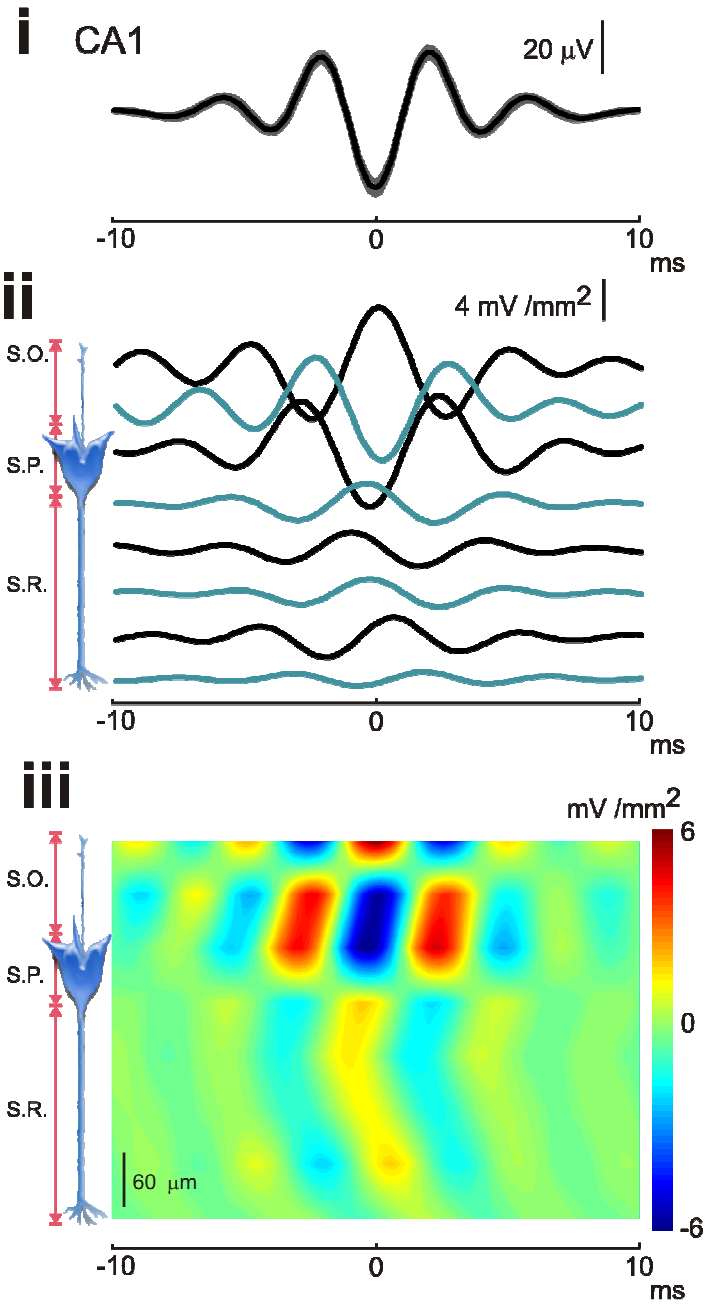
i
CA1
20 μV
-10
0
10
ms
ii
4 mV /mm2
S.O.
S.P.
S.R.
-10
0
10
ms
iii
mV /mm2
6
0
-6
S.O.
S.P.
S.R.
60 μm
-10
0
10
ms

Figure R-17. CSD of the HFA in lesioned CA1. *i*, the averaged 100-300 Hz band-passed waveform of the HFA from CA1 in lesioned slices; *ii*, an averaged CSD of the HFA acquired from CA1 in a lesioned slice, which is averaged according to the most negative troughs of the HFA in stratum pyramidale; *iii*, CSD colour map indicates that the HFA in the lesioned slice also originates from stratum pyramidale and propagates toward stratum oriens and stratum radiatum.

Temporal profile of the neuronal activity during interictal periods after the Schaffer collateral pathway was lesioned

Neuronal firing pattern from thirty-six pyramidal neurons and four interneurons during the normalized interictal periods in the lesioned slices were analysed (Figure R-18A). The trend for firing probability of pyramidal neurons was consistent in the lesioned slices and can be fitted with a linear and a quadratic regression (R squares=0.92 and 0.98, Figure R-18B, *top*). The suppression of the neuronal activity of pyramidal neurons after the previous seizure in the lesioned slices was significantly weaker than that in intact slices ($p<0.05$). The trend of interneuronal activity was not consistent and poorly fitted a linear or a quadratic regression (R squares=0.63 and 0.82, Figure R-18B, *bottom*).

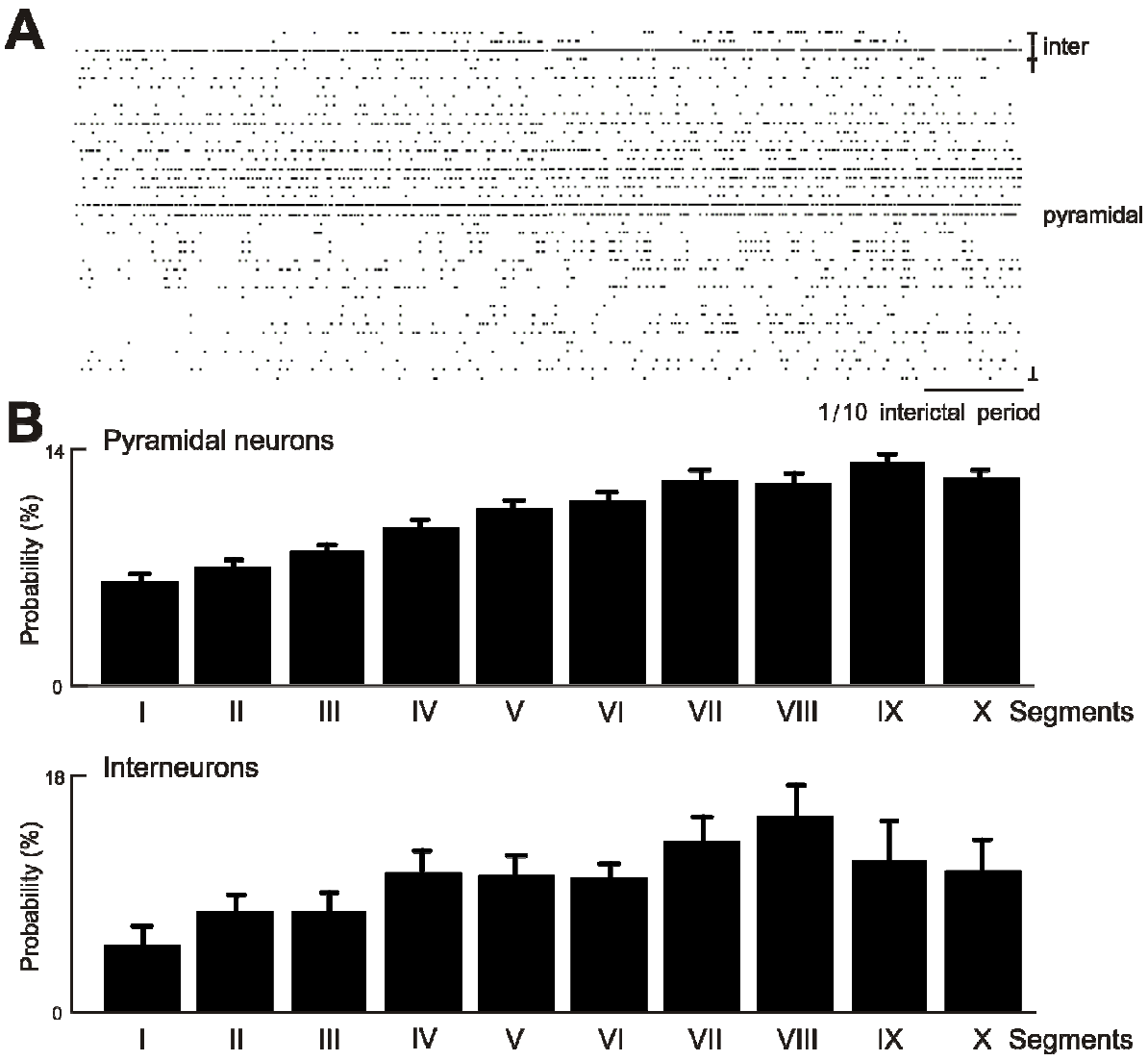
A
inter
pyramidal
1/10 interictal period
B
Pyramidal neurons
14
0
Probability (%)
I
II
III
IV
V
VI
VII
VIII
IX
X
Segments
Interneurons
18
0
Probability (%)
I
II
III
IV
V
VI
VII
VIII
IX
X
Segments

Figure R-18. Unit activities during the interictal periods in CA1 of lesioned slices. **A**, a scatter plot presents unit spikes during the interictal periods in lesioned slices (neurons=40). Cellular types are labeled at the right end. **B**, firing probabilities of the pyramidal neurons and interneurons during the interictal periods. Pyramidal neurons (neurons=36) present an increasing firing probability during the interictal periods. Few interneurons were recorded and the trend of their firing probability is not clear (neurons=4).

Pharmacology of HFA

To further understand the modifications from the distal inputs by CA3 or local circuits in CA1 on the HFA formation and the epileptic features, the involvements of glutamatergic and γ-aminobutyric acid-ergic (GABAergic) receptors were investigated by applying antagonists for these receptors.

The HFA and epileptic features were induced by high K^+ ACSF and lasted 20 minutes at least before the drug tests. Recording of five minutes preceding drug tests was used as control. Thereafter high K^+ ACSF containing drugs were quickly switched. The hippocampal slices were perfused with these antagonists for ten minutes and the drugs were washed away by high K^+ ACSF without drugs for 20-30 minutes. Recordings during the last five minutes with drugs and the periods after 20 minutes wash were used for analyses of drugs' effects.

Involvement of NMDA receptors in HFA formation and epileptic features

The roles of N-methyl-D-aspartic acid (NMDA) receptors in the HFA formation or the epileptic features were tested by D-(-)-2-Amino-5-phosphonopentanoic acid (D-APV, 25 μM). When APV was applied to the intact slices, there was no clear electrographic change on the HFA (Figure R-19A), however it significantly increased the power of HFA (100-500 Hz) in CA1. After wash the power of HFA in CA1 showed no difference to that of control. (Figure R-19B, 8 slices, $p<0.05$). In CA3 of intact slices, APV also significantly increased the power of activities between 100-500 Hz; and the power of HFA was not reduced by wash (Figure R-19C, 12 slices, $p<0.05$). In five slices, both interictal discharges and seizures were weak under the control state; however after application of APV, typical tonic-clonic seizures or seizure-like bursts were induced (Figure R-19D*i*). In these experiments interictal discharges were first enhanced in CA3 region and then to CA1, and seizures were induced in CA1 (Figure R-19D*i* and D*ii*). Interictal discharges and seizures were removed in three of the five slices when we washed APV away, and these epileptic events persisted in the other two (Figure, R-18D*i* and D*iv*).

In lesioned slices APV did not cause clear changes in the morphology of the HFA in

both CA1 and CA3, and no seizure activity was induced by APV in CA1 of lesioned slices (Figure R-20A). The power of activities between 100 and 500 Hz was significantly enhanced in both CA1 (p<0.05) and CA3 (p<0.01) of lesioned slices. This higher power persisted but was not further enhanced after wash (Figure R-20B and C, 12 slices and 11 slices respectively from CA1 and CA3; p<0.05 or p<0.01 individually; comparisions were made by paired-t tests, thus although the means increased there was no significance between drug and wash groups).

The APV effect was poorly reversed in both CA1 and CA3 in lesioned slices and CA3 in intact slices, even in CA1 of intact slices the power of HFA after wash was not significantly different from that in control (but with higher mean with large standard error). Therefore we hypothesized that the HFA may have increased with time rather than as a result of the application of APV. To test the possibility, the baseline of the HFA was studied over the same period but no drug treatment on the slices. In intact slices, no significant change of the power in the HFA band (100-500 Hz) was found in CA1 after 10 minutes or after 15 minutes, which were the times relevant to the drug tests (Figure R-20D, 5 slices). Thus we concluded that the increase of power found under APV in CA1 of intact slices was a genuine effect of APV, and we hypothesised a systematic plasticity prevented the reversal of the HFA after washing. The

comparisons in CA1 of lesioned slices showed a significant increase after 10 minutes, and the power was enhanced further after another 5 minutes (Figure R-20E, 13 slices). Although the HFA which naturally developed with time did not reach the increasing level caused by APV in lesioned slices, this trend was not negligible. Thus we cannot conclude that the significance found under APV in CA1 of lesioned slices was fully due to blocking NMDA receptors.

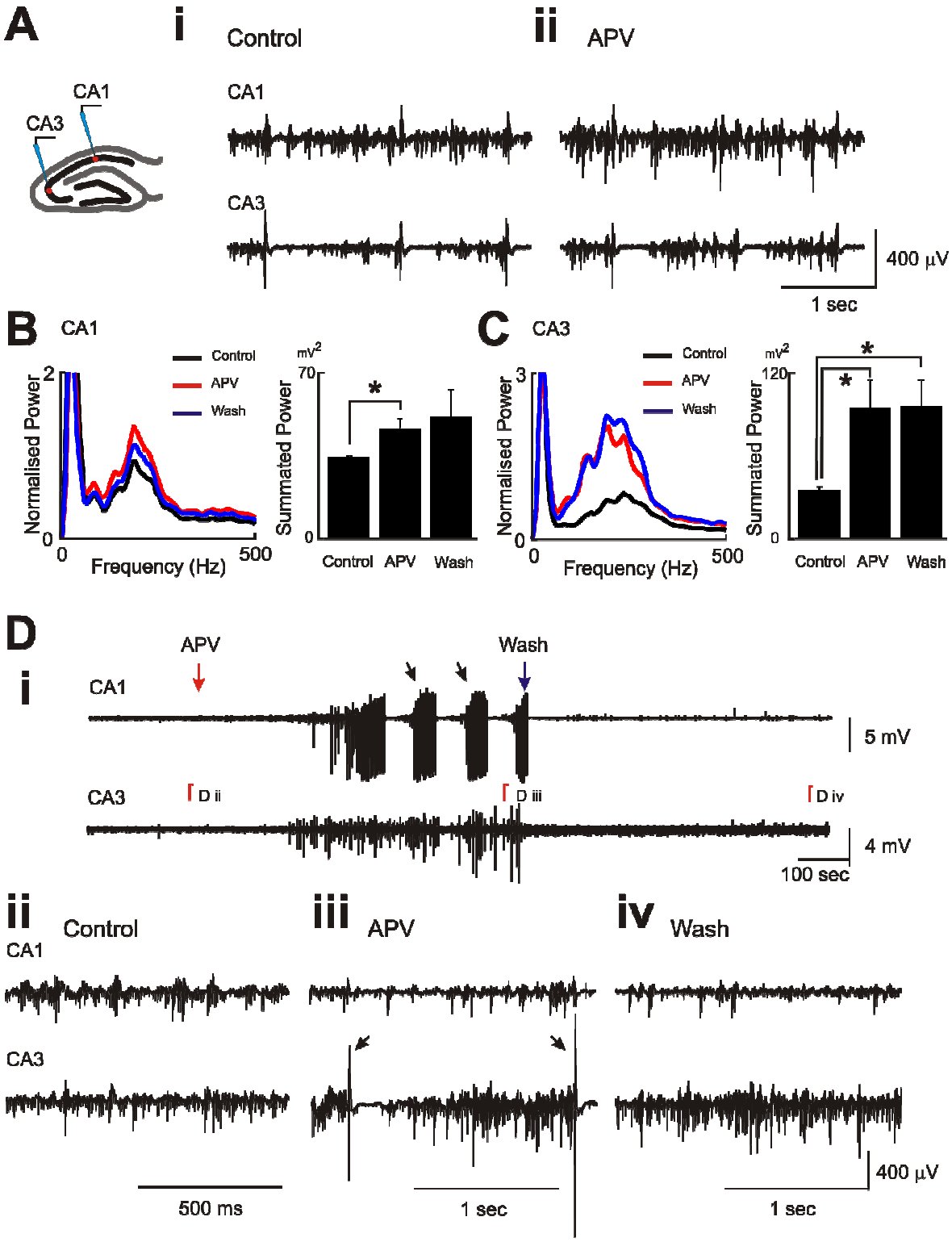
A
i
Control
ii
APV
CA1
CA3
CA1
CA3
400 µV
1 sec
B
CA1
Control
APV
Wash
Normalised Power
2
0
0
500
Frequency (Hz)
mV2
70
0
Summated Power
*
Control
APV
Wash
C
CA3
Control
APV
Wash
Normalised Power
3
0
0
500
Frequency (Hz)
mV2
120
0
Summated Power
*
*
Control
APV
Wash
D
i
APV
Wash
CA1
5 mV
CA3
D ii
D iii
D iv
4 mV
100 sec
ii
Control
iii
APV
iv
Wash
CA1
CA3
500 ms
1 sec
1 sec
400 µV

Figure R-19. APV effects on the HFA and the epileptic features in the intact slices. **A**, a schematic showing an intact slice and two electrodes in CA1 and CA3 individually; *i*, control recordings (>10 Hz) from both regions showing interictal discharges and the HFA; *ii*, recordings while APV (25 μM) was applied. **B**, APV effects on the HFA in CA1; *left*, normalised power spectra from eight slices in control state (black), under APV (red) and after wash (blue); *right*, summated powers between 100 to 500 Hz shows activities were significantly enhanced by APV (*, $p<0.05$, 8 slices). **C**, APV effects on the HFA in CA3; *left*, normalised power spectra from twelve slices in control state (black), under APV (red) and after wash (blue); *right*, summated powers between 100 to 500 Hz shows activities were significantly enhanced by APV, and the effect was not washed out after (*, $p<0.05$, 12 slices). **D**, epileptic features induced by APV; *i*, continuous recordings (>10 Hz) of APV application from CA1 and CA3; complete tonic-clonic seizures (black arrows) were induced in CA1 and interictal discharges were induced in CA3 by APV; and the APV effect was removed after wash out; *ii*, HFA only in CA1 and CA3 in control state; *iii*, interictal discharges (arrows) were induced under APV; *iv*, interictal discharges were removed under wash but HFA was still robust.

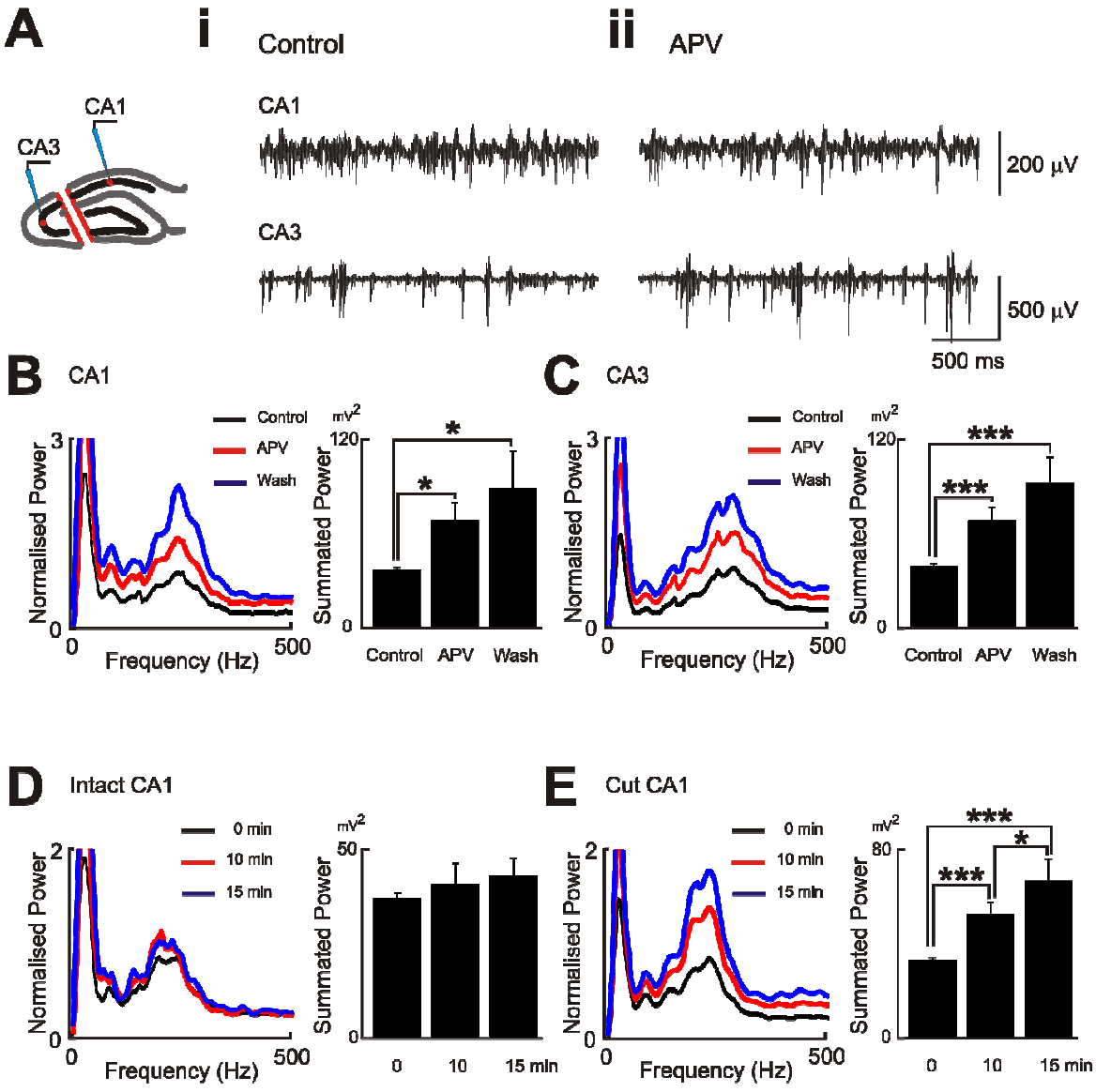
A
i
Control
ii
APV
CA1
CA3
CA1
CA3
200 µV
500 µV
500 ms
B
CA1
C
CA3
Control
APV
Wash
Normalised Power
Frequency (Hz)
Summated Power
mV2
Control
APV
Wash
D
Intact CA1
E
Cut CA1
0 min
10 min
15 min
0
10
15 min

Figure R-20. APV effects on the HFA in the lesioned slices and the long-term changes of the CA1 HFA in intact or lesioned slices. **A**, a schematic showing a lesioned slice and two electrodes in CA1 and CA3 individually; *i*, control recordings from both regions showing the HFA (>10 Hz); *ii*, recordings while APV (25 μM) was applied (>10 Hz). **B**, APV effects on the HFA in CA1; *left*, noramlised power spectra from twelve slices in control state (black), under APV (red) and after wash (blue); *right*, summated powers between 100 to 500 Hz shows activities were significantly enhanced by APV (*, $p<0.05$), and the APV effect was not washed away (*, $p<0.05$, 12 slices). **C**, APV effects on the HFA in CA3; *left*, normalised power spectra from eleven slices in control state (black), under APV (red) and after wash (blue); *right*, summated powers between 100 to 500 Hz shows activities were significantly enhanced by APV (***, $p<0.01$), and the APV effect was not washed away (***, $p<0.01$, 11 slices). **D**, long-term changes of HFA in intact slices; *left*, normalised power spectra from CA1 of five intact slices at time 0 (black), after 10 min (red) and 15 min after (blue); *right*, summated power (100-500 Hz) shows no difference between these three time points. **E**, long-term changes of HFA in lesioned slices; *left*, normalised power spectra from CA1 of 13 lesioned slices at time 0 (black), after 10 min (red) and 15 min after (blue); *right*, summated power (100-500 Hz) indicates the significance on 10 min (***, $p<0.01$) and

the further increase (***, p<0.01 comparing to time 0; *, p<0.05 comparing to 10 min group, 13 slices).

Involvement of non-NMDA receptors in HFA formation and epileptic features

The involvement of non-NMDA receptors in the HFA formations or the epileptic features were tested by 2,3-Dioxo-6-nitro-1,2,3,4-tetrahydrobenzo -[f]quinoxaline-7-sulfonamide (NBQX) disodium salt (20 μM). NBQX was first applied together with APV in intact slices. For those five intact slices (from 12 slices in total) showing only the HFA and interictal discharges under the control state, the combination of APV and NBQX clearly changed the morphology of the HFA into stronger and longer lasting clusters of neuronal bursts in CA1, and the HFA in CA3 was also changed; moreover the interictal discharges were abolished in both regions (Figure R-21A). However the changes of the electrographic patterns did not lead to a significance which can be identified by the test of summated power within the HFA band in CA1 (Figure R-21B, 5 slices). On the other hand, the HFA in CA3 was strongly suppressed by NBQX accompanied with APV, and this drug effect was not removed by wash ($p<0.01$, Figure R21C, 8 slices).

For those seven intact slices (from 12 slices in total) with seizures in CA1 in the control state, the combination of NBQX and APV changed the CA1 tonic-clonic

seizures into seizures with only a tonic phase; and the loss of interictal discharges was also observed both in CA1 and CA3 (Figure R-21D*i*). Changes of seizures and interictal discharges by the NBQX-APV combination were not reversed on removing the drugs. HFA with fewer episodes and smaller amplitudes was observed between the seizures after application of NBQX and APV simultaneously (Figure R-21D*ii*, D*iii* and D*iv*). The summated power of the HFA between seizures was significantly depressed after NBQX and APV were applied, and this drug effect was not reversible (Figure R-21E, 7 slices, $p<0.01$).

For lesioned slices, NBQX was applied alone. NBQX electrographically reduced the HFA in both CA1 and CA3 (Figure R-22A), but induced bursting which resembled the tonic seizures found in CA1 of intact slices under NBQX and APV (Figure R-22A*i* and A*iv*). In these experiments, recordings from CA1 were conducted by either Pt/Ir electrodes or tetrodes. Because of their different sampling rates and the recording sensitivities, which directly affected the summated powers, data from these two different electrodes were analysed separately. In both data recorded by these two kinds of electrodes, the power of the HFA in CA1 was significantly reduced by NBQX, and there was no significance shown after wash comparing to the control by the slices recorded by Pt/Ir electrodes (Figure R-22B*i* and B*ii*, 10 slices by Pt/Ir electrodes and 5

slices by tetrodes individually, $p<0.05$). NBQX significantly reduced the power of the HFA in CA3, and no significance difference of the power was present after wash compared to that in control (Figure R-22C, 8 slices, $p<0.01$). In the slices showing tonic seizures in CA1 under the control state, NBQX switched the seizing pattern to briefer neuronal bursts (Figure R-22D, 4 slices).

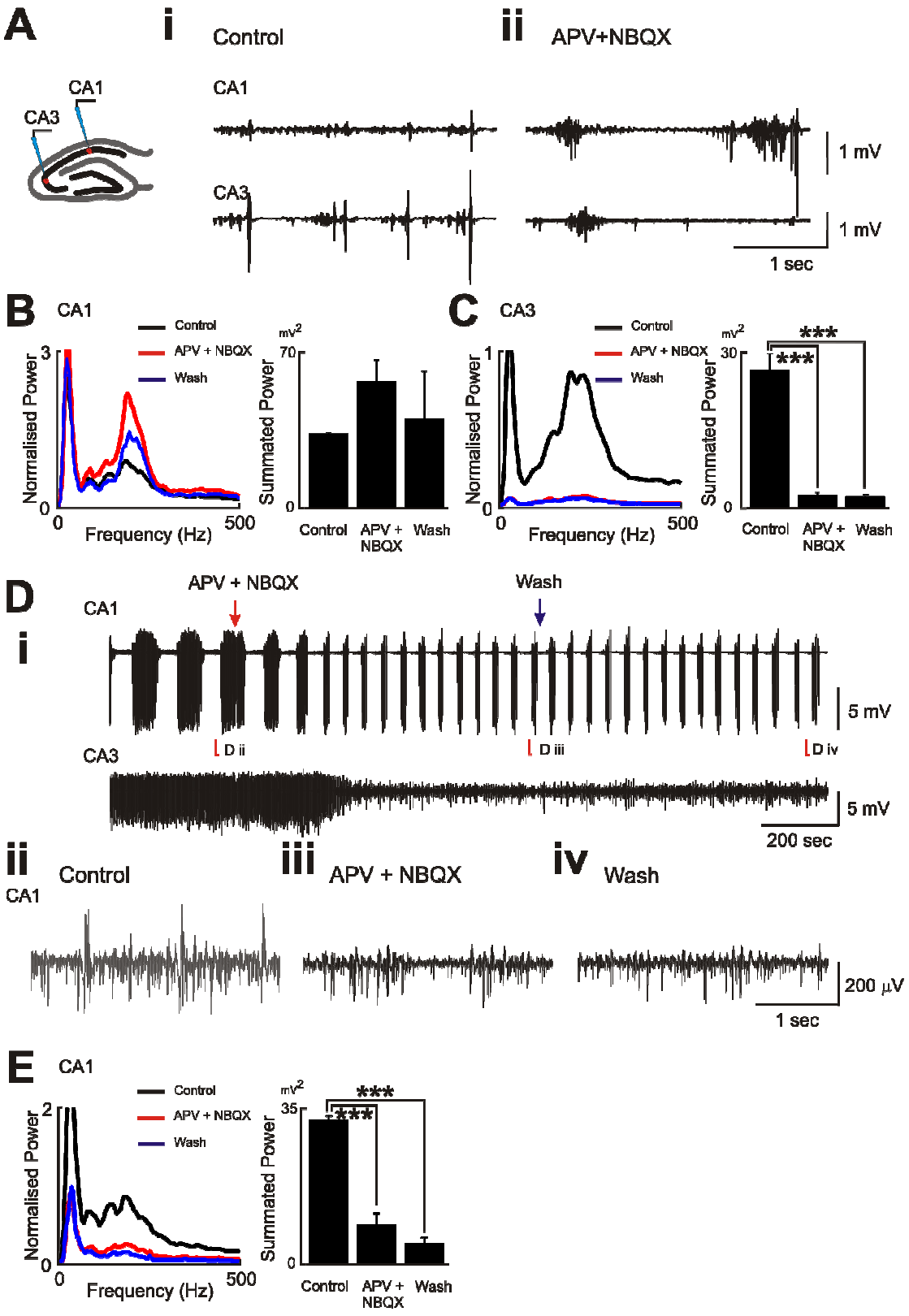
A
i
Control
ii
APV+NBQX
CA1
CA3
1 mV
1 mV
1 sec
B
CA1
Control
APV + NBQX
Wash
Normalised Power
Frequency (Hz)
Summated Power
mV2
Control
APV + NBQX
Wash
C
CA3
***
D
i
APV + NBQX
Wash
D ii
D iii
D iv
5 mV
200 sec
ii
Control
iii
APV + NBQX
iv
Wash
200 µV
1 sec
E

Figure R-21. APV and NBQX combined effects on the HFA and the epileptic features in the intact slices. **A**, a schematic showing an intact slice and two electrodes in CA1 and CA3 individually; *i*, control recordings from CA1 and CA3 show the interictal discharges and the HFA (>10 Hz); *ii*, recordings from CA1 and CA3 under APV (25 μM) and NBQX (20 μM) combination show a different burst firing (>10 Hz). **B**, the effect of APV accompanied with NBQX on CA1 activities in intact slices; *left*, normalised power spectra of five sliced in control state (black), when APV and NBQX applied together (red), and after wash (blue); *right*, summated powers (100-500 Hz) show no difference under introduction of APV and NBQX. **C**, the effect of APV and NBQX on CA3 activities in the intact slices; *left*, normalised power spectra from eight slices on the control state (black), application of APV and NBQX (red) and after wash (blue); *right*, summated powers (100-500 Hz) show the significant suppression under APV and NBQX (***, $p<0.01$), and the effect also remained after wash (***, $p<0.01$, 8 slices). **D**, effects of APV and NBQX combination on the intact slices; *i*, tonic-clonic seizures in CA1 were disturbed after application of APV and NBQX, and the activities in CA3 were dramatically reduced (both traces >10 Hz); HFA before the drugs (D*ii*), with the drugs (D*iii*) and after wash (D*iv*) are shown. **E**, the effects of APV and NBQX on the HFA in the intact slices with seizures; *left*, normalised power spectra of seven slices

with seizures in control state (black), under drugs (red) and after wash (blue); *right*, summated powers (100-500 Hz) show a significant reduction on the activities caused by APV and NBQX (***, $p<0.01$), and the activities were also suppressed after wash (***, $p<0.01$, 7 slices).

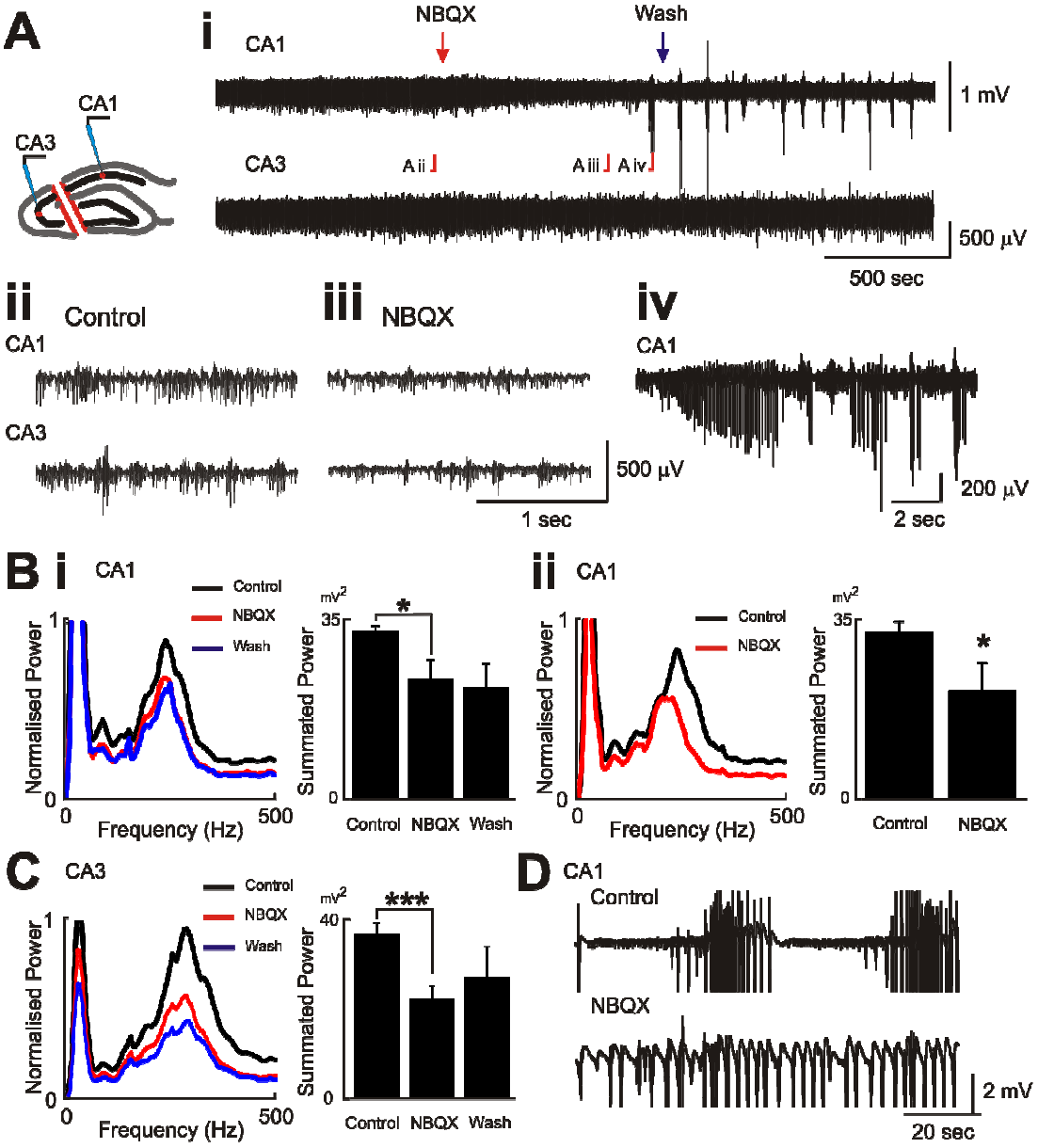
A
i
CA1
NBQX
Wash
CA1
CA3
1 mV
CA3
A ii
A iii
A iv
500 µV
500 sec
ii Control
iii NBQX
iv
CA1
CA1
CA3
500 µV
1 sec
200 µV
2 sec
B i CA1
Control
NBQX
Wash
Normalised Power
Frequency (Hz)
Summated Power
mV2
Control NBQX Wash
ii CA1
Control
NBQX
Normalised Power
Frequency (Hz)
Summated Power
mV2
Control NBQX
C CA3
Control
NBQX
Wash
Normalised Power
Frequency (Hz)
Summated Power
mV2
Control NBQX Wash
D CA1
Control
NBQX
2 mV
20 sec

Figure R-22. NBQX effects on the HFA and the epileptic features in the lesioned slices. **A**, a schematic showing a lesioned slice and two electrodes in CA1 and CA3 individually; *i*, NBQX (20 μM) reduced the activities in CA1 and later caused the burst firing, and the activities in CA3 was reduced by NBQX (both traces >10 Hz); the HFA in both CA1 and CA3 in lesioned slices under control state (*ii*) and after NBQX applied (*iii*) are shown respectively; *iv*, burst firing (or seizure-like activities) were induced in 2 of 10 slices. **B**, effect of NBQX on the HFA in CA1 of lesioned slices; *i*, recorded by Pt/Ir electrodes; *left*, normalised power spectra of the CA1 activities from ten slices under control (black), by NBQX (red) and after wash (blue); *right*, summated powers (100-500 Hz) show the activities were significantly suppressed by NBQX (*, $p<0.05$, 10 slices); *ii*, recorded by tetrodes; *left*, normalised power spectra of CA1 activities in five lesioned slices under control state (black) and under NBQX (red); *right*, summated powers (100-500 Hz) present the significant suppression by NBQX (*, $p<0.05$, 5 slices). **C**, NBQX effects on the HFA in CA3 of lesioned slices; *left*, normalised power spectra of eight lesioned slices under control (black), NBQX (red), and after wash (blue); *right*, summated powers (100-500 Hz) indicate the significant suppression induced by NBQX (***, $p<0.01$, 8 slices). **D**, change of the seizing patterns by NBQX (wide-band recordings, 4 slices).

Involvement of $GABA_A$ receptors in HFA formation and epileptic features

The involvement of $GABA_A$ receptors in the HFA formations or the epileptic features were tested by (-)-Bicuculline methiodide (5 μM). Global excitation of the neurons due to blocking inhibitory receptors was predicted. To prevent over-excitation or spreading depression, slices used for bicuculline tests were perfused with ACSF containing less potassium: in general 6mM potassium or less in the ACSF can induce the HFA, and no interictal discharges or seizures were observed. In intact slices, application of bicuculline strongly induced neuronal bursts from the control state which showed HFA only (Figure R-23A*i* and A*ii*). These new neuronal bursts: 1) were as strong as the clonic part of the seizures we observed in CA1 of intact slices perfused with high K^+ ACSF alone; 2) they fired synchronously between CA1 and CA3 which resembled the characteristic of the interictal discharges, and originated from CA3 as well; 3) several after discharges were present in CA1 (Figure R-23A*ii* and A*iii*). However the HFA were still present and even enhanced between the large neuronal bursts (Figure R-23A*iii*). Corresponding to the dramatic changes seen from the electrographic patterns, significant enhancement of the HFA was also observed from CA1 and CA3 in terms of their power summated in HFA band (Figure R-23B*i* and B*ii* for CA1, 9 slices; Figure

22C*i* and C*ii* for CA3, 6 slices; $p<0.05$). The bicuculline effect can be removed by wash, which was showed by the drop in the summated powers. Previously we hypothesised that the inhibitory circuit may be important in HFA modulation, thus blocking the $GABA_A$ receptors, which represented the majority inhibitory circuit in hippocampus, would be predicted to change the frequency of the HFA. Thus the frequency spread of the HFA under bicuculline was tested. According to the first moment analyses of the frequency spread in the HFA band (100-500 Hz), bicuculline significantly move the distributions of the activities to lower frequencies in both CA1 and CA3 ($p<0.05$, Figure R-23 B*iii* and C*iii*).

In a separate series of experiments bicuculline was applied to lesioned slices. The bicuculline-induced large neuronal bursts present in the intact slices were also observed in the lesioned slices after adding bicuculline. However because the connection between CA1 and CA3 was removed, the synchronisation between the two regions was gone (Figure R-24A). The changes induced by bicuculline were verified by summated power in 100-500 Hz, and no significance between the summated powers of the HFAs was found after introduction of bicuculline (Figure R-24B*i* and B*ii*; Figure R-24C*i* and C*ii*; 6 slices from both CA1 and CA3). Moreover, no significant decrease in the first moment analyses was observed from control to

bicuculline treatment in CA1 or CA3. However a discrepancy of the first moments was present in CA1 between the state of bicuculline and after wash, thus alternatively we believed bicuculline still changed the frequency spread of HFA to lower frequencies.

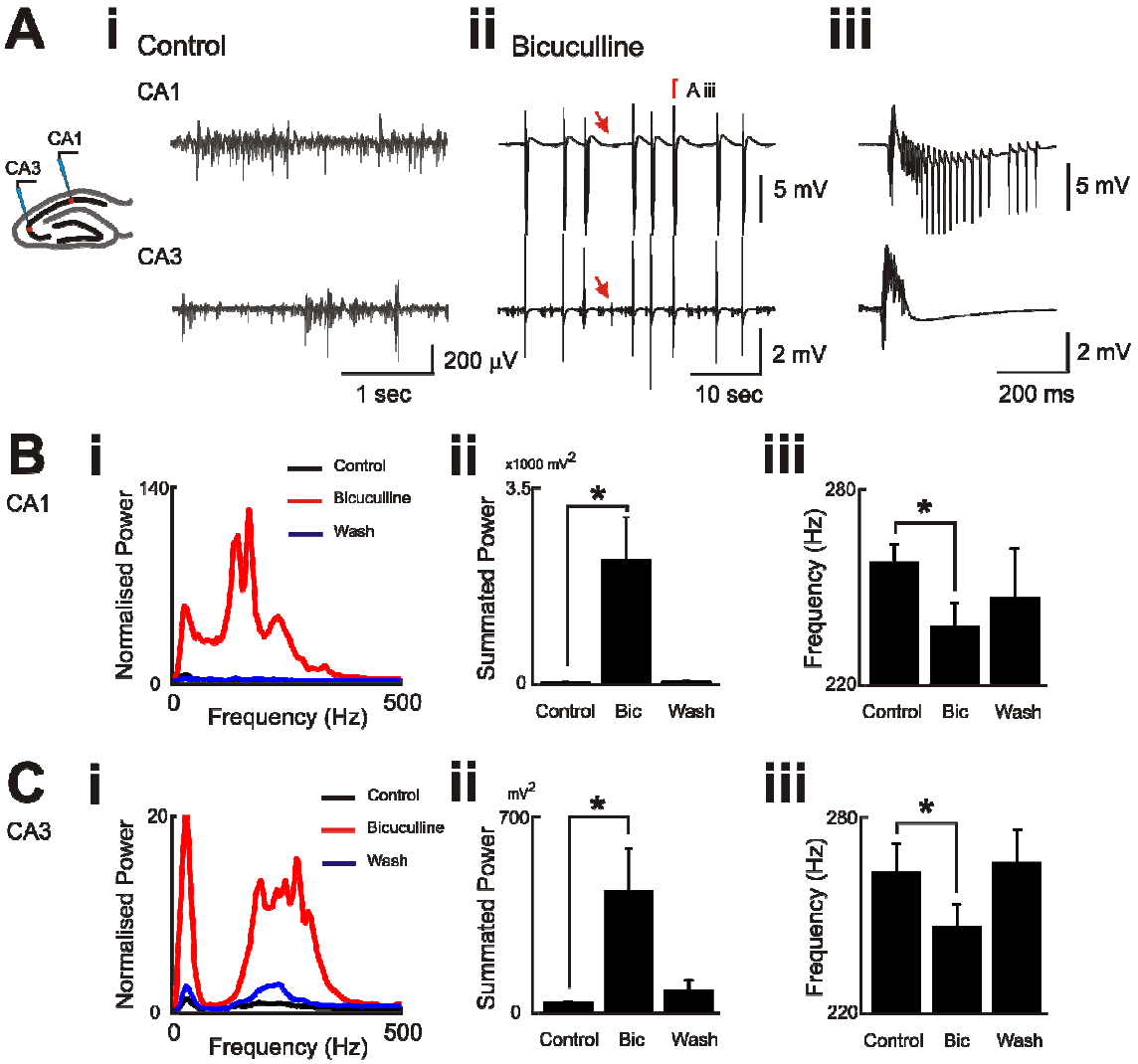
A
i Control
ii Bicuculline
iii
CA1
CA3
CA1
CA3
A iii
5 mV
5 mV
200 µV
1 sec
2 mV
10 sec
2 mV
200 ms
B
CA1
i
Control
Bicuculline
Wash
Normalised Power
140
0
0
500
Frequency (Hz)
ii
x1000 mV2
3.5
0
Summated Power
*
Control
Bic
Wash
iii
280
220
Frequency (Hz)
*
Control
Bic
Wash
C
CA3
i
Control
Bicuculline
Wash
Normalised Power
20
0
0
500
Frequency (Hz)
ii
mV2
700
0
Summated Power
*
Control
Bic
Wash
iii
280
220
Frequency (Hz)
*
Control
Bic
Wash

Figure R-23. Effect of bicuculline on the HFA and the epileptic features in intact slices. **A**, a schematic showing an intact slice and two electrodes in CA1 and CA3 individually; *i*, the HFA of CA1 and CA3 on control state (>10 Hz); *ii*, bicuculline (5 μM) induced strong burst firing in both regions as shown in the wide-band recordings and the HFA was still present (red arrows); *iii*, expanded bursting firing from Aii. **B**, bicuculline effects on the activities in CA1 of the intact slices; *i*, normalised power spectra of CA1 activities from nine slices under control (black), bicuculline (red), and after wash (blue); *ii*, summated powers (100-500 Hz) show the significant enhancement of activities caused by bicuculline (*, $p<0.05$, 9 slices); *iii*, first moment analysis (100-500 Hz) indicates that bicuculline brought the activities to a new distribution on lower frequency (*, $p<0.05$, 9 slices). **C**, bicuculline effects on the activities in CA3 of the intact slices; *i*, normalised power spectra of CA3 activities from six slices under control (black), bicuculline (red), and after wash (blue); *ii*, summated powers (100-500 Hz) show the significant enhancement of activities caused by bicuculline (*, $p<0.05$, 6 slices); *iii*, first moment analysis (100-500 Hz) indicates that bicuculline brought the activities to a new distribution on lower frequency (*, $p<0.05$, 6 slices).

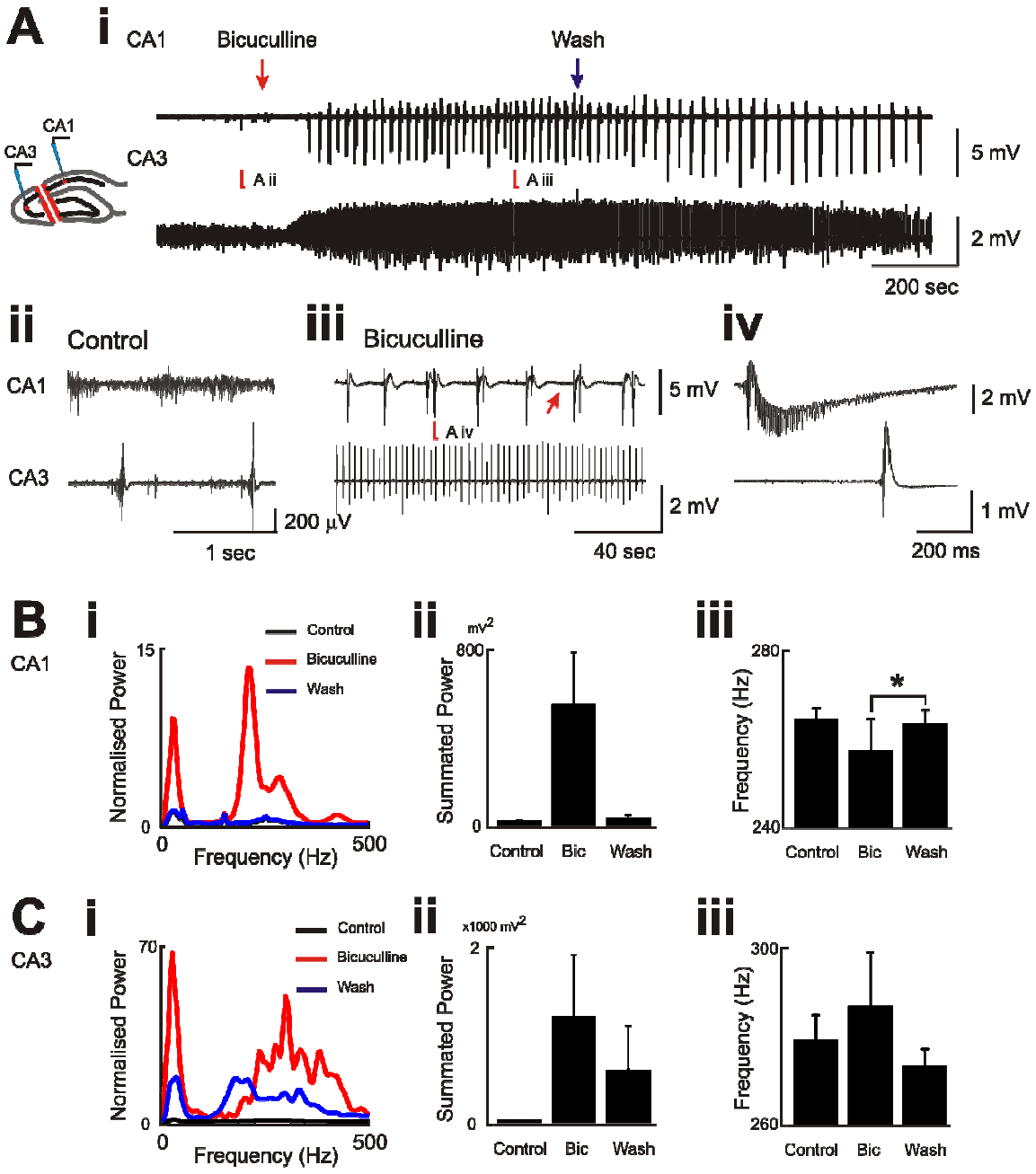
A
i
CA1
Bicuculline
Wash
CA1
CA3
CA3
A ii
A iii
5 mV
2 mV
200 sec
ii
Control
iii
Bicuculline
iv
CA1
CA3
5 mV
A iv
2 mV
200 µV
1 sec
40 sec
2 mV
1 mV
200 ms
B
i
CA1
Control
Bicuculline
Wash
Normalised Power
15
0
0
500
Frequency (Hz)
ii
mV2
800
Summated Power
0
Control
Bic
Wash
iii
280
Frequency (Hz)
240
*
Control
Bic
Wash
C
i
CA3
Control
Bicuculline
Wash
Normalised Power
70
0
0
500
Frequency (Hz)
ii
x1000 mV2
2
Summated Power
0
Control
Bic
Wash
iii
300
Frequency (Hz)
260
Control
Bic
Wash

Figure R-24. Effect of bicuculline on the HFA and the epileptic features in lesioned slices. **A**, a schematic showing a lesioned slice and two electrodes in CA1 and CA3 respectively; *i*, bicuculline (5 μM) induces burst firing in the CA1 of the lesioned slices, and it enhanced the activities in the CA3 (wide-band raw traces); *ii*, the HFA in CA1, and interictal discharges and the HFA in CA3 on control state; *iii*, bicuculline induced strong burst firing in both regions and the HFA was still present in CA1 (wide-band, red arrow); *iv*, expanded bursting firing from Aiii. **B**, bicuculline effects on the activities in CA1 of the lesioned slices; *i*, normalised power spectra of CA1 activities from six slices under control (black), bicuculline (red), and after wash (blue); *ii*, summated powers (100-500 Hz) under the three states, and no significance is observed (6 slices); *iii*, first moment analysis (100-500 Hz) indicates that bicuculline brought the activities to a new distribution on lower frequency while it compared to the wash group (*, $p<0.05$, slices=6). **C**, bicuculline effects on the activities in CA3 of the lesioned slices; *i*, normalised power spectra of CA3 activities from six slices under control (black), bicuculline (red), and after wash (blue); *ii*, summated powers (100-500 Hz) show no significance caused by bicuculline (slices=6); *iii*, first moment analysis (100-500 Hz) indicates no change on frequency distribution of the activities by bicuculline (6 slices).

Discussion

HFA and electrographic seizures were induced by high K^+ ACSF in rat hippocampal slices. HFAs were observed in the pyramidal layer from CA1 to CA3 sub-regions with different frequencies during the interictal periods, and interictal discharges were present in these periods. Seizures in our model were present in CA1 only and comprised tonic and clonic phases. We concluded that the HFA was mainly generated by the synchronous firing of pyramidal neurons; though some of the interneurons participate in the HFA formation either by co-firing with pyramidal neurons or by lag-firing after pyramidal neurons to recurrently modify the HFA. Build-ups of the HFA and unit activities preceded the seizure onsets; however the trends of the build-ups were not continuous. Our results demonstrated that, the interictal discharges interfered with the neuronal activities within wide frequency band in both CA1 and CA3 and the lengths of the refractory periods were different between these two regions. Lesions of the Schaffer collateral pathway shortened the lengths of interictal periods but also abolished the clonic part of the epileptic bursts. Furthermore, the HFAs in the lesioned slices shifted to faster frequencies and the build-ups of the HFA and the unit activities were more robust and developed without suppression preceding

seizures. Thus we suggest that the interictal discharges can modulate the seizure genesis by affecting the formation of the HFA. Glutamatergic or GABAergic blockers did not abolish the HFA but could modify the power of the HFA. Thus the HFA is independent of synaptic mechanisms, however either the local inhibitory circuits or the distal inputs (from CA3 to CA1) can adjust the strength of the HFAs and further might affect the seizure genesis.

Mechanisms for the HFAs

HFA in our high K^+ model starts with a current sink constrained in the pyramidal layer, and the trough of the HFA is correlated with increase of firing probabilities for pyramidal neurons and a subset of interneurons. These results suggested the HFA originates from synchronous firing of mainly pyramidal neurons and some interneurons. Although HFAs were also superimposed on the interictal discharges, most of them occurred without interictal discharges and even a slow deflection of field potential was not observed in the stratum radiatum (data not shown). Furthermore, after a lesion of the Schaffer collateral pathway the HFA persisted in CA1. Moreover, the HFA started earlier than interictal discharges after we increased K^+ concentration. Therefore our finding suggested the HFA can be fully independent of the distal synaptic inputs (e.g. CA3 to the HFA in CA1) and even the local synaptic circuits are less essential for HFA initiation. Our results were consistent with the hypothesis derived from the low Ca^{2+} model that synchronous firing of neurons is due to non-synaptic mechanisms to form HFA, and these non-synaptic mechanisms might be also applicable in the high K^+ model (Jiruska et al., 2010a). In the two models, neurons were tonically excited either by altering the ion gradient across cell

membrane (high K^+) or by removing the divalent cationic shielding (low Ca^{2+}). The spontaneous action potentials from the hyper-activated neurons might further induce co-firing in the neighboring regions by non-synaptic mechanisms (Bikson et al., 2003;Draguhn et al., 1998;Jefferys, 1995;Jefferys and Haas, 1982;Traub et al., 2001;Traub, 2003). In addition, because of the particular cellular architecture in hippocampus, the ephaptic and the electrical field interactions are well-placed to generate neuronal synchronisations (Jefferys, 1995). In this environment even the interneurons in pyramidal layer sharing the similar cellular orientation and positions as pyramidal neurons can be involved in the synchronisation, as we observed a group of interneurons was firing during the trough of the HFA without delay.

Synaptic transmission may not be necessary for HFA formation, but the HFA is substantially modulated either by the local circuits or distal inputs. In the pyramidal layers of the intact and lesioned slices the HFA was superimposed on a positive slow component of field potential present. The current sink of the HFA is quickly followed by a current source which corresponded to the rising phase of the HFA. Comparing to the CSD of the HFA observed in low Ca^{2+} model that no manifest current source followed current sink in pyramidal layer (Jiruska et al., 2010a), this current source here is approximately as strong as the sink. Thus we suggested that the current source may

be as important as the current sink in the formation of the HFA in the high K^+ model. Three mechanisms might contribute to the current source in the pyramidal layer: 1) an intrinsic hyperpolarisation after action potentials from the current-sink-contributing neurons; 2) a passive source caused by a current sink in the surrounding dendrites (like depolarisations of the basal dendrites); or 3) an IPSP of the somata generated by interneurons. Our results did not determine the contributions from each of these origins. However the different firing timings for interneurons made us believe that at least one type takes part in the HFA modulations, and this modulation initiated locally since the lag firing of the interneurons persisted in the lesioned slices.

Although interneurons are just a minority of neurons (~10 %) in the hippocampus, because of their 400-800 μm long axonal extent the inhibition can constrain the activities of principal cells in a very wide range (*in vivo*); and indeed each interneuron forms synapses on thousands of pyramidal neurons, while the pyramidal neurons reciprocally innervate hundreds of interneurons in hippocampus (Buhl et al., 1994;Freund and Buzsaki, 1996;Sik et al., 1995). Thus inhibitory circuits are very prevalent in the hippocampus, as many physiological oscillations, like theta (~10 Hz), gamma (40-100 Hz) and sharp wave ripples (>100 Hz), are related to these inhibitory systems (Freund and Buzsaki, 1996;Klausberger and Somogyi, 2008;Ylinen et al.,

1995). However here we suggested another driver for the HFA formation in our model. Unlike the mechanisms for physiological oscillations that inhibitory circuits are crucial and excited by distal excitatory inputs, the interneurons in our model might fire at the same time as most of the pyramidal neurons through the non-synaptic interactions, and further cause the postsynaptic hyperpolarisations in the pyramidal layer, which are also responsible for the rising phase of the HFA.

Tetrodes were placed in stratum pyramidale during the experiments thus the groups of interneurons we recorded in this study might be assumed as: axo-axonic (chandelier) cells, basket cells, bistratified cells (Klausberger and Somogyi, 2008;Sik et al., 1995). These three types of interneurons are all innervated by distal CA3 inputs and also they can be activated by CA1 pyramidal neurons (Ali et al., 1998;Klausberger and Somogyi, 2008). Our results distinguished the interneurons in two groups in the intact slices and a group only in the lesioned slices by their firing phases correlated to the HFA, but without intracellular recording or morphological information we could not identify which kind of interneuron is categorised in each firing phase or whether they can present both firing correlations. However according to our CSD we could only suggest: 1) the basket cells may contribute the current source for the rising phase of the HFA in the pyramidal layer; 2) the axo-axonic cells and

bistratified cells might generate the source in stratum oriens when the HFA starts with a sink in stratum pyramidale. The alveus/oriens interneurons are innervated by CA1 pyramidal neurons and might be also involved in the modification of the HFA (Sik et al., 1995), but the possible involvement of this interneuron in the HFA was eliminated in this study because of our recording locations.

Region specificity of the HFAs and the interictal discharges

In the high K^+ hippocampal model the frequency of HFA in CA1 (mean of 186 Hz) was slower than that in CA3 (mean of 240 Hz), and the dominant frequencies were consistent in each sub-region but changed promptly at the boundary between the sub-regions as we observed from the spatial power spectra (Figure R-07B). After lesion of the Schaffer collateral pathway, the frequency of the HFA in CA1 significantly moved to a faster rhythm (mean of 234 Hz) but the dominant frequency in CA3 persisted (mean of 249 Hz). There was no significant cross-correlation of the HFA from these two regions in our preliminary tests (data not shown). Thus we concluded that CA3 can modify the HFA in CA1 in form of interictal discharges, although the CA3 inputs are not essential for the HFA initiation in CA1.

In studies of behaving rats, when the subjects were awake sharp waves are associated with consummatory behaviors, like eating or drinking; but generally no *in vivo* behavioural correlate of interictal discharges was reported (Buzsaki, 1986;Buzsaki et al., 1992;Ylinen et al., 1995). However the interictal discharges and the sharp wave became even more ambiguous especially when the subjects were asleep or immobile, and they were roughly distinguished by amplitudes (Bragin et al.,

1999b). Therefore, singular potential deflections as what we described in current model were also studied in other hippocampal slice experiments as the *in vitro* sharp waves, even though the experimental conditions (high K^+ with or without low Ca^{2+}) were not “physiological” at all (Behrens et al., 2005;Foffani et al., 2007;Maier et al., 2003). Fortunately, in our study these abrupt potential deflections were present between seizures though they were also present in CA3, and thus they can be classified as “interictal discharges”. The interictal discharges arose from CA3b or CA3c sub-regions; and then they caused current sinks, which were presumably depolarisations, lasting tens of milliseconds in the stratum radiatum in CA1 region and started CA1 interictal discharges with smaller amplitudes. The causality for the interictal discharges in CA1 in this model is similar to the physiological sharp wave (Buzsaki, 1986) thus the mechanisms for the physiological ripple might be applied on the HFA: during every interictal discharge the CA1 pyramidal neurons and interneurons are both intensely excited, however only the hyper-synchronous firing of the pyramidal neurons can overcome the inhibition. The HFA during interictal discharges may be stronger and slower than the HFA at other times during the interictal periods, perhaps because of the synaptic depolarization responsible for the former. Thus after removing the CA3 inputs, the HFA in CA1 is generated by the local

circuits and non-synaptic mechanisms alone, with a faster frequency and weaker synchronisation.

Even without the interictal discharges, the HFA in CA1 was significantly slower than that in CA3 in the lesioned slices, as shown by our first moment analyses. The regional difference in the physiological ripples between CA1 and CA3 was also observed *in vivo*, and the reasons were not explored (Buzsaki 1992 and Ylinen et al. 1995). Here we suggest an answer based on non-synaptic mechanisms for the HFA formation. The cell bodies of CA3 principal cells are much bigger than CA1 pyramidal neurons. Furthermore, CA1 pyramidal neurons extend longer and thinner apical dendrites with more regular branches (Johnston and Amaral, 2003). In addition to these morphological characteristics of individual cells, the cellular architecture in CA1 is more compact (Jinno and Kosaka, 2010) and has a more compressed interstitial space, where the ephaptic interaction or electrical fields might work more efficiently than in CA3 to produce synchronisation (Jefferys, 1995). These differences could explain the slower frequency of HFA in CA1 we observed. Other differences between the cells from these two regions, such as membrane conductance, the density and/or the properties of the channels might be related to the distinct rhythms of the HFA from CA1 and CA3 (Johnston and Amaral, 2003;Jonas and Sakmann, 1992;Klee et al.,

1995;Spruston et al., 1995). Furthermore we also wondered whether these intrinsic properties for synchronization are also essential for the seizure genesis, since we observed seizures only in CA1 region in our model.

Interestingly, after the lesion between CA1 and CA3, the first moment for the CA3 HFA had significantly increased from 252 Hz to 281 Hz showing that the HFA in CA3 comprise more components in higher frequency after lesions. If this transformation implied a reduction in synchronisation, we suggested the reasons that: 1) CA1 could be a source of accumulated K^+ due to intense neuronal firing, and removing CA1 might withdraw K^+ flow to CA3 thus the neuronal activities and synchronisation may both decrease; 2) back-projection interneurons in CA1 alveus/oriens layer might be activated in phase with the rhythms of local HFA, and thus deliver same firing pattern back to CA3 to modulate the HFA in CA3 (Sik et al., 1994;Sik et al., 1995); once the modulation was deprived, the synchronisation in CA3 thus reduced and presented an intrinsic and faster HFA.

HFA in high K^+ model and in other models

The physiological ripples were present around 150 Hz in rodents and 110 Hz in humans (Bragin et al., 1999b;Buzsaki et al., 1992;Ylinen et al., 1995); but the pathological fast ripples either observed in the kainic acid induced lesional, tetanus toxin induced non-lesional chronic epileptic animal model or in patients were between 250-500 Hz (Bragin et al., 1999b;Bragin et al., 2002b;Bragin et al., 2004;Jiruska et al., 2010b). Thus this discrepancy led to a misunderstanding that (Engel et al., 2009) their dominant frequencies alone reflect the roles of the HFAs in the subjects, where HFA at faster frequency (250-500 Hz) is epileptogenic but that in slower frequency is normal (100-250 Hz). However, this present work and our recent study all demonstrated the HFAs in 100-250 Hz *in vitro*; and their epileptogenic importance was clear because the lower frequency HFAs were strongly related to the seizure onsets (Jiruska et al., 2010a). Thus we question whether the dominant frequency of the HFA is the crucial variable in epileptogenesis.

Gradual developments of sclerosis and mossy fiber sprouting are associated with epileptogenesis before spontaneous seizures develop in clinical or in chronic animal models, and thus these two hallmarks were traditionally believed to be related to

epileptogenesis (Chevassus Au Louis et al., 1997;Jefferys, 1999). In addition, neuronal loss and sprouting fibers were also observed in kainic acid induced epileptic models, in which the pathological HFA around 400 Hz was present; on the contrary HFA around 200 Hz was demonstrated in hippocampal slices from normal rats as we showed in the study. In this decade *in vitro* and *in vivo* evidence suggested that the sprouting fibers are not essential for the initiation of the pathological HFA, but it might expand the epileptogenic areas through the extensive connections (Bragin et al., 2000;Foffani et al., 2007). Alternatively, neuronal loss reduced the resistivity in the interstitial space and might decrease the ephaptic interaction thus neurons fired in less synchrony (Bragin et al., 2000;Foffani et al., 2007). Moreover, the reduction of the spike-timing reliability can disturb the synchronisation between neurons and further make the synchronous ripples decompose into faster oscillations (Foffani et al., 2007). However current findings in our lab suggested sclerosis is not prerequisite for high frequency activities in tetanus toxin induced non-lesional temporal lobe epilepsy model, although fossy fibre sprouting was robust in these epileptic animals (Jiruska et al., 2010b;Mitchell et al., 1996).

HFA and epileptic bursts were found in low Ca^{2+} hippocampal slice model, thus those non-synaptic interactions are sufficient to generate the neuronal synchrony and

seizures (Bikson et al., 2003;Jiruska et al., 2010a). When the synaptic transmission was intact in the high K^+ model, surprisingly we found the HFA was faster in the lesioned slices (234 Hz) than that in low Ca^{2+} model (185 Hz). It would be an interesting question whether the local inhibition disturbed the synchrony and thus decomposed HFA into fragments with faster frequency. In addition, we further wanted to study whether this inhibition is crucial in the seizure genesis since the HFA is highly modulated by the inhibitory circuits.

The discrepancy of HFAs found in our studies, epileptic animals or in patients might be due to the difference of model. In the high K^+ hippocampal slice model we can focus on only several possible circuits and mechanisms which might be responsible for seizure genesis. The simplicity of the brain slice models is also the drawback that we have to ignore the importance of long range afferents in seizure genesis and in HFA. Furthermore, the slice preparation disproportionately truncates excitatory and inhibitory inputs and makes brain slices ~4 times less excitable than that from in vivo (Stepanyants et al., 2009).

Build-up of the HFA, interictal discharges and seizure onset

Temporal build-up of the HFA was described in patients with mesial temporal lobe epilepsy or neocortical epilepsy (Khosravani et al., 2009;Worrell et al., 2004) and also in low Mg^{2+} brain slices model (Khosravani et al., 2005), but the underlying mechanisms for the build-up of the HFA were not discussed. Besides, neuronal firing rate increased before the seizure onsets, which might be responsible for greater population spikes in seizures (de la Prida et al., 2006;Engel et al., 2009). Here we demonstrated a global build-up of the HFA and multi-unit activity which are related to the seizure onset, and particularly the build-ups can be modified by interictal discharges and the seizure genesis is also altered.

Although the role of the interictal discharges are still under dispute, our study supported the notion that interictal discharges are not necessary for the seizure onsets (Jensen and Yaari, 1988). However we suggested the interictal discharges have dual effects on the seizure genesis: 1) to prevent seizure onset and 2) to extend seizures. Interictal-discharge-led refractory period, in our model 200 ms in CA1 and much longer in CA3, is an experimental and clinical manifestation that has been studied for years (de Curtis and Avanzini, 2001). Inhibition of the neuronal activities

was tremendously enhanced by synchronous firing of principal cells in the regions responsible for the interictal discharges (i.e. irritative zone) and caused the lasting hyperpolarisation; where both types of GABAeric receptors ($GABA_A$ and $GABA_B$) might contribute to the sustained refractory periods (de Curtis and Avanzini, 2001). Furthermore, it was also suggested that the de-coupling of gap junctions caused by interictal-discharges-led intracellular/extracellular pH shifts might also play a role in the refractory period (de Curtis and Avanzini, 2001). In our study, we suggested the build-up of HFA is essential for the seizure onset. Refractory periods interfered with the development of HFA and thus prolong the steps to approach seizure onsets.

On the other hand, the rhythmic processes that generate interictal discharges can extend seizures. In the intact slices every CA1 population spike in clonic phases was preceded by a CA3 burst (i.e. the interictal discharges although they were during seizues); after lesion of the Schaffer collateral pathway the clonic population spikes were abolished, thus we suggested the clonic seizures in the high K^+ model were also interictal discharge-like electrographic patterns but more complicated with afterdischarges. The clonic phase of seizures, including the extensive after discharges, are mainly associated with activation of NMDA receptors but also related to increase of extracellular K^+, enhanced inward Ca^{2+} current, active metabotrophic

glutamatergic receptors or even the non-synaptic interactions are involved (Traub et al., 1993;Traub et al., 1995;Traub et al., 1996).

CA3 terminals intensely cover the dendritic regions in CA1 (Li et al., 1994), thus synchronous firing as interictal discharges from CA3 can activate tens of thousands of neurons in CA1 and even initiate seizures; and these synchronous inputs might be the reason for the hypersynchronous onset pattern of seizures (de Curtis and Avanzini, 2001). Previous reports suggested that potentiated recurrent excitatory connections in CA3 were associated with the generation of sharp wave-ripple complex which resemble the interictal discharges as we mentioned in previous section; and the potentiation and synchronization of the interictal discharges were enhanced before the onset of population bursts *in vitro,* which altogether might be supportive for seizure onsets (Behrens et al., 2005;de la Prida et al., 2006;Dzhala and Staley, 2003). Even if seizures were not directly triggered by interictal discharges, the HFA or the unit activities in the sub-regions of CA1 simultaneously recovered from the refractory periods and can start a seizure without lag.

In our experiments, we did not find a linear relation between the irritative zone and the seizure onset zone (Figure R-02). On the contrary, CA1b was susceptible whether CA3b or CA3c were prone to start interictal discharges.

Synaptic transmissions involved in the HFA

In the lesioned slices, HFAs in CA1 and CA3 were both enhanced after applying APV. This phenomenon might be due to the reduced local inhibition caused by less active recurrent principal cell inputs. Enhanced HFA in CA3 could trigger the interictal discharges through their recurrent collaterals (Li et al., 1994); and later the interictal discharges propagate to CA1 region and contribute to the seizure genesis as we observed in several intact slices. We felt it was difficult to interpret the phenomenon that the power of the HFAs persisted in higher level after APV wash-out, especially given that APV is very soluble (see Apendices A.2). First we assumed the consecutive build-up of HFA was the cue to explain the failure of wash-out, but our study on the changes of background HFA level in 15 min did not support the assumption. Thus we suggested blocking NMDA receptors initiated an irreversible plasticity, and this mechanism can potentiate the HFAs.

NBQX reduced the HFAs in both lesioned CA1 and CA3 sub-resions, but it induced bursts in CA1. A previous study had demonstrated that high K^+ induced CA3 fast ripples was gradually abolished after NBQX and APV was applied, and they suggested that synaptic transmissions is crucial in the synchrony between the

neighboring pyramidal neurons in CA3 (Dzhala and Staley, 2004). However after blocking glutamate receptors, other mechanisms might alternatively become predominant to generate bursts in CA1. The non-synaptic interactions can sustain the HFA and seizures on their own, though more active inhibition might reduce the power of HFA. In this case if the robust firing of interneurons is synchronous and rhythmic, these interneurons might constrain the principal neurons to fire correlated to the interneuronal rhythms. Burst firing of GABAergic interneurons was demonstrated in hippocampal slices when convulsant 4-AP or high K^+ was present and glutamatergic transmissions were blocked (Michelson and Wong, 1991;Michelson and Wong, 1994). This GABAergic burst was mediated by GABA itself as an excitatory neurotransmitter to provoke interconnected GABAergic interneurons; in addition they also suggested the electrotonic interactions was involved in the GABAergic synchrony (Michelson and Wong, 1994). Thus this mechanism can be related to the new bursts after blocking glutamate receptors as we saw in our study. Interestingly, it had been suggested that slight blockage on non-NMDA receptors (by 1-1.5 μM NBQX) increased the spike-timing reliability and further enhanced the synchrony as shown by the fast oscillation switching to a lower frequency (Foffani et al., 2007).

Removal of inhibition by $GABA_A$ receptor antagonist presented seizure-like events

in both CA1 and CA3 regions in the intact slices, which had been demonstrated before (Borck and Jefferys, 1999). These events originated from CA3 region and propagated to CA1, but CA1 independently generated different bursts after lesion of the Schaffer collateral pathway. Considerable changes in power spectra or differences in the first moment showed the new HFA in the bicuculline-treated slices might be a distinct activity from the HFAs we described before.

Conclusion

The HFA has attracted much interest in studies of epileptogenesis in recent years, and people envisage that the HFA could be used as a predictor for seizure onset, although the mechanisms of the HFA were not clear. We investigated HFAs and electrographic epileptic features in rat hippocampal slices induced by high K^+ ACSF, and demonstrated the mechanisms and several modulations of the HFA. We addressed the possibility that: potentiated HFA might be the key to activate neurons either through the recurrent synaptic transmission or by the non-synaptic interactions and eventually seizures start in consequence. Thus our findings can help to develop a strategy against HFA that could stop epileptic seizures. Correlations between the growing HFA and the seizure onsets shown in our model emphasize that HFA is a reliable hallmark to predict seizure. However, a threshold of the transient from HFA to seizures has not been found. Thus to understand the transition would be the next step before seizure predictions by HFA is applicable.

Appendices

A.1 Neuronal activities during physiological HFA

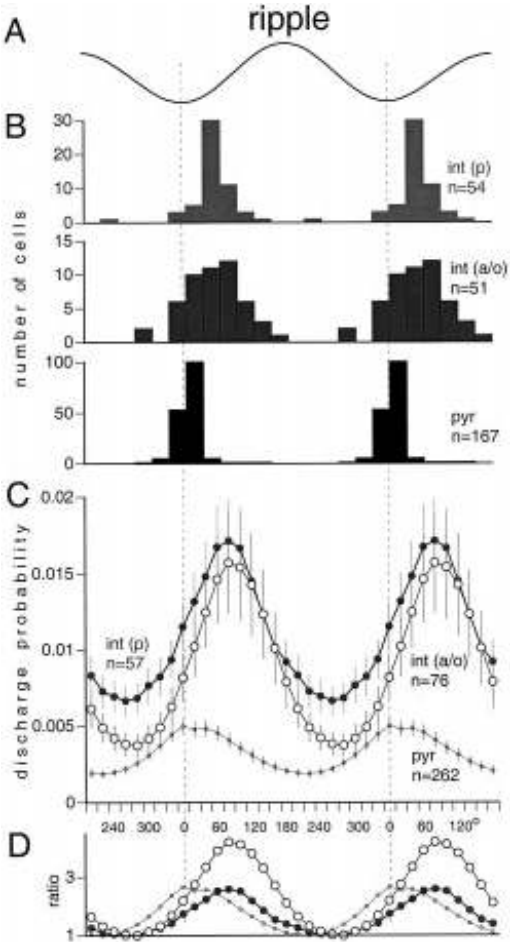

Figure A.1 Ripple phase modulation of pyramidal neurons (*pyr*), interneurons in pyramidal layer (*int(p)*), and interneurons in alveus / oriens (*int(a/o)*). Figure is from Csicsvari et al. 1999b, reprinted from J. Neurosci. *19*, 274-287. **A**, averaged ripple wave (two cycles shown). **B**, phase distribution of single cells relative to the negative peak of the ripple waves (dashed vertical lines). The peak of the phase-corrected cross-correlogram between cell discharge and ripple was used to determine the preferred phase of a single cell. Only neurons with significant ripple phase modulation are shown. **C**, averaged discharge probability of the neuronal subgroups (mean±SE). All neurons are included, independent of whether their crosscorrelograms showed a significant modulation with the ripple waves or not. **D**, normalized probabilities of the different cell groups (depth of ripple modulation). The lowest probability value during the ripple cycle was regarded as the baseline for each neuronal type, and the probabilities were divided by this figure. Note that interneurons follow pyramidal neurons by 90° (~1.2 msec for a 200 Hz ripple).

A.2 APV dynamics *in vitro*

An experiment was conducted to address the question whether APV has quick effect on the slices and can be washed away rapidly in our system. Hippocampal slices were first perfused with ACSF, and two electrodes were placed in CA1 s.pyramidale and s. radiatum respectively to record field potentials which were induced by singular stimuli (strength, 1/4 maximal response; inter-pulse-interval, 45 sec) at the Schaffer collateral pathway. Perfusate was switched to ACSF with low concentration of Mg^{2+} (low Mg^{2+}, 0.1 mM), which reduced the inactivation of NMDA receptors; and NBQX (20 μM) was added to block non-NMDA receptors. This condition was the 'control' for testing APV. After 30 min equilibrium, APV (25 μM) was added to the perfusate. Tem minutes after APV addition, the slice was washed by the control perfusate (low Mg^{2+} and NBQX). Our result suggested that APV had effect on the slice in 2 min after addition; the APV effect started to fade away rapidly after wash and responses recovered in 20 min.

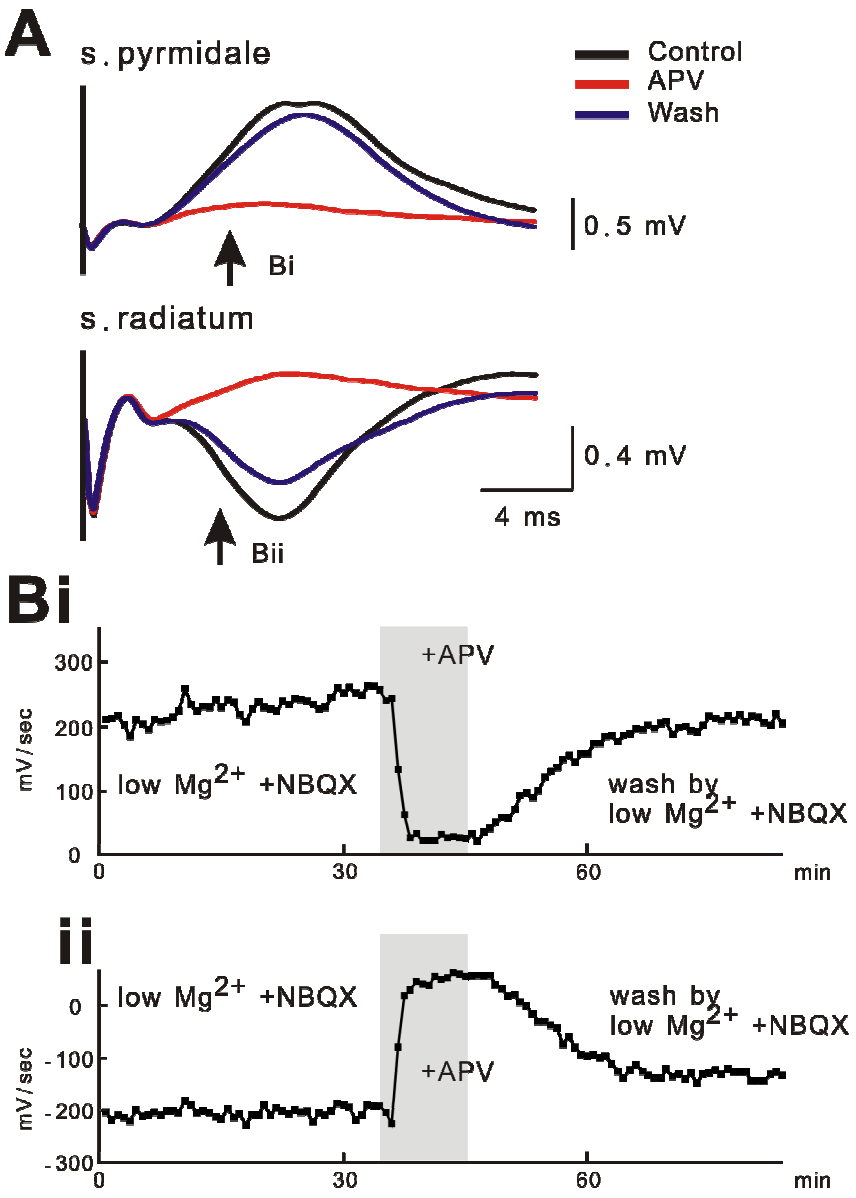
A
s. pyrmidale
Control
APV
Wash
0.5 mV
Bi
s. radiatum
0.4 mV
4 ms
Bii
Bi
+APV
300
200
100
0
mV/sec
low Mg2+ +NBQX
wash by
low Mg2+ +NBQX
0
30
60
min
ii
low Mg2+ +NBQX
wash by
low Mg2+ +NBQX
0
-100
-200
-300
+APV
mV/sec
0
30
60
min

Figure A.2 APV dynamics *in vitro*. **A**, field potentials recorded from CA1 s. pyramidale (*top*) and s. radiatum (*bottom*) during control (black traces), under APV (25 μM, red) and after wash (blue) respectively. Vertical lines at the beginning of the traces indicate the stimuli. Arrows indicate the points where the slopes of the traces were measured for trend plots in B. **B**, trend plots for the slops on the points (indicated in A) of the traces in s. pyramidale (**i**) and s. radiatum (**ii**). Shading represents the addition of APV.

List of References

Ali,A.B., Deuchars,J., Pawelzik,H., and Thomson,A.M. (1998). CA1 pyramidal to basket and bistratified cell EPSPs: dual intracellular recordings in rat hippocampal slices. J Physiol *507 (Pt 1)*, 201-217.

Allen,P.J., Fish,D.R., and Smith,S.J. (1992). Very high-frequency rhythmic activity during SEEG suppression in frontal lobe epilepsy. Electroencephalogr. Clin. Neurophysiol. *82*, 155-159.

Avoli,M., Biagini,G., and de,C.M. (2006). Do interictal spikes sustain seizures and epileptogenesis? Epilepsy Curr. *6*, 203-207.

Bean,B.P. (2007). The action potential in mammalian central neurons. Nat. Rev. Neurosci. *8*, 451-465.

Behrens,C.J., van den Boom,L.P., de,H.L., Friedman,A., and Heinemann,U. (2005). Induction of sharp wave-ripple complexes in vitro and reorganization of hippocampal networks. Nat. Neurosci. *8*, 1560-1567.

Berg,A.T., Berkovic,S.F., Brodie,M.J., Buchhalter,J., Cross,J.H., van Emde,B.W., Engel,J., French,J., Glauser,T.A., Mathern,G.W., Moshe,S.L., Nordli,D., Plouin,P.,

and Scheffer,I.E. (2010). Revised terminology and concepts for organization of seizures and epilepsies: Report of the ILAE Commission on Classification and Terminology, 2005-2009. Epilepsia.

Bikson,M., Fox,J.E., and Jefferys,J.G. (2003). Neuronal aggregate formation underlies spatiotemporal dynamics of nonsynaptic seizure initiation. J. Neurophysiol. *89*, 2330-2333.

Borck,C., and Jefferys,J.G.R. (1999). Seizure-Like Events in Disinhibited Ventral Slices of Adult Rat Hippocampus. J Neurophysiol *82*, 2130-2142.

Bragin,A., Engel,J., Jr., Wilson,C.L., Fried,I., and Buzsaki,G. (1999a). High-frequency oscillations in human brain. Hippocampus *9*, 137-142.

Bragin,A., Engel,J., Jr., Wilson,C.L., Fried,I., and Mathern,G.W. (1999b). Hippocampal and entorhinal cortex high-frequency oscillations (100--500 Hz) in human epileptic brain and in kainic acid--treated rats with chronic seizures. Epilepsia *40*, 127-137.

Bragin,A., Engel,J., Jr., Wilson,C.L., Vizentin,E., and Mathern,G.W. (1999c). Electrophysiologic analysis of a chronic seizure model after unilateral hippocampal KA injection. Epilepsia *40*, 1210-1221.

Bragin,A., Mody,I., Wilson,C.L., and Engel,J., Jr. (2002a). Local generation of fast ripples in epileptic brain. J. Neurosci. *22*, 2012-2021.

Bragin,A., Wilson,C.L., Almajano,J., Mody,I., and Engel,J., Jr. (2004). High-frequency oscillations after status epilepticus: epileptogenesis and seizure genesis. Epilepsia *45*, 1017-1023.

Bragin,A., Wilson,C.L., and Engel,J., Jr. (2007). Voltage depth profiles of high-frequency oscillations after kainic acid-induced status epilepticus. Epilepsia *48 Suppl 5*, 35-40.

Bragin,A., Wilson,C.L., and Engel,J., Jr. (2000). Chronic epileptogenesis requires development of a network of pathologically interconnected neuron clusters: a hypothesis. Epilepsia *41 Suppl 6*, S144-S152.

Bragin,A., Wilson,C.L., Staba,R.J., Reddick,M., Fried,I., and Engel,J., Jr. (2002b). Interictal high-frequency oscillations (80-500 Hz) in the human epileptic brain: entorhinal cortex. Ann. Neurol. *52*, 407-415.

Buhl,E.H., Halasy,K., and Somogyi,P. (1994). Diverse sources of hippocampal unitary inhibitory postsynaptic potentials and the number of synaptic release sites. Nature *368*, 823-828.

Buhl,E.H., Szilagyi,T., Halasy,K., and Somogyi,P. (1996). Physiological properties of anatomically identified basket and bistratified cells in the CA1 area of the rat hippocampus in vitro. Hippocampus *6*, 294-305.

Buzsaki,G. (1986). Hippocampal sharp waves: their origin and significance. Brain Res. *398*, 242-252.

Buzsaki,G. (2004). Large-scale recording of neuronal ensembles. Nat. Neurosci. *7*, 446-451.

Buzsaki,G., Horvath,Z., Urioste,R., Hetke,J., and Wise,K. (1992). High-frequency network oscillation in the hippocampus. Science *256*, 1025-1027.

Chevassus Au Louis,N., Niquet,J., Ben-Ari,Y., and Represa,A. (1997). Cellular plasticity. In Epilepsy: a comprehensive text book, J.Jr. Engel, and T.A. Pedley, eds. (Philadelphia: Lippincott Williams & Wilkins), pp. 387-396.

Chrobak,J.J., and Buzsaki,G. (1996). High-frequency oscillations in the output networks of the hippocampal-entorhinal axis of the freely behaving rat. J. Neurosci. *16*, 3056-3066.

Csicsvari,J., Hirase,H., Czurko,A., and Buzsaki,G. (1998). Reliability and state

dependence of pyramidal cell-interneuron synapses in the hippocampus: an ensemble approach in the behaving rat. Neuron *21*, 179-189.

Csicsvari,J., Hirase,H., Czurko,A., Mamiya,A., and Buzsaki,G. (1999a). Fast network oscillations in the hippocampal CA1 region of the behaving rat. J. Neurosci. *19*, RC20.

Csicsvari,J., Hirase,H., Czurko,A., Mamiya,A., and Buzsaki,G. (1999b). Oscillatory coupling of hippocampal pyramidal cells and interneurons in the behaving Rat. J. Neurosci. *19*, 274-287.

Csicsvari,J., Hirase,H., Mamiya,A., and Buzsaki,G. (2000). Ensemble patterns of hippocampal CA3-CA1 neurons during sharp wave-associated population events. Neuron *28*, 585-594.

de Curtis,M., and Avanzini,G. (2001). Interictal spikes in focal epileptogenesis. Prog. Neurobiol. *63*, 541-567.

de la Prida,L.M., Huberfeld,G., Cohen,I., and Miles,R. (2006). Threshold behavior in the initiation of hippocampal population bursts. Neuron *49*, 131-142.

Draguhn,A., Traub,R.D., Schmitz,D., and Jefferys,J.G. (1998). Electrical coupling

underlies high-frequency oscillations in the hippocampus in vitro. Nature *394*, 189-192.

Dudek,F.E., Snow,R.W., and Taylor,C.P. (1986). Role of electrical interactions in synchronization of epileptiform bursts. Adv. Neurol. *44*, 593-617.

Dzhala,V.I., and Staley,K.J. (2003). Transition from Interictal to Ictal Activity in Limbic Networks In Vitro. J. Neurosci. *23*, 7873-7880.

Dzhala,V.I., and Staley,K.J. (2004). Mechanisms of Fast Ripples in the Hippocampus. J. Neurosci. *24*, 8896-8906.

Engel,J.Jr., Bragin,A., Staba,R., and Mody,I. (2009). High-frequency oscillations: what is normal and what is not? Epilepsia *50*, 598-604.

Engel,J.Jr., and Pedley,T.A. (2008). Introduction: what is epilepsy? In Epilepsy: a comprehensive text book, J.Jr. Engel, and T.A. Pedley, eds. (Philadelphia: Lippincott Williams & Wilkins), pp. 1-7.

Fisher,R.S., Webber,W.R., Lesser,R.P., Arroyo,S., and Uematsu,S. (1992). High-frequency EEG activity at the start of seizures. J. Clin. Neurophysiol. *9*, 441-448.

Foffani,G., Uzcategui,Y.G., Gal,B., and Menendez de la,P.L. (2007). Reduced spike-timing reliability correlates with the emergence of fast ripples in the rat epileptic hippocampus. Neuron *55*, 930-941.

Fox,S.E., and Ranck,J.B., Jr. (1981). Electrophysiological characteristics of hippocampal complex-spike cells and theta cells. Exp. Brain Res. *41*, 399-410.

Freund,T.F., and Buzsaki,G. (1996). Interneurons of the hippocampus. Hippocampus *6*, 347-470.

Gulyas,A.I., Miles,R., Sik,A., Toth,K., Tamamaki,N., and Freund,T.F. (1993). Hippocampal pyramidal cells excite inhibitory neurons through a single release site. Nature *366*, 683-687.

Harris,K.D., Henze,D.A., Csicsvari,J., Hirase,H., and Buzsaki,G. (2000). Accuracy of tetrode spike separation as determined by simultaneous intracellular and extracellular measurements. J Neurophysiol *84*, 401-414.

Hart,Y.M., and Sander,J.W. (2007). Epilepsy: questions and answers (Surrey: Merit Publishing International).

Henze,D.A., Borhegyi,Z., Csicsvari,J., Mamiya,A., Harris,K.D., and Buzsaki,G. (2000).

Intracellular features predicted by extracellular recordings in the hippocampus in vivo. J Neurophysiol *84*, 390-400.

Holt,G.R., and Koch,C. (1999). Electrical interactions via the extracellular potential near cell bodies. J Comput. Neurosci. *6*, 169-184.

Jefferys,J.G. (2003). Models and mechanisms of experimental epilepsies. Epilepsia *44 Suppl 12*, 44-50.

Jefferys,J.G. (1995). Nonsynaptic modulation of neuronal activity in the brain: electric currents and extracellular ions. Physiol Rev. *75*, 689-723.

Jefferys,J.G. (1999). Hippocampal sclerosis and temporal lobe epilepsy: cause or consequence? Brain *122 (Pt 6)*, 1007-1008.

Jefferys,J.G., and Haas,H.L. (1982). Synchronized bursting of CA1 hippocampal pyramidal cells in the absence of synaptic transmission. Nature *300*, 448-450.

Jensen,M.S., and Yaari,Y. (1988). The relationship between interictal and ictal paroxysms in an in vitro model of focal hippocampal epilepsy. Ann. Neurol. *24*, 591-598.

Jinno,S., and Kosaka,T. (2010). Stereological estimation of numerical densities of

glutamatergic principal neurons in the mouse hippocampus. Hippocampus *20*, 829-840.

Jiruska,P., Cmejla,R., Powell,A.D., Chang,W.C., Vreugdenhil,M., and Jefferys,J.G. (2009). Reference noise method of removing powerline noise from recorded signals. J Neurosci. Methods *184*, 110-114.

Jiruska,P., Csicsvari,J., Powell,A.D., Fox,J.E., Chang,W.C., Vreugdenhil,M., Li,X., Palus,M., Bujan,A.F., Dearden,R.W., and Jefferys,J.G. (2010a). High-frequency network activity, global increase in neuronal activity, and synchrony expansion precede epileptic seizures in vitro. J Neurosci. *30*, 5690-5701.

Jiruska,P., Finnerty,G.T., Powell,A.D., Lofti,N., Cmejla,R., and Jefferys,J.G. (2010b). Epileptic high-frequency network activity in a model of non-lesional temporal lobe epilepsy. Brain *133*, 1380-1390.

Jiruska,P., Powell,A.D., Chang,W.C., and Jefferys,J.G. (2010c). Electrographic high-frequency activity and epilepsy. Epilepsy Res. *89*, 60-65.

Johnston,D., and Amaral,D.G. (2003). Hippocampus. In The synaptic organization of the brain, G.M. Shepherd, ed. (Oxford: Oxford University Press, Inc.), pp. 455-498.

Jonas,P., and Sakmann,B. (1992). Glutamate receptor channels in isolated patches from CA1 and CA3 pyramidal cells of rat hippocampal slices. J Physiol *455*, 143-171.

Kandel,A., and Buzsaki,G. (1997). Cellular-synaptic generation of sleep spindles, spike-and-wave discharges, and evoked thalamocortical responses in the neocortex of the rat. J Neurosci. *17*, 6783-6797.

Khosravani,H., Mehrotra,N., Rigby,M., Hader,W.J., Pinnegar,C.R., Pillay,N., Wiebe,S., and Federico,P. (2009). Spatial localization and time-dependant changes of electrographic high frequency oscillations in human temporal lobe epilepsy. Epilepsia *50*, 605-616.

Khosravani,H., Pinnegar,C.R., Mitchell,J.R., Bardakjian,B.L., Federico,P., and Carlen,P.L. (2005). Increased high-frequency oscillations precede in vitro low-Mg seizures. Epilepsia *46*, 1188-1197.

Klausberger,T., and Somogyi,P. (2008). Neuronal diversity and temporal dynamics: the unity of hippocampal circuit operations. Science *321*, 53-57.

Klee,R., Ficker,E., and Heinemann,U. (1995). Comparison of voltage-dependent potassium currents in rat pyramidal neurons acutely isolated from hippocampal

regions CA1 and CA3. J Neurophysiol *74*, 1982-1995.

Kloosterman,F., Peloquin,P., and Leung,L.S. (2001). Apical and basal orthodromic population spikes in hippocampal CA1 in vivo show different origins and patterns of propagation. J Neurophysiol *86*, 2435-2444.

Le Van,Q.M., Bragin,A., Staba,R., Crepon,B., Wilson,C.L., and Engel,J., Jr. (2008). Cell type-specific firing during ripple oscillations in the hippocampal formation of humans. J. Neurosci. *28*, 6104-6110.

Li,X.G., Somogyi,P., Ylinen,A., and Buzsaki,G. (1994). The hippocampal CA3 network: an in vivo intracellular labeling study. J. Comp Neurol. *339*, 181-208.

Litt,B., and Lehnertz,K. (2002). Seizure prediction and the preseizure period. Curr. Opin. Neurol. *15*, 173-177.

Lopez-Aguado,L., Ibarz,J.M., and Herreras,O. (2000). Modulation of dendritic action currents decreases the reliability of population spikes. J. Neurophysiol. *83*, 1108-1114.

Lopez-Aguado,L., Ibarz,J.M., and Herreras,O. (2001). Activity-dependent changes of tissue resistivity in the CA1 region in vivo are layer-specific: modulation of evoked

potentials. Neuroscience *108*, 249-262.

Maier,N., Nimmrich,V., and Draguhn,A. (2003). Cellular and network mechanisms underlying spontaneous sharp wave-ripple complexes in mouse hippocampal slices. J. Physiol *550*, 873-887.

Mathern,G.W., Wilson,C.L., and Beck,H. (2008). Hippocampal sclerosis. In Epilepsy: a comprehensive text book, J.Jr. Engel, and T.A. Pedley, eds. (Philadelphia: Lippincott Williams & Wilkins), pp. 121-136.

Michelson,H.B., and Wong,R.K. (1991). Excitatory synaptic responses mediated by GABAA receptors in the hippocampus. Science *253*, 1420-1423.

Michelson,H.B., and Wong,R.K. (1994). Synchronization of inhibitory neurones in the guinea-pig hippocampus in vitro. J Physiol *477 (Pt 1)*, 35-45.

Mitchell,J., Gatherer,M., and Sundstrom,L.E. (1996). Aberrant Timm-stained fibres in the dentate gyrus following tetanus toxin-induced seizures in the rat. Neuropathol. Appl. Neurobiol. *22*, 129-135.

Mormann,F., Andrzejak,R.G., Elger,C.E., and Lehnertz,K. (2007). Seizure prediction: the long and winding road. Brain *130*, 314-333.

Nicholson,C., and Freeman,J.A. (1975). Theory of current source-density analysis and determination of conductivity tensor for anuran cerebellum. J. Neurophysiol. *38*, 356-368.

Rakhade,S.N., and Jensen,F.E. (2009). Epileptogenesis in the immature brain: emerging mechanisms. Nat. Rev. Neurol. *5*, 380-391.

Ranck,J.B., Jr. (1973). Studies on single neurons in dorsal hippocampal formation and septum in unrestrained rats. I. Behavioral correlates and firing repertoires. Exp. Neurol. *41*, 461-531.

Rosenow,F., and Luders,H. (2001). Presurgical evaluation of epilepsy. Brain *124*, 1683-1700.

Sik,A., Penttonen,M., Ylinen,A., and Buzsaki,G. (1995). Hippocampal CA1 interneurons: an in vivo intracellular labeling study. J. Neurosci. *15*, 6651-6665.

Sik,A., Ylinen,A., Penttonen,M., and Buzsaki,G. (1994). Inhibitory CA1-CA3-hilar region feedback in the hippocampus. Science *265*, 1722-1724.

Spruston,N., Jonas,P., and Sakmann,B. (1995). Dendritic glutamate receptor channels in rat hippocampal CA3 and CA1 pyramidal neurons. J Physiol *482 (Pt*

2), 325-352.

Staba,R.J., Wilson,C.L., Bragin,A., Fried,I., and Engel,J., Jr. (2002). Quantitative analysis of high-frequency oscillations (80-500 Hz) recorded in human epileptic hippocampus and entorhinal cortex. J. Neurophysiol. *88*, 1743-1752.

Stepanyants,A., Martinez,L.M., Ferecsko,A.S., and Kisvarday,Z.F. (2009). The fractions of short- and long-range connections in the visual cortex. Proc. Natl. Acad. Sci. U. S. A *106*, 3555-3560.

Szymusiak,R., and Nitz,D. (2010). Chronic Recording of Extracellular Neuronal Activity in Behaving Animals. In Current Protocols in Neuroscience, C.R. Gerfen, A. Holmes, D. Sibley, P. Skolnick, and S. Wray, eds. (Hoboken, NJ: John Wiley & Sons, Inc.), p. 6.16.1-6.16.24.

Traub,R.D. (2003). Fast Oscillations and Epilepsy. Epilepsy Curr. *3*, 77-79.

Traub,R.D., Borck,C., Colling,S.B., and Jefferys,J.G. (1996). On the structure of ictal events in vitro. Epilepsia *37*, 879-891.

Traub,R.D., Colling,S.B., and Jefferys,J.G. (1995). Cellular mechanisms of 4-aminopyridine-induced synchronized after-discharges in the rat hippocampal

slice. J. Physiol *489 (Pt 1)*, 127-140.

Traub,R.D., Miles,R., and Jefferys,J.G. (1993). Synaptic and intrinsic conductances shape picrotoxin-induced synchronized after-discharges in the guinea-pig hippocampal slice. J Physiol *461*, 525-547.

Traub,R.D., Whittington,M.A., Buhl,E.H., LeBeau,F.E., Bibbig,A., Boyd,S., Cross,H., and Baldeweg,T. (2001). A possible role for gap junctions in generation of very fast EEG oscillations preceding the onset of, and perhaps initiating, seizures. Epilepsia *42*, 153-170.

Traynelis,S.F., and Dingledine,R. (1988). Potassium-induced spontaneous electrographic seizures in the rat hippocampal slice. J. Neurophysiol. *59*, 259-276.

Worrell,G.A., Parish,L., Cranstoun,S.D., Jonas,R., Baltuch,G., and Litt,B. (2004). High-frequency oscillations and seizure generation in neocortical epilepsy. Brain *127*, 1496-1506.

Ylinen,A., Bragin,A., Nadasdy,Z., Jando,G., Szabo,I., Sik,A., and Buzsaki,G. (1995). Sharp wave-associated high-frequency oscillation (200 Hz) in the intact hippocampus: network and intracellular mechanisms. J. Neurosci. *15*, 30-46.